PhD Thesis

submitted in fulfilment of the requirements for the degree of
Doctor of the Università degli Studi di Genova

Italian Academic Field: ING-IND 02
Ship Structures and Marine Engineering

Doctoral School: Polytechnic School - Dept. of Naval Architecture, Electric, Electronic and Telecommunication Engineering.

Presented & Defended publicly on May 24th, 2022
By Nicolò Faggioni

Enabling technologies and decision support systems towards autonomous navigation of ships

---

Supervisor:

Prof. Michele Martelli

In front of a jury composed of:

Prof. Raphael Zaccone

Prof. Vincenzo Piscopo

Prof. Rudy R. Negenborn

Università di Genova
DITEN DIPARTIMENTO DI INGEGNERIA NAVALE, ELETTRICA, ELETTRONICA E DELLE TELECOMUNICAZIONI

Murphy's Law
If anything can go wrong, it will.

Corollaries

1. *Nothing is as easy as it looks.*
2. *Everything takes longer than you think.*
3. *If there is a possibility of several things going wrong, the one that will cause the most damage will be the one to go wrong.*
4. *If you perceive that there are four possible ways in which a procedure can go wrong, and circumvent these, then a fifth way will promptly develop.*
5. *Left to themselves, things tend to go from bad to worse.*
6. *Whenever you set out to do something, something else must be done first.*
7. *Every solution breeds new problems.*
8. *It is impossible to make anything foolproof because fools are so ingenious.*
9. *Nature always sides with the hidden flaw.*

Summary

List of Figures

List of Tables

Preface

Maritime traffic is increasing day by day. Therefore, improving the safety level of life at sea is deeply necessary. The examined statistics show that the primary causes of incidents and accidents are attributable to the human factor: the solution evaluated in this thesis consists of limiting the human factor onboard. In particular, limiting human error could reduce the frequency of incidents and accidents and their severity, positively affecting the protection of human life, environmental conservation, and operating costs. Unfortunately, historically, new technologies and navigation support tools are not always fully exploited and used in the maritime field due to the limited trust against them. Instead, these technological innovation tools are mainly used for limited research project applications, such as autonomous and remote-control navigation. Indeed, these innovations could be used to equip surface vehicles with the tools necessary to achieve situational awareness, allowing the development of a decision support system that be helpful for a bridge operator to take safety navigation decisions or enable autonomous navigation completely overriding the human operator. Due to the several benefits that these technologies promise to bring, global interest has grown enormously in recent years, leading to the creation of international consortia to work on and found several projects concerning autonomous navigation enabling technologies in order to obtain a smart ship. However, the question may arise as to whether it is actually worth investing so heavily in these types of technologies, given that the promises of cost reduction and increased safety are based on hypothetical comparisons as no fully autonomous ship has yet been launched. Fortunately, the significant projects illustrated in the thesis have a near future as their deadline. For these reasons, in the next few years, it will be possible to know and quantify which and how essential the benefits they bring will be. Furthermore, it is also legitimate to question the field of applicability of these technologies. It presented that these technologies are already widely used for small boats, less than 20 m in length, for scientific research purposes and military uses.

Of course, the ship's dimensions are not the only characteristics to be considered but also the task that the ship has to carry out and how much the crew is involved in carrying out more or less complex tasks. For instance, in fishing ships, several tasks performed by the crew might be too complex to be performed by a machine [1]. Thus, removing the crew can be challenging, especially for service ships and fishing ships. Indeed, in such a case, a complete decision support system that helps the bridge operator take correct decisions

during navigation is more suitable than removing the crew onboard. Moreover, the assumption that reaching full autonomous navigation may be limited to smaller ships with the crew performing easily replaceable tasks is supported by the CEO of Maersk, Søren Skou [2]. Regarding the added safety benefit of large autonomous container ships, the impact of removing the crew will be small since there are only a few lives lost on container ships in general. Therefore, the added safety benefit would not be a good reason to invest in (large) autonomous container ships. This thesis wants to emphasise that not all ships will be easily replaced by their autonomous evolutions for various reasons, such as the complexity of the crew's tasks onboard or the impossibility of removing the human factor representing the payload as in cruise ships. In all these cases, in order to improve safety during navigation, it is essential to provide the ship with a decision support system fed with sensors onboard.

Furthermore, the research that is being carried out, and this thesis fits into this context, is studying and developing automated control logics which, if both the achievement of autonomous navigation and the development of a decision support system for the bridge operator, are essential for both developments. In conclusion, the undersigned point of view is that it makes little sense to question whether it will bring significant benefits that justify the potential cost increase. On the other hand, the human being has always been thirsty for knowledge since eating in the garden of Eden of the forbidden fruit of knowledge. For this reason, technological development in this area must be completed and only after implementing the first projects, it will be possible to quantify any benefits and disadvantages effectively. To conclude, in the Divine Comedy, the great navigator Ulysses, placed in Hell by Dante and dead for having wanted to venture beyond the Pillars of Hercules, states: "…*fatti non foste a viver come bruti, ma per seguir virtute e canoscenza*." (…you were not made to live as brutes, but to follow virtue and knowledge.).

It could be sarcastically argued that he bit more than one can chew and that he could have died on terra firma of old age if he had used a bireme equipped with a decision support system that would have been useful to avoid the deadly shipwreck in order to be able reaching the Purgatory island.

Chapter 1

1.1 Introduction

The concept of autonomous or remote control autonomous ships has faraway origins in the past. At the end of the 19th century, Nikola Tesla patented his idea about autonomy in maritime traffic [3]. Indeed, starting from the second half, the 19th century was characterised by scientific and technological improvements in which human beings were relieved of dangerous and tiring tasks, replaced by machinery, and shaping today's world. However, before human beings developed the technology to re-evaluate the possibility of obtaining safe autonomous vehicles, many years of technological innovations had to pass. Indeed, just in recent years, studies concerning the achievement of autonomous vehicles have multiplied. Such an aspect has several reasons. In particular, there is the world market's keen interest due to the countless benefits that these technologies promise in terms of safety and human wellness. The interest in autonomous vehicles has remarkably grown over the past decade. This interest growth is due to the potential benefits for our society that such a technology promises. The potential benefits are manifold and depend on the vehicle's field of use. Indeed, this interest affects all transportation sectors: aviation, automotive and the marine field. For instance, nowadays, air remote unmanned vehicles used for pleasure purposes have become part of everyday life. Numerous disciplines are involved in the study of achieving autonomous vehicles due to the complexity of this challenging task. Indeed, numerous scientific papers deal with the problem by using many approaches, even very different from each other. Currently, the achievement of a completely autonomous vehicle capable of meeting the safety and reliability requirements necessary for use is still under development. In this context, numerous definitions and levels of vehicle autonomy have been ideated to distinguish vehicle capability. Unfortunately, due to the massive amount of studies addressed to this topic, it can happen that the authors, belonging to different fields, confuse or overuse different terms and concepts, causing disorder.

The research project presented in this doctoral thesis fits into the reachability of autonomous navigation or marine surface vehicles. The thesis aims to analyse the complexity of the problem through a deep analysis clarifying and taking into account several characteristics, challenging aspects and threats by presenting the autonomous issue regarding the maritime field with a holistic

point of view. Indeed, in Chapter I, an in-depth analysis of the motivation, the principal aspects, the main potential threats, and the main technical and legislative challenges of autonomous vehicles were conducted and presented. In particular, the thesis focuses on two enabling technology systems, dynamic positioning and sensor-based collision detection, as part of the collision avoidance system. These technologies are essential in order to obtain autonomous navigation or develop a helpful decision support system (DSS) to bridge operators. The decision-maker is the main difference between autonomous navigation and a DSS. In both cases, the raw information gathered by the onboard sensors is processed by algorithms to produce useful information on the ship's self-state and the surrounding environment. In the case of DSS, the output of this analysis is shown to the operator on the bridge so that he can use it to make navigation safer. In the case of autonomous navigation, the operator is not considered within the decision-making loop; moreover, if present or remotely, the bridge operator has only the role of surveillance in case of system failure.

To summarize, these autonomous systems, dynamic positioning and collision avoidance can be helpful for developing a decision support system or a totally autonomous framework development. The difference between a decision support system and a complete autonomous navigation framework was discussed in Chapter II. Moreover, a state of the art of dynamic positioning and collision avoidance was presented.

The dynamic positioning system was studied using three degrees of freedom ship dynamic simulator tailored to a tug testing model owned by the University of Genova. Two different thrust allocations suitable for the testing model have been studied and developed. Moreover, the results have been critically analysed and discussed. Furthermore, the tug testing model is completely controllable, self-propelled and fully actuated and has been part of the experimental benchmark developed in the University's facility, where a video-tracking system has been tested and validated. The description of the experimental benchmark and the developed dynamic positioning system have been reported in Chapter III and Chapter IV, respectively.

The second main research topic presented is the detection, part of the collision avoidance system. Collision detection has been studied by means of a purely experimental approach, indeed, has been developed a multi-obstacle tracking system tailored for the marine environment by a sensor-based data processing approach. In particular, the data processing based on an unsupervised learning approach has been carried out on point clouds gathered by using a LiDAR sensor. Eventually, the proposed multi-obstacle tracking system was evaluated

and tested on a specially developed synthetic scenario and an experimental dataset obtained by means of an experimental campaign. The data collection and processing regarding the collision detection have been shown in Chapter V.

Eventually, in Chapter VI, the research project's contribution to the autonomous navigation field and the future research development concerning autonomous navigation enabling technologies was remarked on and critically discussed.

1.2 Motivation

In this last decade, a new technological era has arisen. As a result, the studies focusing on the achievement of autonomous vehicles have had a remarkable development in every industrial sector. These studies were possible thanks to the considerable technological improvement that has taken place in recent years and is still in progress. Indeed, the new ICT (Information and Communications Technology) solutions have brought to rethink the vehicle design in that equipping vehicles with new capabilities and to improve existing functionality is achievable due to the cost reduction and availability of new technology.

Historically reluctant to sudden changes, the maritime sector was also deeply influenced in this context of significant technological development due to the potential benefits in terms of fuel efficiency, operative cost reduction and greater safety onboard systems. Indeed, many terms related to increased automation have been coined, such as autonomous surface vehicles (ASV), unmanned surface vehicles (USV), and autonomous sea surface vessels (MASS), often misused to describe different vehicles capabilities. The following sections have reported the discussion of these terms, clarifying their terminology and characteristics. A ship with solid automation features such as remote navigation, collision avoidance systems or a decision support system is called a "smart ship". For instance, the "Global Marine Technology Trends 2030" [4] has confirmed the "smart ships" as a development key factor of the maritime sector, in particular, to improve navigation safety profoundly. Indeed, the marine sector has always been sensitive to human life safeguarding at sea. For such a reason, surveys have been conducted to analyse this aspect. Indeed, the need to preserve human life at sea and the environment safeguarding are the primary goals in the maritime field. Inevitably, ship accidents and incidents, e.g., ship collisions, are recorded every year, which causes considerable

economic damage, legal problems, non-negligible risks for human health, fatalities and the dispersion of polluting material in the marine environment.

Yearly European Maritime Safety Agency (EMSA) [5] issues a statistical analysis of accidents in the maritime sector. From 2014 to 2020, more than 3200 ship accidents and casualties happened every year. The unique exception is represented by 2020 with 2600 due to the Coronavirus outbreak. The related investigations are 923 and are classified as: *very serious marine casualties* (49.9%), *serious marine casualties* (41.5%), *less serious marine casualties* (7.5%) and, *marine incident* (1.1.%). There are present 757 investigation reports showing that 20% are human factors while 47% are ship-related procedures. It is essential to underline that these values are probably underestimated. Almost all the investigation reports refer to *severe accidents*, and these are the minority of the 3200 cases per year. On the contrary, the majority of accidents are represented by the remaining *less serious marine casualties* and *marine incidents*; for such a reason, it is foreseeable that many of these accidents are to be considered by the human factor or wrong procedures.

Another critical annual analysis covering the entire yachting industry in the United States is reported in Recreational Boating Statistics [6]. The analysis was conducted by analysing accident and casualties events in detail by analysing their severity, geographical distribution, monthly events, economic weight, length of the boats involved, and reasons for the event. In particular, focusing on the latter case, it is possible to observe that factors attributable to the human factor such as *operator inattention*, *operator inexperience*, *improper lookout*, *excessive speed*, *navigation rules violation*, and *alcohol use* are the preponderant part of all recorded accidents and incidents. In contrast, accidents and incidents due to boat failure or boat equipment malfunctions are a minority of the total events. Neglecting the count of events to which it is difficult to attribute a responsible entity, such as sudden meteorological changes or the cause is unknown, the events undoubtedly attributable to human errors are more than 88% and only 12% to machinery malfunctions.

Moreover, considering accidents and incidents related to environmental conditions attributable to human factors, such as a wrong planning choice for the navigation route, the percentage of machinery breakdowns drops to 9% of the total events. From these analyses, it is essential to underline that in the case of pleasure boats, accidents and incidents attributable to the human factor represent almost all cases. This aspect is due to the analysis carried out by EMSA only considering ships with trained personnel on board.

In this context, the increase in onboard automation, which can take on different meanings depending on the technological level installed onboard (decision support system, onshore remote control or complete autonomous vessel), can undoubtedly help reduce the accidents and incidents attributable to the human factor. Many universities and the industrial sector studies are reported in the scientific literature regarding the potential increase in navigation safety. [7-13].

On the other hand, even a ship with a high level of automation, for example, with a decision support system and remote control systems, can suffer from the same problem as human action is always in the control loop. In this case, the reasons could be many such as the operator's lack of trust towards the decision support system or excessive workload or distraction of the commanded exactly as what already happens onboard the ship, in case of onshore remote control. Furthermore, in the case of the human factor out of the control loop, the decisions must be taken from an appropriately programmed artificial intelligence (AI) based on navigation rules and sensor-based. In this context, the crossing situation of manned and autonomous platforms is the worst-case scenario. Indeed, people's behaviour is often unpredictable, and rules can be neglected [14]. Therefore, the AI system must consider this aspect to avoid potential accidents [15]. (*It is impossible to make anything foolproof because fools are so ingenious – 8th Moody's Law*). Eventually, a critical statistic analysis was conducted by means of the EMSA collision accident data and reductio ad absurdum hypnotising several scenarios with an increased level of autonomous navigation regarding three surface vehicle typologies (small cargo, cargo over 120m, all ships). As a result, it emerges that the introduction of autonomous navigation for all scenarios notably increases safety, assuming the autonomous systems can reduce the number of accidents. Moreover, autonomous navigation alone is able to remove few people from the ship, and in some particular cases, the crew role is crucial to perform the ship task, e.g., in a fishing vessel where a small crew has a fishing and navigation role. Indeed, it is crucial to research technologies that enable the safe elimination of the crew's role in all other ship functions, such as fishing or maintenance, since the crew onshore will not be able to solve onboard issues and specific activities [16].

1.3 Cost Analysis

There are many publications focused on the analysis of safety improvement. Indeed the issue is extensively analysed in every aspect. Moreover, it emerges that the use of technologies enabling autonomous navigation at any level of intervention to support navigation or totally autonomous can significantly reduce the occurrence of incidents and accidents.

Contrary to the safety issue, far fewer scientific publications are based on the analysis of the costs incurred for these new marine units. This lack of cost analysis is because major projects have not yet been completed, and all analyses are based on project estimates. Currently, autonomous navigation is at a preliminary stage with design and testing. Indeed, nowadays, autonomous boats are used mainly for environmental monitoring or remotely controlled and used by navies.

In addition, once the benefit of navigation safety has been ascertained, it remains to be established whether the owner has an improvement in terms of the investment cost. If the new technologies implementing autonomous ships do not have good economic benefits, the shipowners will not invest in such technological solutions due to low ROI (Return On Investment). Indeed, the autonomous navigation topic represents a high-risk outcome. Indeed, as presented in the following section, only the major private companies and international community projects can afford this economic risk, mainly due to the low margin shipping industry [17,18]. For every product, the total cost can be divided into two macro parts CAPEX (CAPital EXpenditures) and OPEX (OPerating EXpenses). In particular, if the case study is a ship is subdivided as follows. CAPEX was defined as a fixed cost corresponding to the total amount of cost regarding the vessel purchasing, e.g., construction cost, financing cost, loan interests, depreciation, taxes, etc. The OPEX in maritime can be subdivided into two main sub-parts Operating Cost and Voyage Cost. The Operating Cost is a semi-variable cost, and the main ones are the crew wages, insurance, maintenance, and administration costs. On the other hand, the Voyage Cost is highly variable. Indeed, it strictly depends on several factors such as the shipping route, the environmental condition, and the amount of transported material. For instance, the Voyage Cost can be subdivided among the fuel consumed, portal and canal charges, harbour tugs and stevedoring [19].

Unfortunately, cost-benefit analyses regarding autonomous and remote-controlled ships are few due to the technical characteristic uncertain of the smart ships. In the literature, a critical analysis is carried out by comparing

CAPEX and OPEX, assuming as a case study a standard Panamax bulk carrier with a length of 230 m, displacement of 90000 t and motorised with 10 MW. This ship was compared with a hypothetical autonomous bulk carrier with the same characteristics, remotely monitored from a shore control station [20]. The analysis is in-depth as it compares multiple items. Within the table was reported the main contributes, a decrease or increase price has referred to the autonomous hypotetical carrier ship:

Table 1: Considered cost changes, [20]

Operating costs	Voyage costs	Capital costs
Crew wages (−)	Air resistance (−)	Deckhouse (−)
Crew related costs (−)	Lightship weight (−)	Hotel system (−)
Shore control centre (+)	Hotel system (−)	Redundant technical systems (+)
Maintenance crews (+)	Boarding crew for port calls (+)	Autonomous ship technology (+)

Minus (-) represents a reduction of costs; Plus (+) an increase.

In particular, three scenarios were taken into account: i) removing crew; ii) removing crew and better fuel efficiency; iii) removing crew, better fuel efficiency and high-grade fuel. The analysis results show that the first scenario guarantees slightly economic benefits; indeed, crew wages the cost savings of crew wages are compensated by the cost of the onshore control station. The second scenario shows advantages to preferring the autonomous fuel efficiency bulker with respect to the standard one due to fuel savings cost. The last scenario is the worst because switching to MDO (marine diesel oil) instead of HFO (heavy fuel oil) is more expensive. To summarise, the analysis was conducted in-depth, and it emerges that the real potential benefit is the fuel savings. Moreover, the cost of emergency arrival of the crew onboard is not considered, and the autonomous ship technology and redundant technical system were estimated based on other concept projects since no autonomous ship has fully in operation nowadays.

However, the results of this analysis may appear not too encouraging from an economic point of view, given that the great advantage in economic terms is linked to the lower fuel consumption, which is not necessarily linked to autonomous navigation. It must be considered that the analysis is conducted on a bulk carrier whereby other types of vessels, such as container carriers for inland waters, could have more economic benefits than the case study analysed.

Indeed, other economic analyses carried out on autonomous container ships used in a short-sea linear network as the working environment were shown several benefits, including a reduction of operating costs between 9% and 13% [21,22]. Furthermore, although the comparison in terms of cost between standard bulkers and autonomous is almost unchanged, slightly in favour of the autonomous ship, it should be emphasised that the autonomous ship would guarantee a significant increase in terms of safety at sea. Therefore, safer units would be obtained at the same cost, and with the affirmation of this technology, the insurance fees related to autonomous ships could also be lower due to reduced safety risk [23]. Eventually, the potential cost-benefits analysis is still uncertain due to application technology immaturity. After realising the first autonomous ship into the shipping industry, CAPEX and OPEX parameters could be valued more precisely and not completely assumed.[24]. On the other hand, in this scenario, CAPEX could be only estimated because a precise value will be known after the consolidation of autonomous ship technology obtained by several autonomous ship construction.

Despite the uncertain regarding autonomous ship projects due to the novelty of the applications of new technologies to naval units, according to a market intelligence report by BIS Research titled "Global Autonomous Ship and Ocean Surface Robot Market: Analysis and Forecast, 2018-2028", the global ocean surface robot market is expected to reach a market size of almost $2,9 billion by 2028, showing a growth rate of 16.8% during 2018-2028. Furthermore, in terms of volume, the autonomous ship market is expected to grow at the rate of 26.7% during the period 2024-2035 and cumulatively generate a revenue of $3.48 billion by 2035 [25]. This forecast is due to the several benefits of using autonomous or unmanned vehicles for scientific research organisations, commercial industries, and naval forces.

1.4 ASV and USV Projects History

In the literature, several projects are documented that refer to studies on the achievement of autonomous navigation. Usually, the research studies for the achievement of autonomous navigation are divided into two main categories; the first concerns the numerical simulation, in which a virtual simulator of the ship is used to test the control logic. The second is represented by the experimental approach in which the studied logics are implemented onboard small models called ASV (autonomous surface vehicle) and USV(unmanned

surface vehicle). In most cases, the development and validation process involves both methodologies. That is, initially, it is virtually developed and tested and then it is implemented onboard the surface vehicles for validation purposes. Furthermore, these surface vessels are used to study autonomous navigation and to carry out risky tasks in which the human factor could lead to the failure of the mission planned. In particular, the scenarios in which these vehicles are used are mainly two, hydrographic research and ocean exploitation and hazardous military scenario. In the first case, the human factor is removed in order to guarantee that the ocean data collection could involve long days of uninterrupted navigation in remote areas or polluted ones. In the second scenario, it is possible to carry out the task in an enemy zone with remotely controlled vehicles without endangering human life during the task. In detail, the application of USVs and ASVs are listed hereinafter:

Table 2: Specific application of ASVs and USVs

Scenarios	Specific applications
Hydrographic research and ocean exploitation	Bathymetric survey; ocean biological phenomena; environmental monitoring, sampling and assessment; pollution measurements and clean-up; Oil, gas and mine exploration; offshore platform/pipeline construction and maintenance.
Military	Port, harbour, and coastal surveillance patrolling; search and rescue; anti-terrorism force protection; remote weapon platform.

A complete overview of ASV and USV projects based on the state of the art and survey on autonomous navigation [26,27,28] is reported in Table 3.

The projects have been listed, showing their name, a brief description of their main purpose, guidance navigation and control (GNC) main characteristics, production year, and literature reference. In particular, the GNC has been subdivided into three main topics, path-following (PF), obstacle avoidance (OA), and dynamic positioning (DP). The listed projects are very heterogeneous hull shape models. They share the main dimension below of about 15 m.

Table 3: USVs & ASVs projects from 1980s

No.	Name	Purpose	GNC			Year	Ref.
			PF	OA	DP		
1	Dolphin	Bathymetric mapping				1983	29
2	Roboski	Fast training target & port surveillance				1990s	30
3	Owl USVs	Harbour & ship security				1990s	31
4	MIMIR	Shallow water search and survey				1990s	32
5	Artemis	Bathymetry sampling	X			1993	33
6	Tito Neri	ASV experimental benchmark			X	1993	34; 35
7	Aces	Oceanographic data sampling	X			1997	36
8	SCOUT	Acoustic fish tracking	X			1998	29; 37
9	MESSIN	Water ecological sampling				1998	38
10	AutoCat	Hydrographic surveying				1998	39
11	Barracuda	Sea-surface target system				2000s	40
12	FENRIR	Multipurpose shallow water operations				2000s	41
13	SWIMS	Mine sweeping				2000s	41
14	Spartan Scout	Port surveillance				2001	29
15	SeaFox	Maritime security operations				2003	42
16	USSV-HTF	Towing various sensors and effectors				2003	31
17	Protector	Reconnaissance and counter-mine	X			2003	43
18	SESAMO	Environmental sampling				2004	44
19	DELFIM and DELFIMx	Oceanographic sampling	X			2004	45; 46
20	UMV series	Ocean and atmosphere exploration				2004	40

No.	Name	Purpose	GNC			Year	Ref.
			PF	OA	DP		
21	CS Saucer	ASV experimental benchmark	X			2004	47
22	Seastar	Port, coastal survey and reconnaissance				2005	48
23	Stingray	Homeland security and coastguard				2005	40
24	WASP	Bathymetric mapping				2005	49
25	Basil and Basil II	Offshore pipelines survey				2005	40
26	MiniVAMP	Remote survey of offshore pipelines				2005	40
27	OASIS	Ocean observing platform	X		X	2005	50
29	SEADOO Challenger 2000	Military patrolling	X	X		2005	51; 52
30	HUSCy	Hydrographic survey				2005	29
31	Proto series	Water quality monitoring sailboat	Heading Following			2005	53
32	WaveGlider	Data sampling	X		X	2005	54
33	ROSS	Oceanographic sampling				2006	55
34	ROAZ and ROAZ II	Search and rescue	Image processing			2006	56
35	Swordfish	Environmental survey	X			2006	57
36	ASV MUN	ASV Scientific Benchmark				2007	58
37	Inspector	Surveillance and reconnaissance				2007	48
38	Circe	USV experimental Benchmark				2007	59
39	Zarco	Hydrologic survey	X			2007	60
40	Tianxiang One	Meteorological survey				2008	61
41	Kaasbøll	GNC benchmark				2008	62
42	Viknes	Multi-purpose benchmark				2008	62

No.	Name	Purpose	GNC			Year	Ref.
			PF	OA	DP		
43	Mariner	High-speed surveillance				2008	62
44	ALANIS	Survey	Veichle following			2008	63
45	AVALON	Autonomous sailing vessles	X			2009	64
46	Charlie	Environmental sampling and survey	X			2009	65; 66
47	SeaWASP	Water mapping				2009	67
48	Ensieta	USV experimental benchmark sailboat	Head Following			2009	68
49	USV-ZhengHe 101	Collecting inshore marine data				2010	48
50	USNA	Sailboat for monitoring and oceanographic research				2010	69
51	Piranha	Reconnaissance				2010	70
52	SailBuoy	Ocean environment monitoring	X			2012	71
53	Lizhbeth	Inland water monitoring	X			2012	72
54	Springer	USV experimental benchmark	X			2012	73; 74
55	CaRoLIME	USV experimental benchmark				2012	75
56	Aurora	ASV experimental benchmark				2012	76
57	WAM-V series	Marine surveys	X			2012	77; 78
58	ASV Roboat	Sailboat for sea-water envioronment sampling				2012	79
59	VAIMOS	Sailboat for oceanographic measurements	X			2013	80
60	ASV SMU	Environment monitoring and hydrologic survey				2013	81

No.	Name	Purpose	GNC			Year	Ref.
			PF	OA	DP		
61	PROPAGATOR series	ASV experimental benchmark	X			2013	82; 83
62	CART and Trimaran	Acoustic characterization of the seafloor				2014	84
63	C-Series	ASV experimental benchmark	X	X		2014	85; 86
64	SCOAP	Environment monitoring and hydrologic survey	X			2014	87
65	CRW	Water quality monitoring	X			2014	88
66	A-TRIMA G1 and G2	Sailboat experimental platform	X			2014	89; 90
67	WUT-I	Underactuated surface vessels	X	X		2014	91
68	ASAROME	Sailboat for environmental monitoring	X	X		2015	92
69	MAINAMI	Scientific investigation and explorations of seabed mineral resources	X			2015	93
70	Seabax	USV Scientific Benchmark	QR-code recognition			2015	94
71	ASV Prototype	USV Scientific benchmark	Sets of commands			2015	95
72	ASV RMUTT	Multipurpose data collecting	X			2015	96
73	N-Boat	Ocean monitoring sailboat	X			2015	97
74	Delfia-1 series	ASV Scientific benchmark	X	X	X	2016	98
75	ERON	USV sampling and monitoring	X			2016	99
76	Dolphin I	USV experimental benchmark	Heading Control			2016	100
77	MARV	Hydrologic research	X			2016	101

No.	Name	Purpose	GNC			Year	Ref.
			PF	OA	DP		
78	DH-01	USV experimental benchmark				2016	102
79	WAM-V Series	USV experimental benchmark	X		X	2016	103; 104
80	ROBOAT AMS	Autonomous floating vessels in metropolitan areas	X	X		2017	105
81	Barlavento	Sailoboat for Ocean Monitoring	X			2017	106
82	Halycon	ASV Scientific benchmark	X			2017	107
83	Morvarid	Energy system				2018	108
84	SWAMP	Shallow water navigation	X	X		2019	109
85	USV TU	USV experimental benchmark	X	X		2020	110
86	VTec S-III	USV experimental benchmark	X	X		2020	111
87	MF-USV	Monitoring and cleaning water	X	X		2021	112

It is essential to underline that despite being a considerable number, the listed projects refer only to projects present in scientific literature, that is, published. Many other projects have not been included because they are not present in the literature, for example, military vehicles covered by military secrecy or projects of small private companies active in recent years.

1.5 Industrial State of Art

This section shows the most ambitious projects that explicitly have the achievement of autonomous navigation as a primary objective. Unsurprisingly, these projects belong to large corporations, international bodies and classification registers.

Indeed, as a long-term sustainability approach to shipping, a research project co-founded by the European Commission called MUNIN (Maritime Navigation through Intelligence in Networks) had the task of developing a concept for

unmanned and autonomous merchant vessels and investigating the feasibility during the deep-sea voyage [113]. The study has been conducted taking into account that the more likely scenario shortly is the simultaneous operation of manned and unmanned vessels on the oceans and researching the autonomous vehicle impact would have on the existing international legal framework of shipping. Therefore, the research project budget was 3.8 mln EUR to study the autonomous topic's legal, economic, and technical aspects.

Meanwhile, concerning the industrial sector, another crucial research project has been conducted by Rolls-Royce, named AAWA (Advanced Autonomous Waterborne Applications Initiative). The research budget was 6.6 mln EUR, and the aim was to study the specification and preliminary designs for the next generation of ships. Moreover, to underline the importance of autonomous navigation being considered for the company, the first sentence of the technical report whitepaper [114] has been reported: "Autonomous shipping is the future of the maritime industry. As disruptive as the smartphone, the smart ship will revolutionise the landscape of ship design and operations." Mikael Makinen, President Rolls-Royce Marine. The MUNIN and AAWA projects have already been finished (in 2015 and 2017, respectively).

Indeed, Rolls-Royce and Finferries started the collaboration SVAN (Safer Vessel with Autonomous Navigation) [115] to develop and build an autonomous ship based on the AAWA project knowledge. Furthermore, in 2018, navigation was successfully demonstrated aboard Falco, "the world's first fully autonomous ferry" in Finland [116]. During the demonstration, Falco, 53.8-metre double-ended car ferry, conducted the voyage under fully autonomous control. The vessel detected objects utilising sensor fusion and artificial intelligence and conducted collision avoidance. In addition, also automatic berthing was carried out. Furthermore, all the navigation was conducted without any human intervention by the crew.

Another important autonomous shipping project EU funded started in 2019, AUTOSHIP – Horizon 2020 [117], aims to speed up the transition towards the next generation of autonomous ships in the EU by means of an increase in coastal short-sea and inland waterways shipping to reduce road freight transport. The project has a consortium composed of several partners, including Bureau Veritas and Kongsberg (which acquired Rolls-Royce Commercial Marine in 2019). The project aims to build and operate two different autonomous vessels, demonstrating their operative capabilities in short sea shipping and inland waterways scenarios, focusing on goods mobility.

In cooperation with Yara, Kongsberg, active in autonomous navigation, is working on the "world's first fully electric and autonomous container vessel with zero emissions" called Yara Birkeland [118]. The aim is to obtain a ship able to be manned by a remote position and fully autonomous, equipped with electrical propulsion, battery and control systems used for coastal navigation along with the Norwegian coast. On November 18, 2021, Yara Birkeland took its first manned trip to Oslo before it was put into operation. Nowadays, it has started a two-year trial to become autonomous and certified as an autonomous, fully electric container vessel.

Classification society DNV-GL conducts another similar project regarding unmanned, zero-emission, short-sea vessel navigation. The project is named ReVolt and aims to develop a 60 metres long fully battery-powered autonomous vessel. For the purpose of testing the autonomous capabilities of ReVolt, a 1:20 scaled model has been built thanks to a collaboration with the Norwegian University of Science and Technology (NTNU) [119].

This great interest from Norway has resulted in the concession of a large area of Trondheimsfjord designated as an official test bed for autonomous trials. As a result, Trondheimsfjorden Test Area was established in 2016 as the world's first test area for autonomous ships to transform from traditional to autonomous shipping [120]. At the head of this project, SINTEF, Norway's largest research institute.

Another important site for the autonomous navigation tests was created in the Great Lakes region in USA and Canada in the US waters area, called Marine Autonomy Research Site (MARS) [121]. Indeed, the Smart Ships Coalition announced a Great Lakes testbed area open to all companies, research institutions, and government agencies to test autonomous surface and sub-surface vehicles and related technologies.

The Oceanalpha announcement in Zhuhai represents another important event in China, on December 3rd, 2019 [122]. Oceanalpha is an unmanned surface vessel company (USV). It announced that its parent company Yunzhou Intelligent Technology Co., in partnership with the Wuhan University of Technology, the China Classification Society (CCS), and the Zhuhai city government, created the test site for autonomous vehicles called "Wanshan Unmanned Test Site". The testing site for autonomous navigation is the largest in the world and the first in Asia. The test site is located in the Wanshan Islands and covers an area of 771 square kilometres. The test field would allow the testing of technologies suitable for the achievement of autonomous navigation,

such as the prevention of obstacles (collision avoidance) and the pursuit of a route (track keeping).

Another significant and ambitious project based in the East is supported by The Nippon Foundation MEGURI, which aims to promote the development of completely autonomous ships. In particular, on 2022 January 17, the world's first fully autonomous ship navigation system on a 222-meters car ferry was carried out, conducted on the Iyonada Sea from Shinmoji, Kitakyushu City. The ferry is able to autonomous port berthing and unberthing using turning and reversing movements and high-speed navigation of up to 26 knots. In addition, the advanced, fully autonomous operation system includes sensors to detect other ships using infrared cameras, a remote engine monitoring system, and a sophisticated cyber security system. [123]

As shown, the interest in achieving autonomous navigation is widespread worldwide. As a result, a consortium called INAS (International Network for Autonomous Ships) was created. The INAS members are research institutes for each nation interested in the theme of autonomous navigation [124]. From these numerous projects, a very high interest in autonomous navigation, especially for navigation in restricted waters to reduce the transport of goods by road, emerges. Indeed, most of the projects concern coastal applications in northern Europe, where transport by sea can drastically reduce the delivery time compared to road transport due to the morphology of the territory.

1.6 Autonomous Vessels Taxonomy

From the review previously shown, there is a lot of ambiguity and confusion regarding the terms of autonomous vehicles. In particular, many terms, hereinafter an example of terms used ASV, USV, ASC (autonomous surface craft), MASS (Maritime Autonomous Surface Ships) and AUSV (armed unmanned surface vehicle), very often are used as synonyms when they are not, in particular ASV and USV. Indeed, an unmanned surface vehicle, USV, does not necessarily mean that a vehicle is capable of acting without human intervention. Usually, the correct use of the USV term is to represent an unmanned vehicle commanded by a remote station or acting automatic instruction a priori imposed. Contrarily, the term ASV focuses not on human beings' presence or not on board but on the ability to perform a navigation task autonomously. Obviously, an ASV could be unmanned, but this characteristic

does not have to change the term to describe it. In general, an ASV can be unmanned as a function of its purpose, but the contrary is not valid. Indeed, a USV cannot be an ASV.

In general, an ASV must have the situational awareness capability to the knowledge of the surrounding environment. Indeed, a vehicle to be categorised as autonomous must have the following technical characteristics, indispensable for autonomously accomplishing the task: automatic route generation and path planning control, object detection capability and collision avoidance capability, and autonomous decision-making system [125].

1.7 Autonomous Vessels Regulations

Initially, in 1978 [126], the definition of autonomy level pioneer was the Sheridan's classification. Sheridan has defined ten levels of interaction between human beings and autonomous systems. As shown in Table xxx, the higher levels represent increased computer autonomy over human action.

Table 4: Sheridan's classification

Levels	Description
1	The computer offers no assistance: humans must take all decisions and actions.
2	The computer offers a complete set of decision/action alternatives
3	Computer narrows the selection down to a few
4	The computer suggests one alternative
5	The computer executes a suggestion if the human approve
6	The computer allows humans a restricted time to veto before automatic execution
7	The computer executes automatically, then necessarily informs human
8	The computer informs humans only if asked
9	The computer informs humans only if it (the computer) decides to
10	The computer decides everything acts autonomously, ignoring the humans

The levels are based on the classic four control concepts:

- Information acquisition: sensing and acquiring input data through the continuous monitoring of the environment around or through a communication channel.
- Information analysis: elaborating received data, creating predictive algorithms or integrating different input variables.
- Decision and action selection: evaluating different proposals, selecting decision and action.
- Action implementation: receiving the inputs from the decision made and having the goal to execute the actions.

Each of these functions can be automated to differing degrees or many levels.

Nowadays, in February 2017, during the Maritime Safety Committee (MSC) 98th session, IMO (International Maritime Organization) started the process to create a regulatory framework for MASS and the interaction among the manned ships within the existing IMO rules [127]. In particular, MASS could be subdivided into different autonomous classes with different impacts regarding the legislation and the operativity:

Table 5: 98th MSC session MASS subdivision [128]

Type	Description
Autonomy Assisted Bridge (AAB)	The ship bridge is always manned, and the crew can immediately intervene in ongoing functions. This will not generally need any special regulatory measures except perhaps performance standards for new functions on the bridge.
Periodically Unmanned Bridge (PUB)	The ship can operate without a crew on the bridge for limited periods. The crew is on board the ship and can be called to the bridge in case of problems.
Periodically Unmanned Ship (PUS)	The ship operates without a bridge crew on board for extended periods.
Continuously Unmanned Ship (CUS)	The ship is designed for unmanned operation of the bridge at all times, except perhaps during special emergencies.

Following the indications of IMO, the major classification societies wrote their guidelines regarding autonomous navigation: Lloyd's Register (LR Code for Unmanned Marine System, 2017) [129], Bureau Veritas (Guidelines for Autonomous Shipping – NI641 R01, 2019) [130], and Det Norske Veritas Germanischer Lloyd (Autonomous and remotely operated ships - DNVGL-CG-0264, 2018) [131]. In particular, classification societies reported their levels of navigation automation.

Table 6: LR, Levels of navigation autonomy [129]

Autonomy level		Description of autonomy level
AL0	Manual	All action and decision-making performed manually (n.b. systems may have level of autonomy, with Human in/ on the loop.), i.e. human controls all actions.
AL1	On-board Decision Support	All actions taken by human Operator, but decision support tool can present options or otherwise influence the actions chosen. Data is provided by systems on board.
AL2	On & Off-board Decision Support	All actions taken by human Operator, but decision support tool can present options or otherwise influence the actions chosen. Data may be provided by systems on or off-board.
AL3	Active' Human in the loop	Decisions and actions are performed with human supervision. Data may be provided by systems on or off-board.
AL4	Human on the loop, Operator/ Supervisory	Decisions and actions are performed autonomously with human supervision. High impact decisions are implemented in a way to give human Operators the opportunity to intercede and over-ride.
AL5	Fully autonomous	Rarely supervised operation where decisions are entirely made and actioned by the system.
AL6	Fully autonomous	Unsupervised operation where decisions are entirely made and actioned by the system during the mission.

Table 7: BV, Levels of navigation autonomy [130]

Degree of Automation		Manned	Definition	Information Acquisition	Information Analysis	Authority to make decisions	Action initialised by
A0	Human operated	Yes	Automated or manual operations are under human control. Human makes all decisions and controls all functions	System Human	Human	Human	Human
A1	Human Directed	Yes/No	Decision support: system suggests actions. Human makes decisions and actions.	System	System Human	Human	Human
A2	Human Delegated	Yes/No	System invokes functions. Human must confirm decisions. Human can reject decisions.	System	System	Human	System
A3	Human Supervised	Yes/No	System invokes functions without waiting for human reaction. System is not expecting confirmation. Human is always informed of the decisions and actions.	System	System	System	System
A4	Full Automation	Yes/No	System invokes functions without informing the human, except in case of emergency. System is not expecting confirmation. Human is informed only in case of emergency.	System	System	System	System

Table 8 DNV-GL, Levels of navigation autonomy [131]

Autonomy level	Description of autonomy level
M	Manually operated function.
DS	System decision supported function.
DSE	System decision supported function with conditional system execution capabilities (human in the loop, required acknowledgement by human before execution).
SC	Self controlled function (the system will execute the operation, but the human is able to override the action. Sometimes referred to as 'human on the loop).
A	Autonomous function (the system will execute the function, normally without the possibility for a human to intervene on the functional level).

Eventually, the autonomous ship study and regulatory framework in order to establish what is meant when the term MASS is used started in the MSC 98th session and ended with the MSC 100th session [132]; as a result, IMO established new levels with specific characteristics that the ship must possess.

Table 9. 100th MSC session MASS subdivision

Type	Description
Degree one	Ship with automated processes and decision support: Seafarers are on board to operate and control shipboard systems and functions. Some operations may be automated and at times be unsupervised but with seafarers on board ready to take control.
Degree two	Remotely controlled ship with seafarers on board: The ship is controlled and operated from another location. Seafarers are available on board to take control and to operate the shipboard systems and functions.

Degree three	Remotely controlled ship without seafarers on board: The ship is controlled and operated from another location. There are no seafarers on board.
Degree four	Fully autonomous ship: The operating system of the ship is able to make decisions and determine actions by itself.

Despite this intense interest in the autonomous navigation sector and its achievement, the current scenario shows a lack of homogeneity, an unclear regulatory framework where each entity proposes its own regulatory framework similar to the others but not perfectly superimposable. Furthermore, at the moment, the IMO prohibits navigation in deep water, allowing it only in coastal areas. This scenario potentially slows the development of autonomous boats from a legal, administrative and insurance point of view. On the other hand, since the autonomous ship is an objective that has never yet been achieved, it is expected that there has been confusion in recent years. A defined regulatory framework will be possible only when the first autonomous will be built and tested the ship's potential in terms of safety and reliability.

Chapter 2

2.1 Decision Process Structures

As shown in the previous chapter, there is a great deal of interest in autonomous navigation due to the promises of increased navigation safety guaranteed using this now mature and available technology.

Before discussing a possible structure and any differences between frameworks regarding the presence of a human being on board, delegated to make decisions on the route to follow, with respect to a completely autonomous ship, it is essential to define what is meant by Guidance Navigation and Control (GNC) by means of a brief description of the parts that make it up the system.

Guidance refers to determining the desired navigation path (the "trajectory"). The path is information as a function of the task of the vehicle, from the actual location to the desired position, potential obstacles, desired changes in velocity, rotation, and acceleration for following that path or achieving the task.

Navigation refers to the determination, at a given time, of the vehicle's state. Knowing the vehicle's state means knowing several characteristics of the vehicle, e.g. location and velocity or/and the surrounding environment vehicle, e.g. other ships or fixed obstacles. The knowledge of this data is guaranteed by sensors installed onboard.

Control refers to the manipulation of the forces required to execute guidance commands while maintaining vehicle stability.

Achieving full autonomous navigation is a very ambitious and challenging task. Nevertheless, it is conceivable that the studies carried out so far could contribute to the development of an increasingly safe and efficient decision support system obtaining a crew's decision-making on the bridge. Indeed, studies and research focused on new guidance logics such as collision avoidance can be used as a source of additional information to the commander to modify the original route to prevent a collision by route changing advice. In the following have been reported the architecture of a potential framework for manned and autonomous ships, in

Figure 1 and Figure 2, respectively. The proposed workflow is based on scientific literature [133, 134].

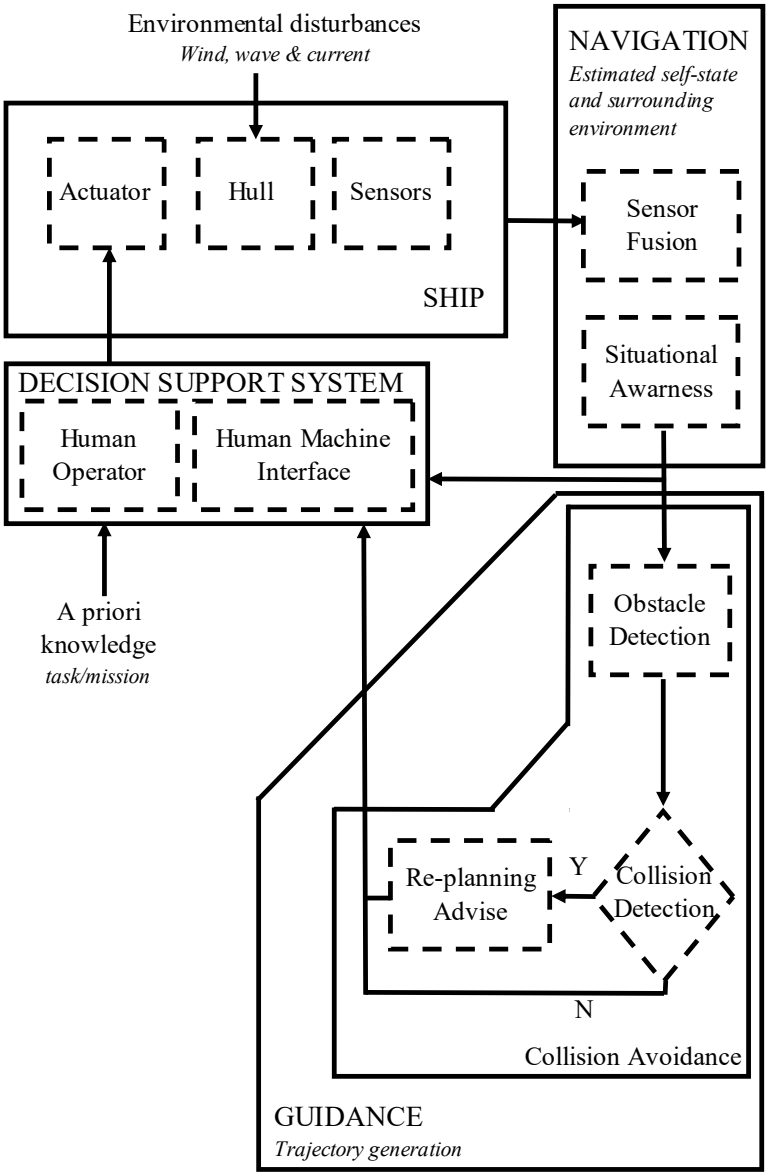

Figure 1. The decision process in a manned ship

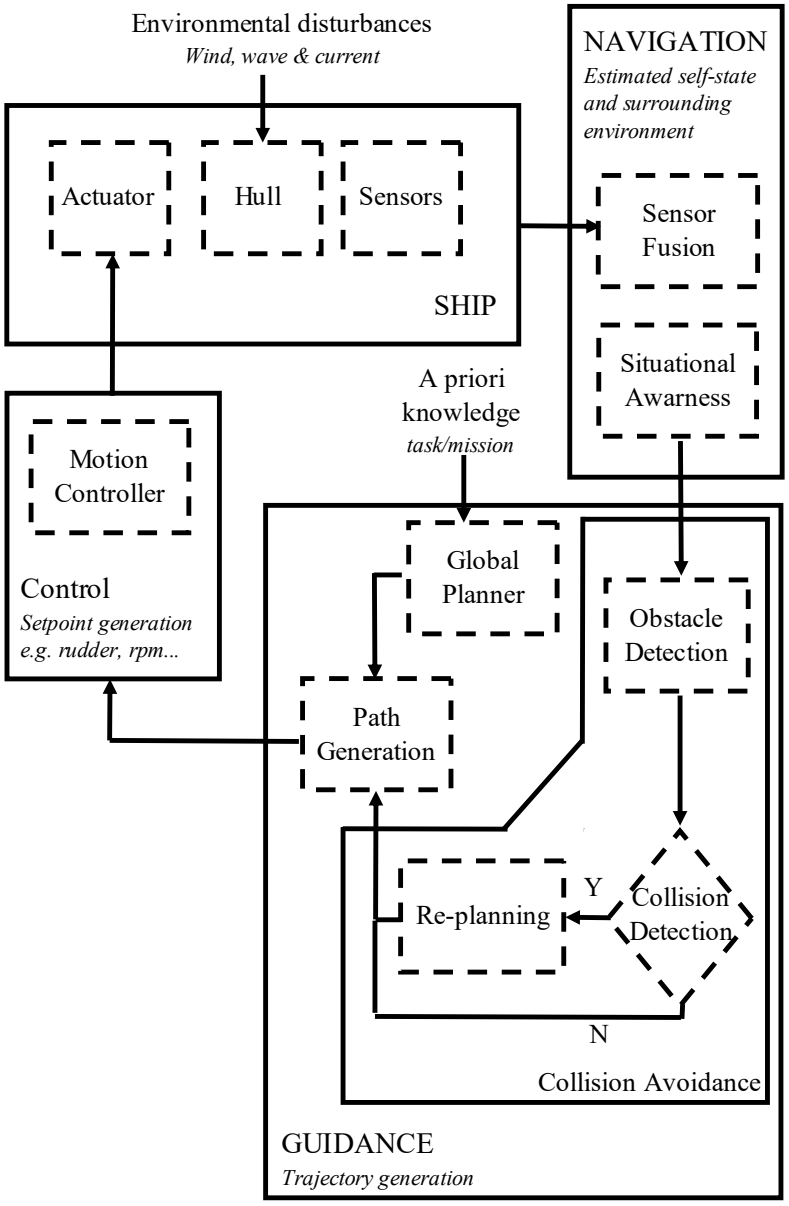

Figure 2. The decision process in autonomous ship

The decision-making process for the manned ship, shown in

Figure 1, is composed of the ship block, the Navigation system, the Collision Avoidance (CA) System and the Decision Support System. The subsets communicate with each other respecting a well-defined hierarchy. The ship block is characterised by three main parts, the actuators, the hull and the sensors. The actuators have the task of exerting and directing the thrusts in order to obtain the desired manoeuvre. The hull is the rigid body on which environmental forces act. The sensors gather data on the ship's state and about the surrounding environment. These can be RADAR (RAdio Detection And Ranging), AIS (Automatic Identification System), GNNS (Global Navigation Satellite Systems), torque transducers, revolution counter, etc. The collected sensor data is used as input in the Navigation block, which combines the collected information according to a hierarchy of importance to obtain specific information on the self-state of the ship and the surrounding environment. The output of the Navigation block can be used immediately as visual or audible feedback to the operator on the bridge, or the CA system can further process it. Indeed, the CA system has the task of verifying that the own current route of the ship is not in conflict with obstacles detected by the sensors. In the event of a conflict, the CA provides the operator with valuable information in order to resolve the conflict. For example, this can be the change in heading or rudder angle. Eventually, the human operator, aware of the mission he must carry out, can decide the route based on the decision support obtained.

The proposed framework without the human factor, shown in Figure 2, has an additional set of instructions. In particular, the guidance block has the path generation and the global planner. The path generation system aims to produce and upload, every time step, a safe navigation path. It is obtained by means of the knowledge of the obstacle presence and the global navigation path, evaluated by the global planner by using the information regarding the navigation task to achieve. The output of the guidance system flows in the motion controller that is programmed to evaluate the magnitude and direction of the thrusts as a function of the requested displacement and ship's speed (different control logics request different ship's data). Eventually, the motion controller sends the requested signal to the actuator to close the control loop.

It should be emphasised that the frameworks exposed and discussed represent two extremes where for example, navigation with a human operator excludes a control block, and when there is a Control part, the human operator is completely removed. Indeed, in a real scenario, it is straightforward that hybrid

frameworks can occur in which tasks are entrusted to the control system due to the physiological limits of the human operator, who would not have the capabilities in terms of reactions or sensitivity to perform the desired manoeuvre. In these hybrid systems, some manoeuvres are carried out autonomously, and the operator has the task of supervising the execution of the manoeuvre and possibly, in case of system failure, can intervene by overriding the system.

In this context, the studies carried out and shown in the following chapters refer to two distinct framework topics: Control and Collision Avoidance. In particular, the dynamic positioning system obtained by means of a tug dynamic simulator and sensor-based collision detection and multi-obstacle tracking have been studied and developed. For such reasons, the detailed descriptions of the aforementioned automatic control logics have been reported in the following.

2.1.1 Dynamic Positioning system

The history of Dynamic Positioning (DP) began in the 1960s for offshore drilling applications. In particular, the first ship equipped with a DP system was a drillship – Cuss 1 – in 1961 [135], since DP systems have been one crucial interest topic for the oil industry [136]. Indeed, from its first applications, DP has proved to be a fundamental tool for equipping ships able to work in the offshore environment, operating in blue water, where the other station-keeping options (jack-up barge & anchoring) were too expensive or unsuitable.

Technology progress has improved the DP systems from the first applications, such as accuracy, thanks to the global navigation satellite systems (GNSS). Furthermore, more precise and less expensive technologies nowadays available [137] lead to the use of DP systems for other maritime fields. Moreover, in the last ten years, due to the strong push for the complete automation of land and sea vehicles, research studies related to DP systems are solving autonomous navigation challenges at very low-speed.

Undeniably, autonomous navigation has been a hot topic in recent years as a solution to reduce gas emissions, optimising fuel consumption; or improve navigation safety by avoiding human errors [138]. Indeed, many industrial and University projects have been developed that focus on achieving it. For instance, some model-based and experimental studies were conducted to analyse the controller behaviour [139, 140]. Model-based design is one of the most widely used approaches to designing the DP controller structure [141,

142, 143]. Indeed, it has the advantage to emulate real system behaviour. On the other hand, it requires the knowledge of a multitude of vessel parameters that increases with the degrees of freedom of the dynamic simulator that is used. These parameters are not always available, and for such a reason, other approaches should be considered [144, 145].

The DP systems control logic structure is a complex subject based on automatic ship motion control. For such a reason, it requires the integration of several subsystems and a thorough knowledge of their mutual interactions. It is composed of three main sub-sets: the controller, the force allocation logic (FAL), and the thrust allocation logic (TAL). The controller and the thrust allocation development are the kernels of a DP systems design; they can be developed in several manners with profoundly different approaches [146, 147]. The case study, used to validate the proposed idea, refers to a fully actuated tug testing model equipped with two azimuth thrusters and one bow-thruster. The structure of the developed DP system, the purpose of the research, and the results are shown and critically discussed in the following chapter, in particular Chapter IV.

2.1.2 Collision Detection and Avoidance

The need to preserve human life and the environment's health is crucial. For such a reason, the collision avoidance system has been deeply studied in scientific literature. Indeed, the study and use of the Collision Avoidance system is not a new topic in the marine field. The first assessment of collision avoidance dates back to 1960 [148].

While the task of avoiding collisions looks simple, in particular in a marine environment, accomplishing this task is not. Furthermore, despite the automotive or aircraft sector, the ship can be seen as a single model, a prototype, as it is complicated to standardise the product. This difficulty implies that as the ship varies, there will be a variation in the actuators and the sensors installed onboard. For this reason, numerous different approaches to the development of the Collision Avoidance System can be found in the literature. Indeed, there are different approaches based on different sensors installed onboard. Generally, those always present onboard RADAR and AIS are used.

Most of the marine applications are based on classic heuristic algorithms, reducing computational time, such as genetic algorithms (GA) [149, 150, 151]. Also, iterative methods set up the minimum rudder angle to avoid a collision

[152]. In addition, also potential field methods are also widely used for various unmanned vehicles [153, 154, 155]. Potential field methods are based on the concept of associating a potential for every element present in the scenario. Sources are associated with obstacles, while the target is modelled as a sink. Indeed, the trajectory is found by solving the minimum potential path. Eventually, some of the most recent works are based on random sampling algorithms, which conjugate a relative simplicity and flexibility with great computational performances. The random sampling philosophy inspired a considerable number of different algorithms [156, 157].

A significant number of the papers presented in the literature review deal with the collision avoidance problem does not consider compliance with the regulations defined by the International Maritime Organisation (IMO). This aspect is true, but more and more publications have dealt with COLREG within the collision avoidance problem in the last three years [158, 159, 160, 161]. In particular, when the case studies are on large ships, COLREG, or the Convention of International Regulations for Preventing Collisions at Sea [162], which includes several rules and regulations for the proper conduction of marine vehicles for safe navigation.

As shown before, the input most used for the CA system is represented by AIS and RADAR data. However, in a real scenario, in which there are surface vehicles of very different dimensions, ranging from the 300-meter container ship to the small 5-meter pleasure vessel, it is possible to demarcate the various types of tools used. In particular, instruments such as AIS (mandatory on ships with gross tonnage over 300 tons and on all passenger ships) and RADAR can be considered reliable and usable instruments for long distances, as they have an operating range above ten nautical miles. However, these instruments represent strong limits in this context, such as the failure to detect an obstacle not equipped with an AIS system or an obstacle that does not have a magnetic signature (small pleasure boat). Therefore, it is conceivable to use other instruments to detect any obstacle in a real scenario for these cases. These can be LiDAR (Light Detection and Ranging) or Cameras (also infrared cams for night detection or in case of adverse weather conditions). In this case, the use of these technologies can be made for a different range of applications, in the order of 100 meters. Hence, in a real scenario, assuming equipping a ship 100 meters long with these devices, it can be assumed that the obstacle detection can be a function of the obstacle distance or to use the different sensors in different scenarios, for instance, when navigating away from the coast use AIS and RADAR while when navigating near the coast or in a harbour scenario, use LiDAR and Cameras.

In this context, the research study has been carried out by means of a tug testing model of 1m length unequipped of these sensors. For such a reason, the purpose of research has been to test and develop a collision detection based on LiDAR able to detect potential obstacles and track them. In this case, developing an obstacle tracking system based on a LiDAR sensor means working in an operating range of 100 ship lengths, so only in the case of a small ship, it is possible to use this type of sensor for the detection of obstacles in close to the ship and for long distances (100 ship lengths). In Chapter V, the sensor-based obstacle detection developed framework and the tracking results have been shown and discussed.

Chapter 3

3.1 Lab Description

The laboratory was assembled during the PhD period. This includes different instruments, including a remote controllable and self-propelled ship model, a video-tracking system used to know the model's position inside the tank, different sensors purchased in order to equip the boat with the capability of situational awareness, and finally, two small and medium-sized tanks in which to carry out the experimental tests.

3.1.1 Available Sensors

Initially, the sensors selected to allow the ship to assess the distance from any obstacles were ultrasonic. Specifically, the HC-SR04 modules were used, with which it is possible to make distance measurements. According to the radar principle, an ultrasonic pulse can measure the “small” distances (the datasheets declare an operating range between 2 - 400 cm) acceptably accurate. An ultrasonic transducer emits a few pulses of a signal with a frequency of 40 kHz. This signal is reflected on an object in the aforementioned distance range and with a minimum surface area of 0.5 m^2. The reflected signal is captured by the second transducer and amplified. Therefore, measuring the time between sending and receiving pulses can accurately measure the distance from the transducers to the object. The speed of sound in air at sea level at 0 ° C and 0% relative humidity is 331.4 m/s. The distance is evaluated as the measured signal return time times (time between sending and receiving divided by 2) speed of sound in the air.

$$dist. = \frac{t_{sign.}}{2}\, v_{sound.air} \tag{1}$$

Furthermore, knowing that the operating conditions in which the experimental tests will be carried out do not correspond to the reference values at which the speed of air is given, to increase the accuracy of the distance obtained, it is necessary to take into account the local temperature and humidity of the air. The following relation gives the speed of sound:

$$v_{sound.air} = 331{,}4 + [0{,}606\ T] + [0{,}0124\ TH] \quad (2)$$

where: *T* is the air temperature in °C and *TH* is the relative humidity in %.

In order to obtain the speed of air, the DHT22 module was used. The sensor is capable of reading the instantaneous air temperature and relative humidity values. The manufacturer provides the following technical characteristics:

- Operating range; Relative humidity 0-100% RH; Temperature -40 ~ 80 Celsius;
- Error; Humidity +-2% RH (Max + - 5% RH); Temperature <+ - 0.5 Celsius;
- Sensitivity; Humidity 0.1% RH; Temperature 0.1 Celsius;

Moreover, modules (ACS712 of 20 A) were adopted to know the voltage and amperage that motor controllers send to the actuators to work. The ACS712 provides economical and precise AC or DC sensing solutions in industrial, commercial, and communications systems. Indeed, typical applications include motor control and load detection.

Eventually, a GPS and IMU are available. In particular, the MTi-G-710 is a GNSS/INS system capable of providing information relating to position and speed (integrated GPS and GLONASS receiver) and movements in space (Roll, Pitch and Yaw) by combining the use of the merging algorithm of the XKF data, the innovative XEE filter (Xsens Estimation Engine) and the raw data coming from the internal sensors (accelerations - angular velocities - variation of the magnetic field). The proprietary software provides orientation data in real-time with high accuracy. Moreover, the libraries allow users to easily integrate sensory data with custom software or with existing analysis applications such as MATLAB, FlexPro or LabVIEW.

The system is IP67 (complete dust protection and protected from temporary immersion), with a USB and RS232 interface.

Product overview

		MTi-G-710 GNSS/INS
Calibrated Sensor Data		yes
Roll/pitch	Static	0.2°
	Dynamic	0.3°
Yaw	In homogenous magnetic field	1.0°
Position and velocity		
Horizontal position	1σ STD (SBAS)	1.0 m
Vertical position	1σ STD (SBAS, baro)	2.0 m
Velocity accuracy	1σ RMS	0.05 m/s

All above specifications based on typical application scenarios

Figure 3. MTi-G-710 spec techs

In recent years, LiDAR-type instrumentation has become increasingly frequent due to price reduction and more precise data acquisition. LiDAR uses ultraviolet to acquire information regarding the environment and target a wide range of materials, including non-metallic objects. The operation is similar to the best-known RADAR. The object distance is asses by measuring the time elapsed between the emission of the pulse and the reception of the backscattered signal. Therefore, the interest in this technology by the autonomous vehicles research fields grows more and more, especially in the automotive sector to achieve obstacle detection.

A typical layout of a LiDAR device includes different principal systems:

- Laser, whose task is to generate the light beam pulse.
- Scanner and optics system; that mechanically creates the scan and collects the return signal.
- Receiver and electronics system; that exploit optical sensor to acquire the return signal.

Many types of LiDAR are available, differing on the path of the laser beam, wavelength, optical scanner technology, field of view (FOV), acquisition range and intended use. A 360° FOV laterally oriented rotating LiDAR, optimized for short-range acquisition, is often adopted in automotive obstacle detection applications. These types of LiDAR generally work, adopting a divergent spinning beam of the laser channel. A 360° FOV laterally oriented rotating LiDAR, optimized for short-range acquisition, is often adopted in automotive obstacle detection applications.

The LiDAR model used for the experimental campaign is HESAI PandarXT LiDAR. It is a rotating multi-laser beam type. It provides 32 equally spaced channels on vertical axes. It emits in the infrared spectrum and with tunable

rotation (5-10-20) [Hz] speed defining different resolutions (in the horizontal plane), while the vertical resolution is of 1-degree. The declared functioning range is 120m. The dimension and laser beam cone are reported in Figure 4, while the LiDAR's own reference frame has been reported in Figure 5

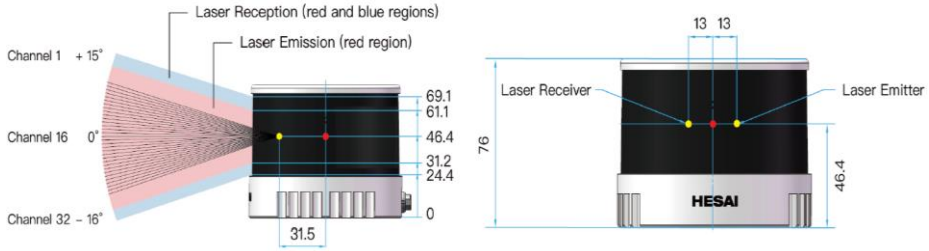

Figure 4. HESAI Pandar XT-32 characteristics (unit, mm)

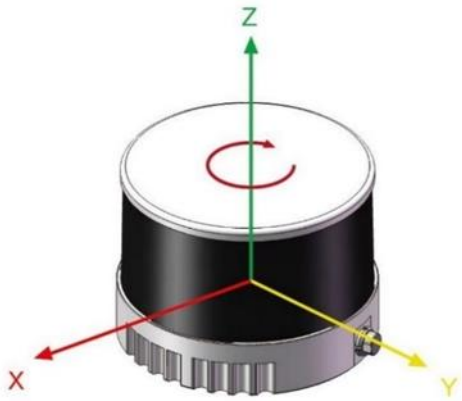

Figure 5. HEASI Pandar XT-32 reference frame

As previously written, the horizontal resolution is related to the rotor's revolutions. In particular, the 5 Hz frame rate guarantees a horizontal resolution of 0.09°. Considering the computational time needed to process a scan, a frame rate greater than 5 Hz does not provide any benefits in terms of time accuracy in a real application, but it implies a poor horizontal resolution; for this reason, a 5 Hz frame rate has been adopted for all the acquisition performed with the HESAI PandarXT LiDAR.

3.1.2 Model Scale Tug

The UNIGE testing model represents a tugboat with a 1:33 scale; TU-Delft provides the original mock-up. The large hull shapes allow the researchers to work efficiently inside of it, facilitating the preparation of the hardware, as there is a large volume that allows easy management of internal hull devices set up. Besides, the hull has excellent seakeeping behaviour to successfully carry out without any waterboarding in future tests in an outdoor environment. This characteristic is fundamental because all hardware components are inside the hull, and the tug's deck does not have a watertight feature. The tugboat model called "Tito Neri" has a length (Loa) equal to 0.97 meters, a maximum width of 0.30 meters and about 13 kg of displacement. It is a completely electric (equipped with a 12V Pb battery pack) self-propelled model thanks to two azimuthal propellers and a bow thruster remotely controlled. The wireless communication is done via the Xbee module mounted on the microprocessor (Arduino) presented onboard. The Arduino installed onboard plays a low-level controller role and communication with the remote console and can be powered with a maximum voltage input of 5 V. This has made it essential to insert a chopper that regulates the voltage between the batteries and the microprocessor, guaranteeing a constant 5V. The communication could also be via cable directly connected to the Arduino board.

The tugboat model propulsion plant is composed of:

- Two azimuth thrusters: one for each shaft-line of the ship, are a configuration of marine propellers placed in pods that can be rotated to any horizontal angle (azimuth) in a range between [-180, +180], making a rudder unnecessary. The type of azimuth thruster present on the model has a duct. It is used to improve the propeller's efficiency in heavy load conditions near the condition of zero speed.
- Two electric motors are coupled with the azimuth propellers by a Z-drive gearbox; dedicated DC drives control DC motors.
- Bow thruster: has a separate electric motor, controlled by its relative DC drive. It aims to improve the tug's manoeuvrability by generating a controllable thrust in the bow part of the hull nearby zero-speed.

The tugboat model propulsion gives the capability to the tug model to be fully actuated in the horizontal plane. In addition, the boat is not only equipped with actuators but also with sensors:

- Two rpm encoders: on the shaft line, they are mounted between the DC motor and the azimuthal component. The information of the revolutions of the main propellers is given by these types of equipment, which allow for closed-loop control through the action of different input parameters.
- Three current sensors were installed downstream of the DC drives. This layout will be used for feedback logic application; indeed, it enables knowing the current absorbed by the DC motors. Moreover, by means of the information of current and voltage is possible to evaluate the DC motor delivered power.
- Four ultrasonic sensors: Through an ultrasonic pulse, it is possible to measure the "small" distances in an acceptably accurate manner. An ultrasonic transducer emits some pulses of a signal with a frequency of 40 kHz. The reflected signal is captured by the second transducer and amplified. By means of measuring the time between sending and receiving pulses, the distance from the transducers to the object can be evaluated, which is useful for auto berthing and collision avoidance application.
- One humidity & temperature sensor: The sound speed in air is used to evaluate the obstacle distance. In order to obtain a better measure of the distance, the humidity and temperature sensor is used to evaluate the sound speed in the air locally. Indeed, sound speed is deeply influenced by air temperature and humidity.
- The superstructure was re-designed in order to perform a video-tracking activity. The new superstructure was projected and 3D printed with 5 (infrared) LED mounting. The particular shape of the superstructure, in particular the position of the LEDs and their relative distances, has been designed to increase the performance of the video-tracking system; for this purpose. As a result, the LEDs have been positioned on different planes, and it is possible to detect the ship's motion at 6 DOF.

The listed sensors are not sufficient for the intended purpose, i.e., equipping the ship with situational awareness capability. For this reason, a LiDAR sensor has been purchased and used as the primary input sensor in order to develop the experimental detection and tracking that represents the first step to obtaining a collision-avoidance system. In addition, an IMU (Inertial Measurement Unit) coupled with a GPS to be installed onboard was selected and purchased. With the IMU and GPS, even in an outdoor environment, it is possible to track the model position and its motions in 6DOF.

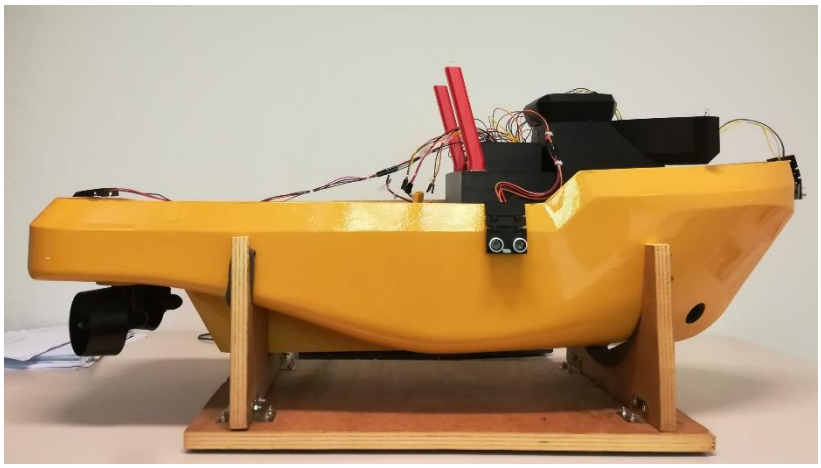

Figure 6. Tito Neri testing model

Moreover, the hydrodynamic characteristics and the lines plan are reported hereinafter:

Table 10: Geometric characteristic of the hull at model scale

$L_{WL}[mm]$	$B_{WL}[mm]$	$T[mm]$	$\nabla[dm^3]$	L/B	B/T
891	301	103	13.28	2.96	2.92
$A_W[dm^2]$	$A_x[dm^2]$	C_b	C_p	C_x	C_{wl}
22.21	2.71	0.48	0.54	0.87	0.82

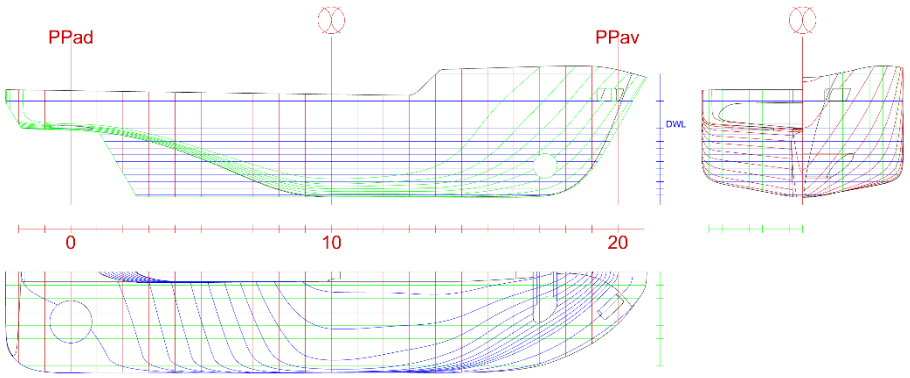

Figure 7. Tito Neri lines plan.

3.1.3 Indoor Localization System

By carrying out the tests in an indoor environment, the choice of positioning tracking via GPS is not possible. It was decided to set up a video-tracking system for such a reason. In summary, the video-tracking system is used to mimic the GPS within a closed space.

A 6-DOF video-tracking system has been implemented, tested, and validated to know the position of the testing model inside the indoor tank. The implementation is necessary to know the instantaneous position of the ship as feedback during the tests. The video-tracking system is able to track infrared (IR) bright spots in a dark room. In particular, the case study concerns a testing model with a predetermined number of fixed points (landmarks) identified by point-like light sources (IR bright LED spots) with the known 3D. The wanted information is the position during the tests carried out within a test area.

First of all, the video-tracking system requires to be calibrated to determine the optical camera parameters. In particular, the calibration of the camera is carried out, assuming the validity of the pin-hole model with distortion. Moreover, it assumes that the camera makes a linear 3D-2D projection of the world observed on an image plane quantized in digital elements (pixels). By means of a 3x3 type K matrix (intrinsic matrix), the optical parameters (e.g. focal length), which start from a generic point (XYZ), produce a pixel with coordinates (u, v).

The linear pin-hole model is then applied to real cameras by introducing a variable set of coefficients capable of modelling the inevitable distortion effects introduced during manufacturing. The general model includes both radial-type effects and tangential-type effects. The general model is able to handle even low-quality commercial cameras (e.g. webcam).

Calibration is usually carried out by shooting planar 2D patterns (e.g. black and with a checkerboard) from different viewing angles by observing the points of the chessboard arranged on a regular 2D grid.

Moreover, the automatic search for LEDs on a generic image was conducted, assuming that they appear as bright regions (spots) of predictable size. A convolution operator (filter) has been defined whose response peaks localize the position of the LEDs. The detector has the classic Laplacian of Gaussian (LoG). It has two parameters: the expected size of the light spot in pixels and the binarization threshold of the image expressed in grey level. The automatic detection procedure returns the image coordinates of all the light spots found,

represented in an Nx2 matrix. Candidates are selected so as to be compatible with some geometric assumptions on the 2D shape of the spot (min/max area, eccentricity, min/max diameter). In the analyzed tested scenes, by adjusting the ambient lighting so that only the spots are visible, the function achieves 100% correct detection, with a false alarm rate close to zero. In this context, false alarms represent false spots due to other light sources, such as water reflection. Since these are practically absent, the function has been parameterized not to have false negatives. If any spurious points remain, they will be removed in the next recognition phase.

The estimation of the relative pose of the model concerning the camera involves calculating the geometric transformation (RT roto-translation matrix), which describes how the camera sees the 3D model in a certain image. The problem is challenging because the bright spots are not indistinguishable from each other, and therefore only through a geometric check it is possible to establish the correct correspondence between the points of the 3D model and the spots observed. It should also be considered that spurious spots may also exist in real ones. The problem was solved by exploiting the fact that the points of the model are few (five bright spots), and the incidence of false spots is very low. Knowing N spots makes it possible to enumerate all the arrangements of 5 elements starting from N and for each of these to establish whether there is a reliable mapping between the 3D model and 2D image - The permutation choice that minimizes the error is the correct one.

Compared to the research conducted on independent images (script detection), the tracking process introduces variants that do not repeat useless calculations and quickly converge on the correct association between light spots and LEDs. Once a valid frame has been found, the processing of the next one is conditioned by launching the search for spots only on five small square regions centred on the positions already calculated. In this way, two results are obtained: a clear speeding up of the search process and a direct association between spot and 3D point.

The result is a process in which each 3D point numbered from 1 to 5 is followed in each sequence frame. The model position is always calculated at each frame, expressed by three translation components and three rotation angles, as shown in Figure 8.

Figure 8. Video-tracking system acquisition

The video tracking system described comprises a FullHD 1920x1080 camera with 2MP resolution and variable focal length. The camera is suspended at 2 meters from the tank, and the field of view is 3x2 meters. The system has a high level of accuracy on the plane. Furthermore, it has an accuracy depending on the field of view. In particular, using the previously set up conditions, the accuracy on the plane is 1 cm for translation and 1/10 of a degree for rotation.

To summarize, the proposed video-tracking system makes it possible to trace the ship's position during the manoeuvres within the tank. The position of the ship data inside the tank represents fundamental data as used as feedback for the control logic. The video-tracking system estimates the pose concerning the model regarding the camera and a fixed reference frame (in the case study, the frame is placed equal to one of the tank corners). As described previously, the problem of the evaluation of the model's rotations and translations is challenged because the light spots onboard the model are among them indistinguishable, and it is therefore only through a geometric verification that it is possible to evaluate the correct correspondence between the known points of the 3D model and the observed spots. In addition, it could also occur that spurious spots can appear in addition to the real ones due to the reflection of the water or other luminous sources. The problem was solved thanks to the high-fidelity level of false spots and the position knowledge of light spots.

3.1.3.1 Superstructure video-tracking system project

As described, the light spots used for position tracking are five. Initially, the ship model had only three light spots available for video tracking. The need to redesign the superstructure was dictated by three identified spots representing the minimum number to accurately identify an object's bright spots moving in space through the available video-tracking system. The new superstructure was designed to accommodate five IR LEDs. The passage from three to five LEDs is because, in some conditions, it could happen that the LED was not detected, as the light spot of the LED is visible when the LED is placed perpendicular to the camera lens. In particular conditions, such as very accentuated roll motion, this condition was not verified, causing tracking loss. By using five LEDs, this phenomenon is mitigated.

The particular shape of the superstructure, particularly the position of the LEDs and their relative distances, was designed to maximize acquisition by the video-tracking system. For this purpose, they were positioned on different planes and with symmetry concerning the plane of ship symmetry plane. Furthermore, by redesigning the superstructure, it was possible to know the position and distances between the various light spots with extreme precision. The superstructure was redesigned through software for 3D modelling and realized by employing 3D printing (Fused Filament Fabrication - FFF or FDM).

The 3D project is shown in the following figure and the dimensions of the light spots on the table.

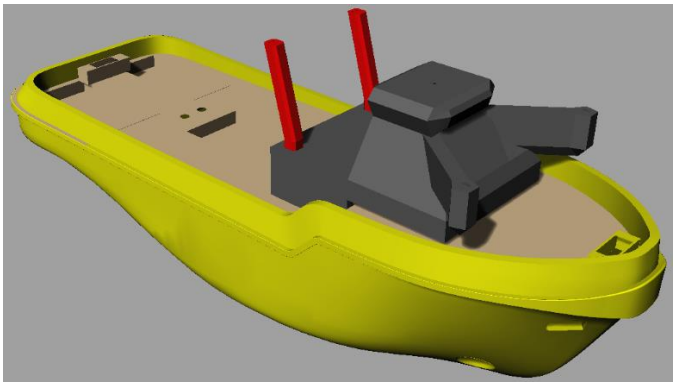

Figure 9. Superstructure redesign

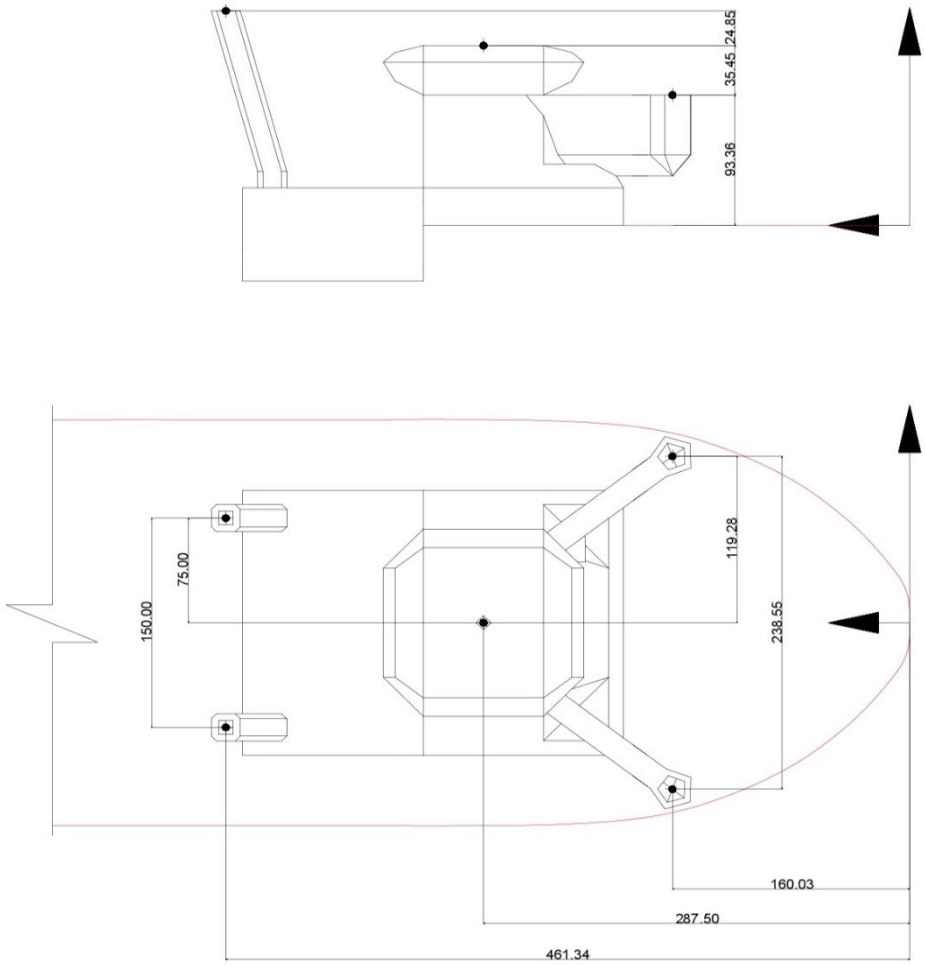

Figure 10. Spots contour plan [mm]

3.1.4 Communications Infrastructures

There is a need to know the instantaneous ship position during the tests as previously described. For the reason that the tests are carried out in a closed environment, the choice of tracking the position via GPS is not suitable. In addition, GPS guaranteed tolerance is not sufficiently precise for the testing purpose. It was decided to adopt a video-tracking system for all these reasons. In summary, the video-tracking system is used to simulate the GPS inside a closed space on the test model. The used video-tracking is an infrared type and provides the information of three translations and three rotations.

In addition, another essential video-tracking system feature is the specific communication with the PC. A UDP communication has been developed because it is possible to separate the PC which controls the model from the video-tracking system. In this case, the PC save computational resources.

Currently, this feature is not entirely used because a single PC laptop perfectly manages the computational resource requested for only one camera and the Simulink control code to command the testing model. However, this feature is essential for future development where enhance the Simulink command model in which a completely integrated architecture with a guidance system and collision avoidance logic is implemented and a video-tracking system composed of multi-camera. In this case, only one PC that has to elaborate all information could be costly resourced computational consuming. To summarize, the testbed used for the trials are shown in the following:

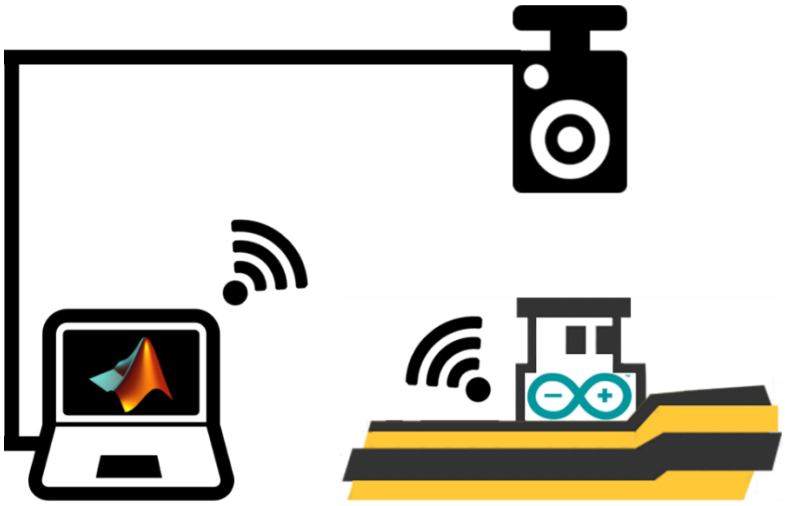

Figure 11: Test-bed Layout

The PC laptop simultaneously runs the video-tracking system and Simulink command interface for the testing model. The communication between the laptop and the testing model is a wireless type. The signals that the laptop sends to the model are the angular position of the starboard and the portside azimuthal thruster (2 variables), the thrust of the starboard and the portside azimuthal thruster (2 variables) and the thrust of the bow-thruster (1 variable). The camera that communicates with the laptop with UDP (User Datagram Protocol) sends the information of the position and the velocity of the ship by evaluating the 2D image of the infrastructure in which are collocate the infrared light spots.

Chapter 4

4.1 Digital Model 3DOF

In this Chapter, the mathematical models used to develop a simulation platform to be used as a preliminary benchmark are shown. The developed dynamic simulator accounts for the x-y plane motions: surge, sway, and yaw. The mathematical model describes the system behaviour and consists of a set of rules of a mathematical nature, which emulate the behaviour of the set of the single components that compose the real system. As a result, the system's dynamic performance prediction can be more or less accurate according to the degree of detail used for mathematically describing it. The simulator has been developed in the MATLAB/Simulink environment and is composed of sets of mathematical sub-models, which reflect the physics, each used to simulate a specific system. In particular, the 3 DOF dynamic simulator is composed of several subsystems:(i) Two independent Propulsive Line Subsystem; composed of Electric Motor, Shaft Line Dynamic, and Azimuth Propeller; (ii) Bow Thruster; (iii) Hull Forces; (iv) Environmental Disturbances; (v) Motion Solver. Each of the previous models has been detailed in the following paragraphs. The aim is to emulate the behaviour of the ship dynamically. The simulator workflow diagram is shown in Figure 12.

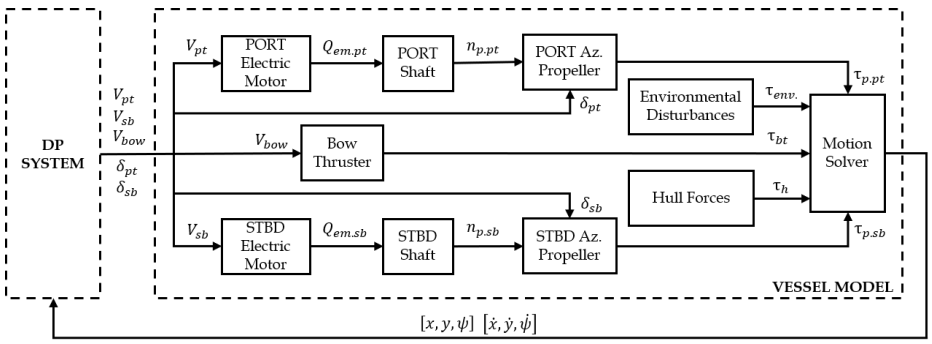

Figure 12. Simulator platform conceptual layout.

A 3 DOF model has been chosen because the actual case-study propulsive layout is unsuitable for counteracting forces and moments in the vertical plane

[163]. However, a 3 DOF simulator is sufficient for designing and evaluating actuators' performance for a DP system at a preliminary design stage. A DP capability performance assessment through a 6 DOF including vertical plane motions (heave, pitch, and roll) is remarkable indeed; the motions also affect the forces and moment in the x-y plane [164], influencing several operational aspects [165]. However, the information needed to create a 6 DOF simulator at the preliminary design stage is often unknown. For such a reason, further investigations will be carried out in future. The proposed simulation framework emulates the dominant dynamics of the tug testing model. Then, every subsystem that composes the vessel has been mathematically described by reproducing their functioning and mutual interactions. Ship fixed frame $(\underline{b}_1, \underline{b}_2, \underline{b}_3)$ centred in $L_{pp}/2$ and earth fixed frame $(\underline{n}_1, \underline{n}_2, \underline{n}_3)$, are used and shown in Figure 13.

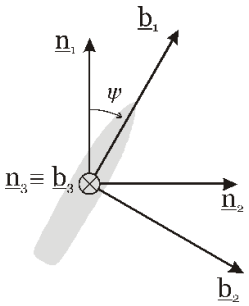

Figure 13. Reference frames

4.1.1 Towing Tank Test

In order to obtain the realistic behaviour of the dynamic ship simulator, towing tank tests were conducted to assess the hull resistance.

One of the critical points to adequately describe the ship dynamics in the sea is the knowledge of the hydrodynamic hull forces. Towing tank consists of towing a ship model (built following a geometrical scale) at a prescribed speed (following the Froud similarity) and measuring its experienced longitudinal force. Some guidelines to perform a correct towing tank test are collected in the ITTC guideline.

The first step in order to carry out the tests in the tank was the preparation of the hull. The original deck has been replaced with one explicitly created to carry out the towing tests. The characteristic of this specific deck is that it is not

continuous but divided into two parts; the forward and aft parts are distinguished. Furthermore, both deck parts are equipped with guiding plates to forbid hull rotation during the towing test, as shown in Figure 14.

The choice of equipping the model with this type of bridge lies in the fact that the model must be towed by means of a load cell connected to the hull by means of a spring. The connection must be at the lowest possible altitude, possibly at the same level at which it is finding the propellers. The towing by means of the carriage, as the speed varies, allows knowing the drag resistance of the hull.

Eventually, some model components were removed, such as the superstructure equipped with LEDs, used by the video-tracking system, and some electrical devices. The removal of these components caused a new weight distribution and a new displacement. For this reason, the model has been ballasted to regain the weight and the starting position.

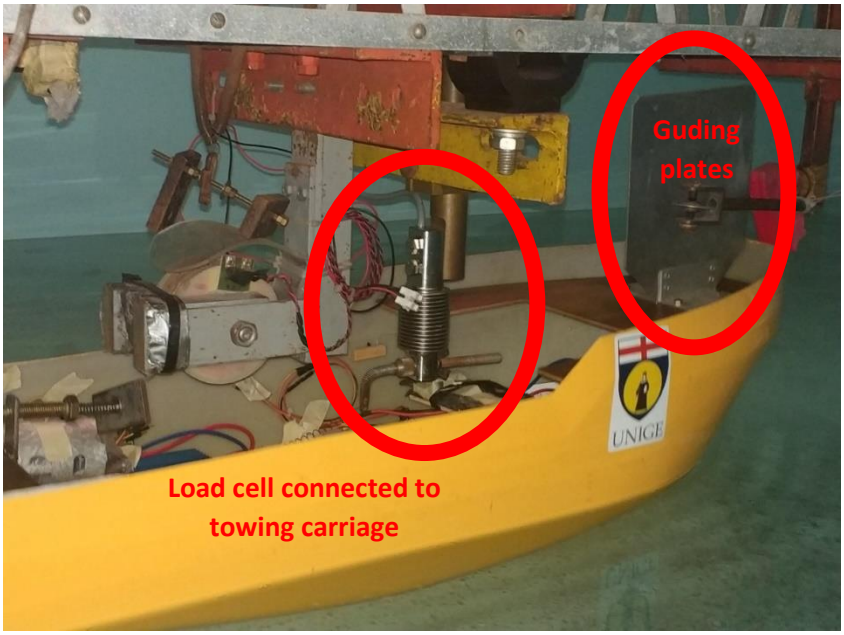

Figure 14. Hull outfitting for towing tests

Moreover, the analysis was carried out that allowed the comparison of the detected through experimental tests and simulated through CFD simulation models, the latter not conducted by the undersigned. Indeed, to validate the CFD analysis, a 3D model of the towing model has been created. The partial modelling of the azimuth thrusters is because the towing tests were conducted with only part of the propulsors assembled; indeed, it was not possible to

completely disassemble the entire azimuth thruster. The recreated 3D model of the tug boat hull is shown in the trim conditions in the towing tests performed, Figure 15.

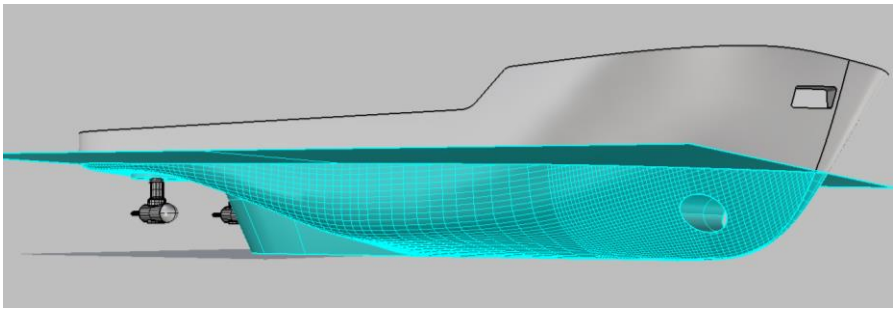

Figure 15. 3D hull

The reported towing tank tests had been performed in the University of Genova testing facility. It is a 60 meters tank with a transversal width of 3 meters wide and a water depth of 2.5 meters. Even if relatively small for industrial applications, these dimensions are adequate for a short model of only a 0.89 m length water line. On the other side, the carriage speed can reach three m/s of stabilized speed. It is equipped with a longitudinal load cell connected with the model through a free to move connection that does not interfere with the ship's motion. The model, therefore, is free to sink and trim during the tests to reach its dynamic attitude. The dynamic trim can be recorded thanks to two vertical lasers positioned at the ship extremities.

Three sets of tests were performed. For each test, six runs at different speeds with a maximum equal to 1.1 m/s were carried out. The max speed value was chosen because the boat reaches a maximum speed of 1.0 m/s when it is self-propelled. Another reason for the limitation of the maximum speed was to avoid that the wave train that is created during the towing tests could risk damaging the boat, as the new bridge is not watertight due to the positioning of the load cell, and any boarding on the water would have compromised the trim and the electrical instrumentation that has not to be possible remove. The three resistance curves obtained through the tests carried out are reported. Furthermore, it is possible to observe the comparison between the experimental data and the curve obtained through hydrodynamic calculations in Figure 17 (CFD analyses carried out by Genova's Hydrodynamic research group, in Figure 16 was reported the prepared 3D hull during a CFD analysis).

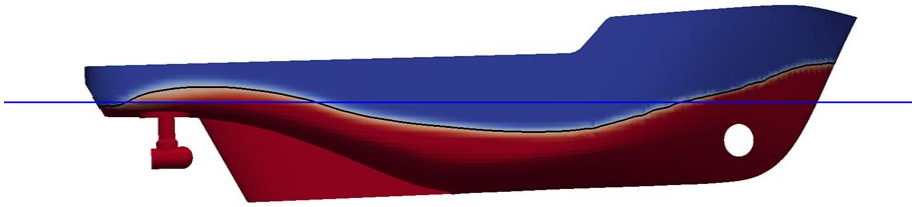

Figure 16. CFD analyses performed by the UNIGE Hydrodynamic research group

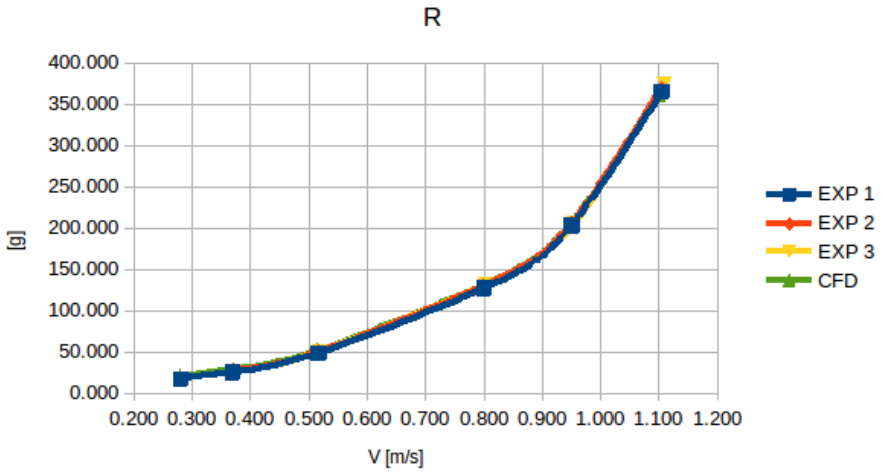

Figure 17. Towing tank and CFD hull resistance comparison

The hull resistance curves that indicate the experimental value are blue, red and yellow. It can be observed that the values of the repetitions are very similar to each other, as well as the curve obtained through CFD calculations which perfectly repeats the experimental curves. Another consideration regarding the resistance trend is the change in slope for the speed of 0.9 m/s. This phenomenon is because the boat's attitude changes profoundly when that speed is exceeded, bringing the model to sink the bow part. A pic obtained during the towing test carried out at maximum speed is shown, in which the immersion of the bow and the generated bow wave on the side is distinguishable.

Figure 18: Towing tank test capture

4.1.2 Dynamical Simulator Structure

As briefly described previously, the dynamic simulator is composed of several subsystems connected. In particular, the 3 DOF dynamic simulator is composed by:

- *Two independent Propulsive Line Subsystem*; composed by Electric Motor, Shaft Line Dynamic, and Azimuth Propeller. The propulsion plant has the aim to output the propeller thrust of the ship. This model has a symmetrical propulsion plant composed of DC electric motors, shaft lines, and azimuthal thrusters. All elements and their details are modelled in their subsystem through math equations, and they describe propulsion details as much as possible;
- *Bow Thruster;* as the propulsion plant aim to evaluate the thrust by the manoeuvering device, a DC electric motor delivers the thruster. The BT is composed of a double propeller that implies a theoretical symmetric behaviour of manoeuvering.
- *Hull Forces*; described by Oltmann & Sharma model, and the hull resistance has been obtained through experimental towing tank tests.
- *Environmental Disturbances*; These forces are considered to evaluate the total environmental force acting on the hull. The DNV-GL formulation has been used to evaluate the forces and moment due to wind, wave and current.

- *Motion Solver*; the ship is considered a rigid body with six degrees of freedom (surge, sway, heave, roll, pitch, and yaw). In particular, in the case study, the degrees of freedom have been set equal to three (surge, sway, and yaw. It is possible to obtain the ship acceleration, speed, and position reached during the simulation by means of the Newton – Euler formulation.

In the following, each subsystem has been analysed and mathematically described.

4.1.2.1 Propulsive line subsystem

The propulsion system consists of two independent shaft lines, and each one is modelled as the cascade of three mathematical sub-models: (i) a dynamic equation of DC electric motor; (ii) the dynamic equation of the shaft line; (iii) the ducted azimuth propeller. In detail, the DC electric motor is modelled by the electromechanical relation described by a differential equation, as reported hereinafter:

$$\frac{di}{dt} = \frac{1}{L}\left[V_{app} - Ri - K_e\omega\right] \tag{3}$$

where: $i(t)$ is the current $[A]$; L is the inductance $[H]$; V_{app} is the applied voltage $[V]$; R is the resistance $[\Omega]$; $\omega(t)$ is the motor angular speed $\left[\frac{rad}{s}\right]$; and K_e is the electric constant related to DC wiring $\left[\frac{V\,s}{rad}\right]$. Through the integration process, it is possible to obtain the DC magnitude. The output of the DC motor subsystem is the DC delivered torque, $Q_{em}(t)$ evaluated as follows:

$$Q_{em} = K_m\, i \tag{4}$$

where K_m is the mechanical constant related to construction characteristics of the electric motor $\left[\frac{Nm}{A}\right]$. Furthermore, under certain assumptions, it is possible to approximate the electric constant, K_e, equal to the mechanical one, K_m, [166]. The following differential equation describes shaft-line dynamical behaviour:

$$2\pi\, I_T \frac{dn_e}{dt} = Q_T \tag{5}$$

where: I_T is the total propulsive inertia $[kg\ m^2]$; n_e is the motor angular speed $[rps]$; and Q_T is the sum of the torques acting on the shaft line $[Nm]$. In particular, the several torques considered are reported hereinafter:

$$Q_T = Q_{em} - Q_f - Q_p \tag{6}$$

where: $Q_{em}(t)$ is torque delivered by the electric motor; $Q_{fric}(t)$ is the friction torque; and $Q_p(t)$ is the required propeller torque. In particular, the friction torque, $Q_{fric}(t)$, is described by the following relation:

$$Q_f = Q_{em}\,[1 - \eta_{TR}(n_e)] \tag{7}$$

where: η_{TR} is the transmission efficiency as a function of the motor rotational speed (n_e). The transmission efficiency behaviour is described by a function that asymptotically increases up to the maximum efficiency value [167]. The lower and upper bounds correspond to idle condition and maximum engine speed, respectively; and are equal to $\eta_{TR}(n_e) \in [0.65 - 0.98]$. The absorbed propeller torque, $Q_p(t)$, is described by the following relation:

$$Q_p = \frac{Q_O}{\eta_R} \tag{8}$$

where: Q_O is the required open water torque; η_R is the relative rotative efficiency that is assumed constant. The propeller geometry model is described by Kaplan 19A propeller [168]. To evaluate the delivered thrust and required torque, the thrust coefficient, C_T, and the torque coefficient, C_Q, were used. Such coefficients are described as a function of hydrodynamic pitch angle, β. These coefficients, which replace the K_T, K_Q are described as a function of the advance coefficient, J, have been adopted to consider the operation of the propeller in the four quadrants. In particular, a quasi-static approach is used to evaluate the propeller forces and moment time histories. The formulation relative to the propeller in the four quadrants used is reported in the following:

$$\beta = \text{atan}\left[\frac{V(1-w)}{0.7\,\pi n_p D}\right] \tag{9}$$

$$V_r = \sqrt{V^2\,(1-w)^2 + (0.7\,\pi\,n_p\,D)^2} \tag{10}$$

$$T_O = \frac{1}{8}\rho\, C_T(\beta)\ \pi\, D^2\, V_r^2\ ;\ Q_O = \frac{1}{8}\,\rho\, C_Q(\beta)\,\pi\, D^3\, V_r^2 \tag{11}$$

where: V is the ship's speed $[m/s]$; w is the wave factor $[-]$; n_p is the propeller's angular speed $[rps]$; D is the propeller diameter $[m]$; V_r is the relative speed $[m/s]$; ρ is the water density $[kg/m^3]$; T_O is the open water thrust $[N]$; and Q_O is the open water torque $[Nm]$. Hence, the forces, X_p, Y_p and moment, N_p, expressed in the ship fixed frame, are obtained in the function of the geometric azimuth angle, δ, as follows:

$$\tau_p = \begin{cases} X_p = T_O \cos\delta \\ Y_p = T_O \operatorname{sen}\delta \\ N_p = Y_p x_p - X_p y_p \end{cases} \tag{12}$$

where x_p and y_p are the coordinates of the propeller concerning the ship fixed frame along $\underline{b_1}$ and $\underline{b_2}$, respectively. In particular, the assumed values of δ, i.e., the operating range of the propeller position is equal to [-180°, 180°]. This aspect guided the fixed angle allocation logic development reported in the following paragraphs.

4.1.2.2 Bow thruster subsystem

Beyond low-speed manoeuvring, the bow thruster is essential for unconventional manoeuvrings, such as auto berthing and station keeping. The bow thruster can have a single propeller, with an asymmetric behaviour (the flow that crosses the propeller is disturbed from the presence of the hub), or a double propeller, in this case, with symmetric behaviour. A double propeller bow thruster is present and commanded by an electric motor in this application. Hence, if the bow thruster is used, the manoeuvrability will be considerably improved, especially at low speed. The bow thruster has been approximated as a ducted propeller. By means of this approximation, it has been possible to evaluate the thrust delivered and torque required. The channelled propeller of the Wageningen Ka series, with the following characteristics: number of Z blades equal to 3, Ae/Ao ratio equal to 0.65, nozzle 19A and pitch equal to 1, has been taken as the referred propeller. By means of the information of thrust coefficient, $K_T(J)$, and the torque coefficient, $K_Q(J)$, the forces, X_b, Y_b, and moment, N_b, have been evaluated as follows:

$$J = \frac{v + r\, x_{BT}}{n_p D}$$
$$T_{Ob} = \rho K_T(J)\, {n_p}^2 D^4 \;\; ; \;\; Q_{Ob} = \rho K_Q(J)\, {n_p}^2 D^5 \tag{13}$$

where: v is the sway speed, i.e., the velocity component along $\underline{b_2}$ $[m/s^2]$; r is the yaw speed, i.e., the angular speed around $\underline{b_3}$; and x_{BT} is the bow-thruster tunnel position in the ship fixed reference frame $[m]$. Hence:

$$\tau_{bt} = \begin{cases} X_{bt} = 0 \\ Y_{bt} = T_{Ob} \\ N_{bt} = Y_p x_{bt} \end{cases} \tag{14}$$

4.1.2.3 Hull forces subsystem

Oltmann & Sharma's hull forces model provides a realistic representation of the hydrodynamic force performance for low-speed manoeuvres at high drift angles [169]. For such a reason, since the dynamic simulator is used for research focused on the study of DP system performance, it has been used for the evaluation of hull forces, X_h, Y_h and moment, N_h. The main idea behind the model is that the total hydrodynamic force is composed of three main contributions: ideal fluid forces, lift forces, and cross-flow drag forces. The contribution of the hull resistance, R_T, in explicitly considered as a separate term. The hull resistance is known accurately since the testing model conducted towing tank tests. The ideal fluid forces are assessed using the potential theory, i.e., neglecting viscosity effects. The hydrodynamic forces generated by a body that moves in an ideal, irrotational fluid that does not generate lift can be expressed through a mass matrix and added inertia depending exclusively on the body shape. The wavefield formation phenomenon can be ignored (simplification is acceptable for considering low Froude numbers).

Lift forces can be assessed by comparing the hull as a low aspect ratio wing. In particular, a body in a fluid that moves at a given speed with a certain angle of attack generates lift forces equivalent to a wing profile.

Cross-flow drag forces represent the resistance due to the viscous forces generated by a moving body in a real fluid. Such a term considers the hull divided into mutually non-influential sections and analyses each section of length dx placed at a distance x from the axes' origin.

Eventually, the formulation for 3-DOF for the hull forces and moment evaluation is the reported after this, with the subscripts referred to as ideal fluid forces (I), lift forces (HL), and cross-flow drag (HC):

$$\tau_h = \begin{cases} X_h = X_I + X_{HL} - R_T \\ Y_h = Y_I + Y_{HL} + Y_{HC} \\ N_h = N_I + N_{HL} + N_{HC} \end{cases} \tag{15}$$

4.1.2.4 Environmental disturbances subsystem

DNV-GL formulation has been used to determine the environmental forces; in particular, all disturbances (wind, wave, and current) have been considered to assess the DP system and evaluate the dynamic positioning capability plots (DPCPs). The total forces, X_{env}, Y_{env} and moment, N_{env}, have been evaluated under the hypothesis of the linear superposition principle as follows:

$$\tau_{env} = \begin{cases} X_{env} = X_{wind} + X_w + X_c \\ Y_{env} = Y_{wind} + Y_w + Y_c \\ N_{env} = N_{wind} + N_w + N_c \end{cases} \tag{16}$$

where: $w, c, wind$ subscripts refer to wave, current, and wind, respectively. The DNV-GL rules provide the formulation for all disturbance models. In the following, all the relations to evaluating the disturbances forces and moment have been reported.

$$\begin{cases} X_{wind} = -0.7 \dfrac{1}{2} \rho_{air} {V_{wind}}^2 A_{F,wind} \cos \gamma_{rel} \\ Y_{wind} = 0.9 \dfrac{1}{2} \rho_{air} {V_{wind}}^2 A_{L,wind} \sin \gamma_{rel} \\ N_{wind} = Y_{wind} \left[x_{L,air} + 0.3 \left(1 - 2 \dfrac{\gamma_{rel}^i}{\pi} \right) L_{pp} \right] \end{cases} \tag{17}$$

$$\gamma_{rel}^i = \begin{cases} \gamma_{rel}, & 0 \le \gamma_{rel} \le \pi \\ 2\pi - \gamma_{rel}, & \pi \le \gamma_{rel} \le 2\pi \end{cases}$$

where: ρ_{air} is the air density $[kg/m^3]$; V_{wind} is the relative wind speed $[m/s]$; $A_{F,wind}$ is the frontal projected wind area $[m^2]$; $A_{L,wind}$ is the longitudinal projected wind area $[m^2]$; $x_{L,air}$ is the longitudinal position of the lateral

projected area centre (in the body-fixed frame)[m]; and γ_{rel} is the relative wind direction [rad].

$$\begin{cases} X_w = \frac{1}{2}\,\rho g {H_S}^2 B\ \ h\left(\gamma_{rel}, bow_{angle}, C_{WLaft}\right) f(T'_{surge}) \\ Y_w = \frac{1}{2}\,\rho g {H_S}^2 L_{OS}\ (0.09 \sin\gamma_{rel}\ )\, f(T'_{sway}) \\ N_w = Y_w \left[x_{LOS} + \left(0.05 - 0.14\ \frac{d\gamma_{rel}^i}{\pi} \right) L_{OS} \right] \end{cases} \tag{18}$$

where: H_S is the significant wave height [m]; g is the gravity acceleration [m/s^2]; B is the maximum breadth at the waterline [m]; L_{OS} is the longitudinal distance between the foremost and aft-most point under the keel line [m]; and X_{LOS} is the longitudinal position of $L_{OS}/2$ [m]. The following relations should also be assessed:

$$h\left(\gamma_{rel}, bow_{angle}, C_{WLaft}\right) = 0.09\ h_1\left(\gamma_{rel}, bow_{angle}, C_{WLaft}\right) h_2(\gamma_{rel})$$

where:

$$h_1\left(\gamma_{rel}, bow_{angle}, C_{WLaft}\right) = \ 0.8\ {bow_{angle}}^{0.45} + \frac{\gamma_{rel}^i}{\pi}\left(0.7\ {C_{WLaft}}^2 - 0.8\ {bow_{angle}}^{0.45}\right)$$

$$h_2(\gamma_{rel}) = \ 0.05 + 0.95\,\mathrm{atan}[1.45\ (\gamma_{rel}^i - 1.75)]$$

and :

$$f(T') = \begin{cases} 1 & T' < 1 \\ {T'}^{-3} e^{1-T'^{-3}} & T' \geq 1 \end{cases} \tag{19}$$

$$T'_{surge} = \frac{T_Z}{0.9\ {L_{pp}}^{0.33}} \quad ; \quad T'_{sway} = \frac{T_Z}{0.75\ B^{0.5}}$$

where: bow_{angle} is the angle between the vessel x-axis and a line drawn from the foremost point in the water line [rad]; C_{WLaft} is waterplane area coefficient and can only assume the values within the range $\in [0.85, 1.15]$ [$-$]; T_Z is the main wave period [s]; and γ_{rel} is the relative wave direction [rad].

$$\begin{cases} X_c = -0.07 \frac{1}{2} \rho \, {V_c}^2 B \; draft \cos \gamma_{rel} \\ Y_c = 0.6 \; \frac{1}{2} \rho \, {V_c}^2 A_{L,c} \sin \gamma_{rel} \\ N_c = \; Y_c \left[x_{L,c} + \max(minimum \, , -0.2) \, L_{pp} \right] \end{cases} \tag{20}$$

$$minimum = \min \left[0.4 \left(1 - 2 \; \frac{\gamma_{rel}^{i}}{\pi} \right), 0.25 \right]$$

where: V_c is the current speed $[m/s]$; $draft$ summer load line draft $[m]$; $A_{L,c}$ is the longitudinal projected submerged current area $[m^2]$; $x_{L,c}$ is the longitudinal position of the area centre of $A_{L,c}$ (in the body-fixed frame) $[m]$; and γ_{rel} is the relative current direction $[rad]$.

The wind speed is considered through the Davenport spectrum model [170], tailored to generate allowable wind gusts for the proposed testing model. The wind speed V_{wind}, implemented in the simulator is evaluated by means of the following formulation:

$${V_{wind}}^2 = (V_{m,wind} + \; v_{g,wind})^2 \cong {V_{m,wind}}^2 + 2 V_{m,wind} v_{g,wind} \tag{21}$$

where $V_{m,wind}$ is the average wind speed $[m/s]$, and $v_{g,wind}$ is the wind gust speed $[m/s]$.

4.1.2.5 Ship dynamic subsystem

The ship motions and displacements have been evaluated by assuming the vessel as a rigid body and considering a constant displacement; the latter hypothesis is entirely true as the case study is electrically powered. Therefore, the weight does not vary during its operation. Hence, using the II[nd] Newton's law is possible to evaluate the ship acceleration and, consequently, through the integration of the velocity and displacement. The formulation used to evaluate the ship velocity components is shown hereinafter:

$$\begin{cases} M(\dot{u} - x_G r^2 - uv) \; = X_h + X_{p\,stbd} + X_{p\,port} + X_{env} \\ M(\dot{v} + x_G \dot{r} + ur) \quad = Y_h + Y_{p\,stbd} + Y_{p\,port} + Y_{env} + Y_{bt} \\ I_{zz} \dot{r} + M x_G (\dot{v} + ru) = N_h + N_{p\,stbd} + N_{p\,port} + N_{env} + N_{bt} \end{cases} \tag{22}$$

where: u, v, r are the ship's quasi-velocity components, in particular, surge, sway, and yaw, concerning the ship's fixed frame ($\underline{b}_1, \underline{b}_2, \underline{b}_3$) centred in $L_{pp/2}$; M is the total mass equal to the sum of both the ship's mass and added mass; I_{zz} is the ship's inertia along $\underline{b}_3$; x_G is the longitudinal position of the centre of gravity concerning $L_{pp}/2$; X, Y, N are the forces and moment concerning the frame ($\underline{b}_1, \underline{b}_2, \underline{b}_3$) and the subscripts h, p, env, bt refer to the hull, propellers, environmental disturbances and bow-thruster, respectively.

4.2 Dynamic Positioning and Change Positioning systems

The proposed DP system consists of three main parts: the controller, the force allocations logic (FAL) and the thrust allocation logic (TAL). In particular, for this application, the same controller and TAL were used, and two different force allocation logics (FAL) were developed. The controller structure is based on a PID structure with anti-windup [171]. The FAL's input can switch between open and closed loops in this application. In particular, forces and moment requirements can be either the joystick or motion controller output fed with the vessel model output, as sketched in Figure 19. The joystick outputs are forces and moment independent of the position requirements. On the contrary, the motion controller outputs are forces and moment necessary to counteract the environmental disturbances, and they were assessed by means of the position and speed errors. For the sake of compactness, quantities are presented in matrix form. In particular, the array $\tau_i = [X_i, Y_i, N_i] \in \Re^n$ contains forces components along $\underline{b}_1$, $\underline{b}_2$ and the moment around $\underline{b}_3$, respectively. The subscripts R and D refer to the requested and delivered quantities, respectively. In the following, the forces, moment, and thrusts are referred to with superscript $*$, which represents those quantities are divided by the maximum allowable thrust of the azimuthal propeller ($T_{pt\,max}$). The general structure the requested forces and moment τ_R^* are defined hereinafter, the first set is referred to the joystick mode, while the second one is related to the DP.

$$\tau_R^* = \begin{cases} X_{joystick}^* \\ Y_{joystick}^* \\ N_{joystick}^* \end{cases} \quad \text{or}$$

(23)

$$\tau_R^* = \begin{cases} K_{P_x} e_x^* + K_{D_x} e_{\dot{x}}^* + K_{I_x} \int e_x^* - K_{AW_x}(X_R^* - X_D^*) d\zeta \\ K_{P_y} e_y^* + K_{D_y} e_{\dot{y}}^* + K_{I_y} \int e_y^* - K_{AW_y}(Y_R^* - Y_D^*) d\zeta \\ K_{P_\psi} e_\psi^* + K_{D_\psi} e_{\dot{\psi}}^* + K_{I_\psi} \int e_\psi^* - K_{AW_\psi}(N_R^* - N_D^*) d\zeta \end{cases}$$

where: $X_{joystick}^*, Y_{joystick}^*, N_{joystick}^*$ are the non-dimensional forces corresponding to joystick lever positions, $[K_{P_x}, K_{P_y}, K_{P_\psi}]$, $[K_{D_x}, K_{D_y}, K_{D_\psi}]$, $[K_{I_x}, K_{I_y}, K_{I_\psi}]$, and $[K_{AW_x}, K_{AW_y}, K_{AW_\psi}]$ are proportional, derivative, integral, and anti-windup controller coefficients, respectively. An anti-windup component is added to limit windup integral divergences to assess the DP controller accurately [172]. In Figure 19, the schematic system's view is reported. As previously illustrated, the joystick and DP controller output are required forces and moment, necessary to follow a user-defined direction or keep the required position. Then, a unique force allocation logic can accomplish both requirements.

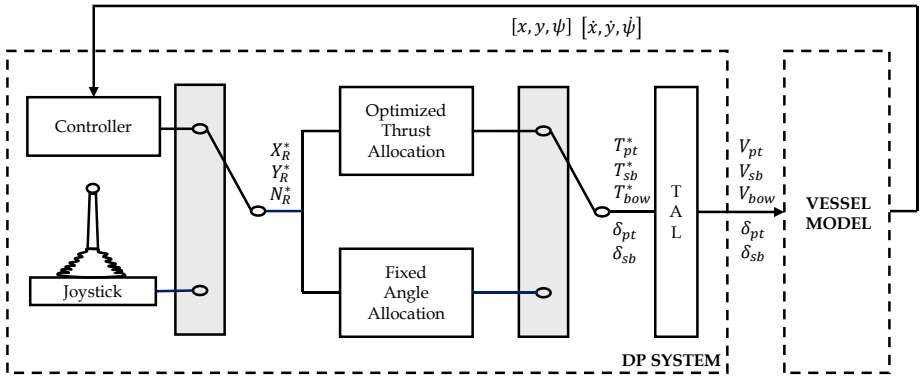

Figure 19. Dynamic positioning system structure.

4.2.1 FAL – Optimised Thrust Allocation

This section reports the allocation logic implemented to assess dynamic positioning capabilities. The logic is based on a constrained optimisation problem that uses the Lagrange multiplier method to minimise an objective function under certain constraints. The required thrust is optimised by changing the azimuth position to compensate for the environmental disturbances. In particular, The actuators can exert the required thrust according to the following rules:

- The bow-thruster has the ability to push on both sides, which means that the rotation of the azimuth thrusters can be both clockwise and anti-clockwise;
- The two azimuth thrusters can only push in one direction. In order to vary the thrust change direction, the angles of the azimuths have to be changed. As a result, the azimuth thrusters are completely uncoupled (different azimuth angles and thrusts).

The graphical representation is reported hereinafter in Figure 20:

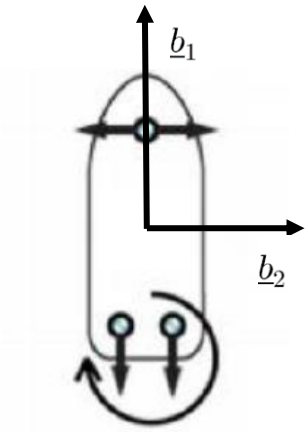

Figure 20. Thrust optimized allocation

In particular, the domain of the function is $\underline{x} = \left[T_{pt}^*, T_{sb}^*, T_{bow}^*, X_{pt}^*, Y_{pt}^*, X_{sb}^*, Y_{sb}^*\right] \in \mathbb{R}^7$ where $\underline{T}_{pt}^* = X_{pt}^* \underline{b}_1 + Y_{pt}^* \underline{b}_2$ is the vector of portside thrust, $\underline{T}_{sb}^* = X_{sb}^* \underline{b}_1 + Y_{sb}^* \underline{b}_2$ is the vector of starboard thrust and $\underline{T}_{bow}^* = Y_{bow}^* \underline{b}_2$, is the vector of the bow thruster thrust. The problem is formulated as it follows:

$$\min_{\underline{x}} f(\underline{x}) \quad \text{with} \quad h_i(\underline{x}) = 0 \quad \text{and} \quad g_j(\underline{x}) > 0 \tag{24}$$

where $f(\underline{x})$ is the objective function $f(\underline{x})$: $\mathbb{R}^n \longrightarrow \mathbb{R}$

$$f(\underline{x}) = \left(\frac{T_{pt}^*}{T_{max}^{tot}}\right)^2 + \left(\frac{T_{sb}^*}{T_{max}^{tot}}\right)^2 + \left(\frac{T_{bow}^*}{T_{max}^{tot}}\right)^2 \tag{25}$$

The constraints $h_i(\underline{x})$: $\mathbb{R}^n \longrightarrow \mathbb{R}^m$ are the following

$$\begin{cases} h_1(\underline{x}) = X_R^* - X_{pt}^* - X_{sb}^* \\ h_2(\underline{x}) = Y_R^* - Y_{pt}^* - Y_{sb}^* - T_{bow}^* \\ h_3(\underline{x}) = N_R^* - x_{bow}\ T_{bow}^* - x_{pt}\ Y_{pt}^* + + y_{pt}\ X_{pt}^* - x_{sb}\ Y_{sb}^* + y_{sb}\ X_{sb}^* \\ h_4(\underline{x}) = T_{pt}^{*^2} - X_{pt}^{*^2} - Y_{pt}^{*^2} \\ h_5(\underline{x}) = T_{sb}^{*^2} - X_{sb}^{*^2} - Y_{sb}^{*^2} \end{cases} \tag{26}$$

where: $[X_R^*, Y_R^*, N_R^*]$ are the required forces and moment. In the closed-loop, such components are the controller's output when the automatic motion control is active. Alternatively, they can be the joystick output in the open loop when the lever is active. In addition, the following constraints are added to guarantee the relationship between the vector components and their modules:

$$g_1(\underline{x}) = T_{pt}^* \quad \text{and} \quad g_2(\underline{x}) = T_{sb}^* \tag{27}$$

4.2.2 FAL – Fixed angle allocation

This allocation was developed with the opposite concept of the previous one. In this case, the goal was to minimise the azimuthal movements to reduce the mechanism wear. The allocation layout is the following: one azimuth thruster compensates the environmental disturbances along $\underline{b_2}$ together with the bow-thruster, while the second one counteracts the disturbances along $\underline{b_1}$. Both azimuth thrusters work only with two available fixed directions, in particular these positions: ±90 and 0-180. The graphical visualisation of the allocation is reported hereinafter in Figure 21.

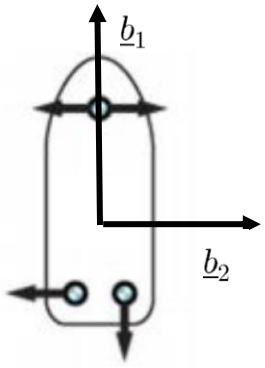

Figure 21. Fixed angle allocation

This allocation was studied for experimental purposes; indeed, the lab testing model is not able, as a full-scale system, to precisely respect the continuous variable angle request, which is the output of the thrust optimised allocation. In such a way, with the propeller fixed positions allocation, the thrusters counteract external disturbances acting mainly on the propeller rotation speed with a quasi-fixed position. This force allocation has the double advantage of being more easily solved from a mathematical point of view and easily implemented in a real PLC, as it can be described by a system of three linearly independent equations and three unknowns as follows:

$$\begin{cases} X_R^* + T_{sb}^* = 0 \\ Y_R^* + T_{pt}^* + T_{bow}^* = 0 \\ N_R^* + x_{pt}T_{pt}^* + x_{bow}T_{bow}^* - y_{sb}T_{sb}^* = 0 \end{cases} \quad (28)$$

4.2.3 TAL – Thrust Allocation Logic

The thrust allocation logic is needed to convert the actuators' thrust signals into command signals for the actuators. Generally, in real applications, the signals to be sent can be shaft revolutions or fuel mass flow. The TAL output is represented by the electric motors' voltage in the testing-model case study. In particular, the relationship to assess the voltage versus the DP system's thrust is reported hereinafter. The relation between thrust and voltage was found by means of a model-based approach by carrying out a simulation campaign in the bollard pull condition.

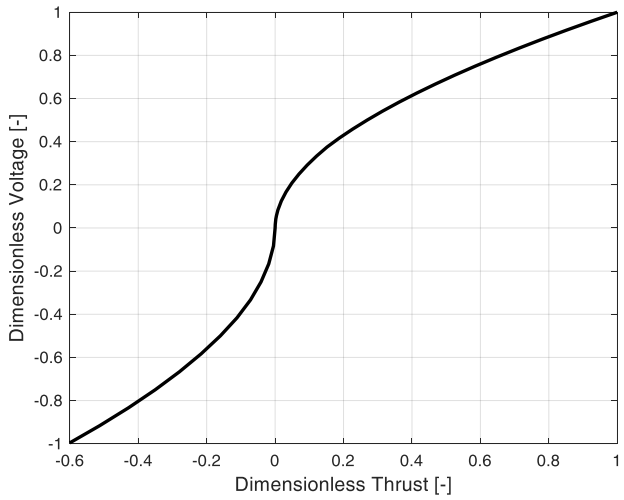

Figure 22. Dimensionless relation between thrust and voltage for the azimuth thrusters.

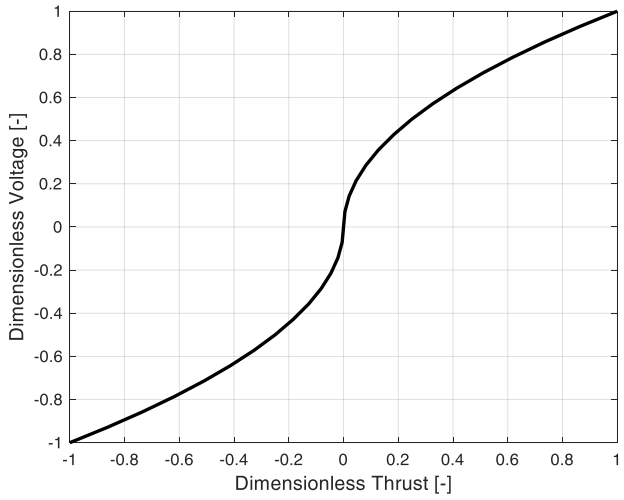

Figure 23. Dimensionless relation between thrust and voltage for the bow thruster.

In Figure 22, the dimensionless relation between thrust and voltage for the azimuth propellers is reported. The asymmetrical thrust behaviour of propellers is experienced, i.e., with a positive voltage, which is more significant than that obtained with a negative voltage. This aspect has also been validated via experimental tests.

In Figure 23, the bow thruster behaviour is symmetrical due to its propulsive layout (duo propeller).

4.3 Dynamic Positioning Capability Plot

DP system performances are usually assessed through the DP capability polar plots (DPCPs), focusing on the reliability of environmental disturbances. This section presents station-keeping results employing the static and dynamic approach. The main idea is to compare DPCPs obtained by static approaches and those obtained by dynamic simulations varying the allocation force and the environmental disturbances, called to distinguish them from the other Time-domain Dynamic Positioning Capability Plots (T-DPCPs). Briefly, before introducing how the T-DPCP were created using the dynamic simulator, the equilibrium condition for creating the static DPCP is reported in the following:

$$\begin{cases} X_R^* = \dfrac{X_{wind} + X_w + X_c}{T_{pt\,max}} \\ Y_R^* = \dfrac{Y_{wind} + Y_w + Y_c}{T_{pt\,max}} \\ N_R^* = \dfrac{N_{wind} + N_w + N_c}{T_{pt\,max}} \end{cases} \tag{29}$$

Through the force allocations previously shown, it is possible to evaluate the dimensionless thrust $(T_{pt}^*, T_{sb}^*, T_{bow}^*)$ and consequently also the thrusts $(T_{pt}, T_{sb}, T_{bow})$. These thrusts, calculated according to the environmental disturbance acting on the hull, are compared with the maximum values that can be exercised ($T_{pt} < T_{pt\,max},\ T_{sb} < T_{sb\,max},\ T_{bow} < T_{bow\,max}$).

If the required thrust is lower than the maximum available, the environmental condition analysed is considered satisfied; otherwise, not. Moreover, the interaction with the disturbances and the vessel dynamics is neglected in the static approach.

For such a reason, the developed simulation platform is used to obtain the T-DPCPs by dynamic results. The input data have been defined:

- the disturbances' main incoming directions starting from 0° to 180° with a step of 10°;

- the main wind speed with the range from 0.5 $[kn]$ to 15 $[kn]$ with a step of 0.5 $[kn]$;
- the current magnitude was considered independent from the Davenport spectrum and was varied between 0 - 0.1 - 0.2 $[m/s]$;
- the wave disturbances are aligned with the wind, and the magnitude is considered constant and equal to 0.1 m and 3.5 s for main wave height and main wave period, respectively. The worst-case in terms of disturbances acting on the hull is considered, with the direction of disturbances aligned.

The same discretisation range regarding the environmental conditions was used in the static approach for the evaluation of requested forces and moment (X_R^*, Y_R^*, N_R^*).

The vessel and the wind's actual encounter angle replaced the dynamic analysis's absolute disturbance direction. Eventually, the controller structure and its coefficients have been left unchanged to compare the differences between the two force allocations fairly.

A set of more than 1700 simulations for each force allocation have been carried out to obtain the T-DPCPs using the dynamic simulator. The simulation time was set to 1800 s. The dynamic simulation has been validated by introducing the maximum allowable offsets from the desired position according to environmental disturbances. Such constraints were evaluated during the simulation after the initial transient (600 s) was expired to allow the controller to be initialised.

Hence, the dynamic simulation is valid when the maximum displacement from the desired position is below 0.3 L_{OA} and the bow angle error is below then ± 5°. During the simulation, it is possible to continuously overcome the previous bounds only for 30 s or exciding the constraints for a maximum of 90 s for all manoeuvre duration; otherwise, it is considered a failure. The latter time constraint was imposed to avoid rapid transients of less than 30 s, which are repeated continuously, causing a false valid manoeuvre. These could occur due to the low boat inertia and the high response speed of the actuators, which are characteristics of the tug testing model.

4.3.1 Optimised Thrust Allocation DPCPs

A comparison between static and dynamic approaches is shown in this section, taking into account the optimised thrust allocation. In particular,

Figure 24 shows the capability plot obtained with a static approach, while Figure 25 represents T-DPCP obtained by simulating several manoeuvres as a function of changing magnitude and direction of environmental disturbances. In order to highlight the differences between the two analyses, Figure 26 sketches the DP performances for the selected disturbance incoming directions. The first bar (yellow) represents the results obtained through the static approach, while the second (purple) belongs to the time-domain simulations. Notably, as expected, the static approach always provides a better DP performance prediction. The main difference regards results for the stern seas, between 170°-180°. This particular behaviour is due to the real azimuth propeller functionality. For such a reason, whenever the direction of the disturbance corresponds to 180°, the controller cannot symmetrically handle oscillation around that angle; because of the device limitations, when the required azimuth overcomes 180°, the propeller has to turn in the opposite direction to reach the desired angle and vice-versa, causing further instability. The latter is the main reason that led the authors to develop a force allocation logic based on fixed thrusters.

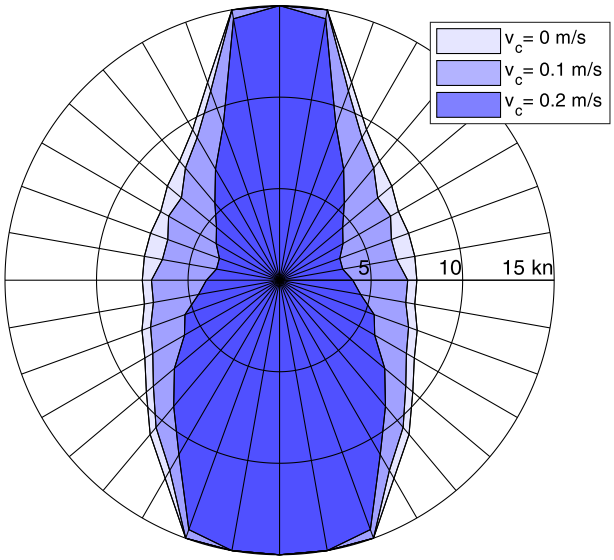

Figure 24. Static DPCP thrust optimised allocation.

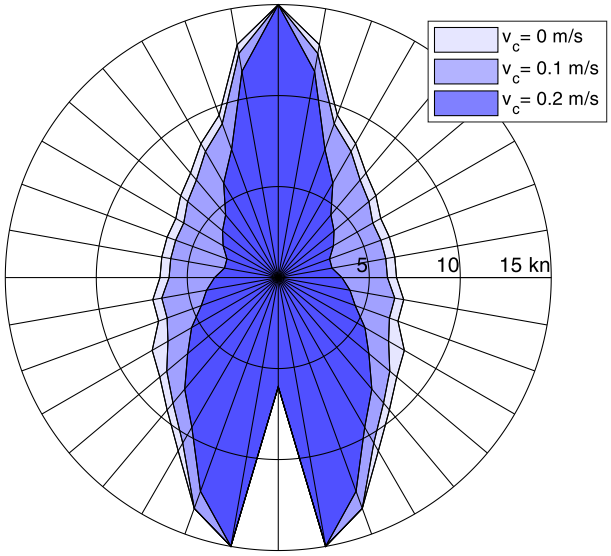

Figure 25. T-DPCP thrust optimised allocation.

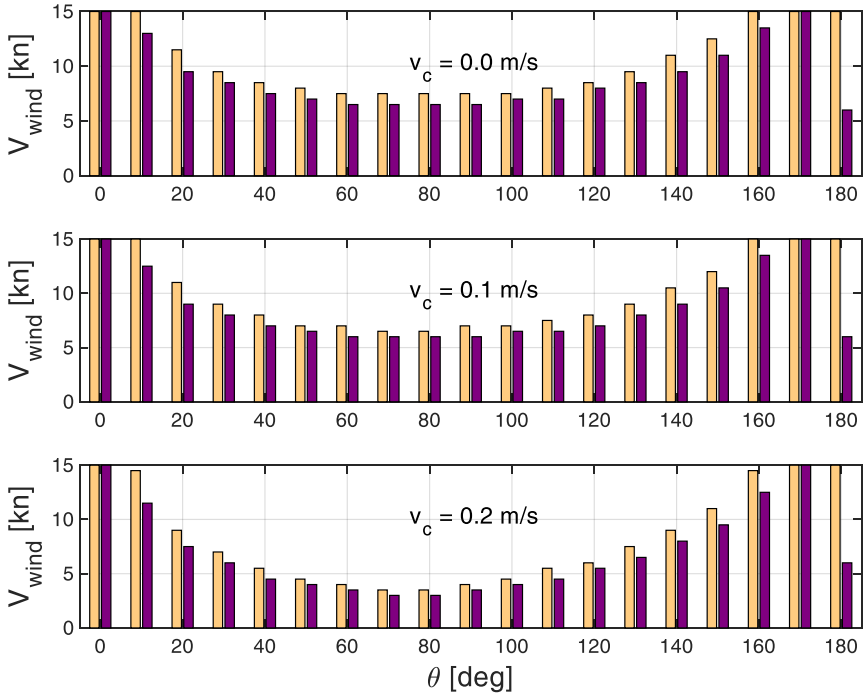

Figure 26: Comparison thrust optimised allocation

4.3.2 Fixed Angle Allocation DPCPs

As reported in the previous section, a comparison between the two different approaches is reported for a fixed angle allocation. Figure 27 shows the DPCP obtained with a static approach; instead, Figure 28 shows T-DPCP obtained by several time-domain simulations. Both of them are referred to as the fixed position propeller allocation. In such a case, it is immediately notable that the area of the plot decreases with the time dynamic approach, and, concerning the previous allocation, it is not experienced any particular behaviour at 180°. That means that the allocation logic with a fixed azimuth angle gives a more stable performance for all environmental directions. A quantitative analysis concerning the differences between the two previous capability plots is shown in Figure 29, where the first bar (blue) represents the results obtained through the static approach, while the second (red) is through time-domain simulations. The static approach results are always more promising for all directions and current speed.

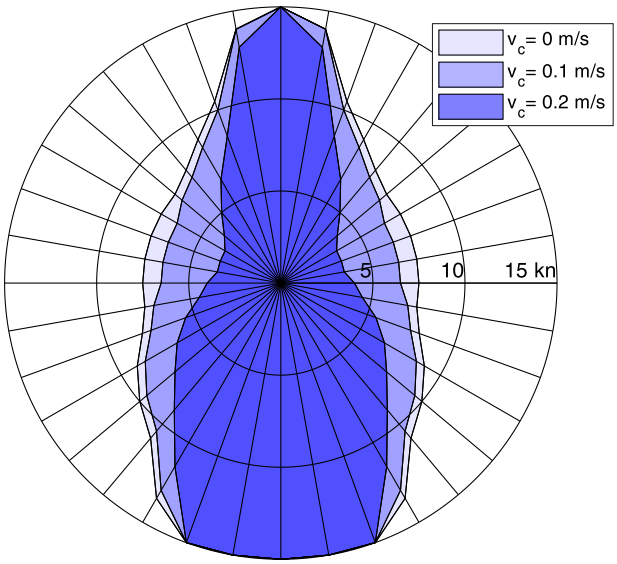

Figure 27. Static DPCP fixed angle allocation.

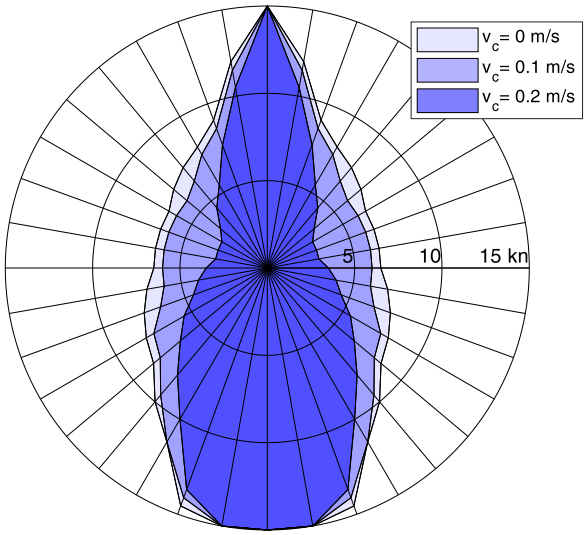

Figure 28. T-DPCP fixed angle allocation.

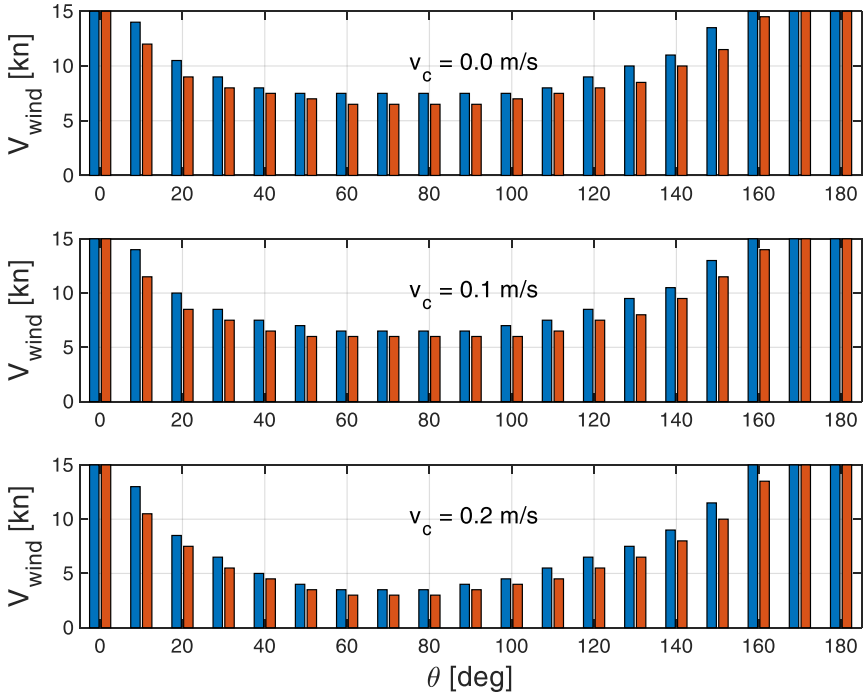

Figure 29. Comparison of fixed angle allocation

4.3.3 Time-domain DP Manouvre Comparison

In order to emphasise the additional information obtained by using a simulation-based design approach, the time history results obtained during a simulation near a limit condition for both allocations are shown. Therefore, the manoeuvre has been considered valid for both allocations and has been carried out with the following environmental characteristics. The wind mean speed of 9 kn, the main wave height of 0.1 m, the main wave period of 3.5 s, the current speed of 0.2 m/s and the incoming direction of 150°. In addition, all the time-domain results have been shown without the initial transient equal to 600 s.

In Figure 30 and Figure 31, the dimensionless vessel path for thrust optimised and fixed angles, respectively, is reported with a cyan line. The black dashed circle line represents the maximum allowable position error. The setpoint position is represented with a green dashed hull waterline, while the position at the end of the simulation is shown in red. The blue waterline represents the position every 50 s. The manoeuvre is considered valid for both allocations, indeed; the constraints are respected.

Figure 32 and Figure 33 show dimensionless displacements for x and y-axes (over L_{OA}) and rotation along z-axis in three different subplots for thrust optimised and fixed angles, respectively. The centre of the body-fixed frame's current position is shown with a dashed red line, while the setpoint is represented with a blue line. Moreover, the maximum allowable error is reported with a black line. The mean heading error for both allocations is equal to 1°, showing the proper design of the controller. A difference between allocations is that for the x-direction, the displacement of fixed angle allocations is deeply oscillatory, more than the other allocations, around the setpoint position.

Figure 34 and Figure 35 show three subplots regarding the exercised thrust for thrust optimised and fixed angles, respectively. In particular, the figures report, from top to bottom, the dimensionless thrust of port side azimuth, starboard side azimuth and bow thruster, respectively. The required thrust is reported in blue and actuated with a red dashed line. For both allocations, the time histories of azimuth propeller thrusts are about 0.1; for the thrust optimised allocation, the mean required thrust value is lower than 0.1. It means that the required azimuth thrust is below 10% of the maximum available. Instead, the time history of the required thrust of the bow thruster presents several spikes greater than 1, which means that the controller asks for something not available and works in saturation. This aspect is a well-known issue; indeed, the bow thruster

is the bottleneck in terms of available thrust in a real system. This is a critical aspect; indeed, the mean thrust value required for bow-thruster is very close to 1; with a static approach, exceeding the value of 1 means that the system cannot maintain the set position. On the other hand, the dynamics approach could maintain the ship within the allowable positional limits working in thrust saturation for a brief time. Generally, the bow thruster working point is the bottleneck of force allocation because the bow thruster's maximum thrust is much lower than the azimuth one, so it has to work near its maximum thrust. Moreover, the difference in requested thrust is clearly distinguishable for the starboard thruster. Indeed, in the optimised thrust allocation, the requested thrust is less oscillatory with a smaller magnitude than fixed angle allocation, where the required thrust is not optimised.

In Figure 36 and Figure 37, the time histories of the azimuth angle are reported. Also, in this case, the difference between the allocations is clearly distinguishable. Indeed, the azimuth angle value for the thrust allocation, for both portside and starboard side, continuously oscillates within a maximum range of 30°. Such oscillations in a real scenario could cause the azimuth moving mechanisms to malfunction and wear. On the other hand, the angles do not change during the manoeuvre for the fixed angle allocation.

Figure 38 and Figure 39 are composed of three subplots in which the required (blue line) and actuated (red dashed line) forces and moment are reported. Within the same figure, also reported the environmental forces and moment (black dashed line). X, Y and N converge to the environmental disturbances; this means that the actuators succeed in counteracting environmental disturbances and maintaining the desired position. All these forces and moment are evaluated along $\underline{b}_1$, $\underline{b}_2$, $\underline{b}_3$. The saturation effect comes out, particularly in the moment time history. Indeed, the number of requested moment spikes is due to the bow thruster's behaviour, described in Figure 34. Moreover, the number of bow thruster spikes is greater than the fixed angle allocation for the optimised thrust allocation. Indeed, it is possible to notice three not fulfilled spikes for the requested moment in 300, 550, and 1100 s corresponding in Figure 35 to the requested bow thruster thrust greater than 1.

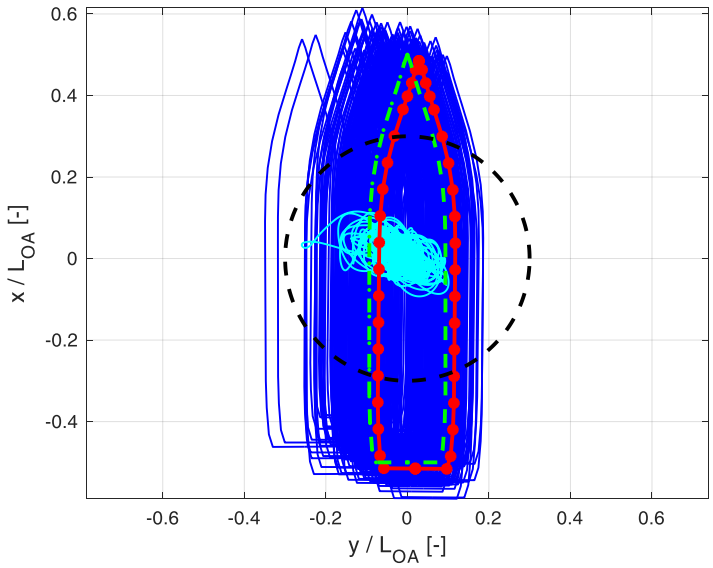

Figure 30. Dimensionless path – thrust optimised allocation.

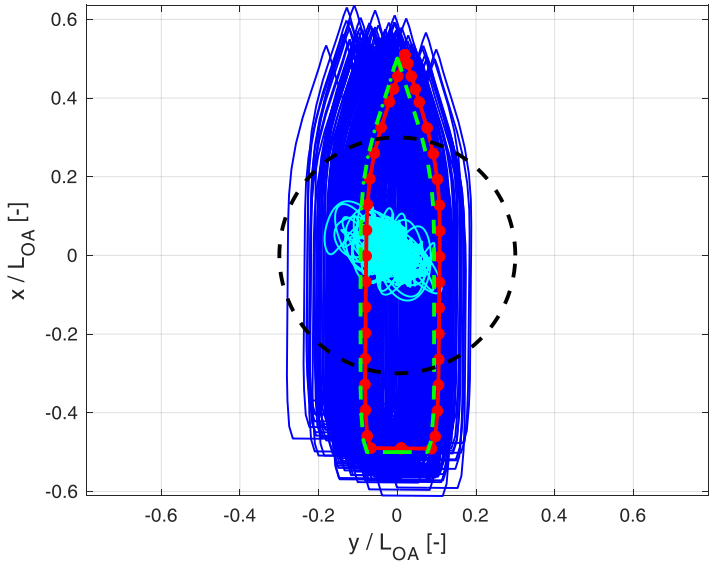

Figure 31. Dimensionless path – fixed angle allocation

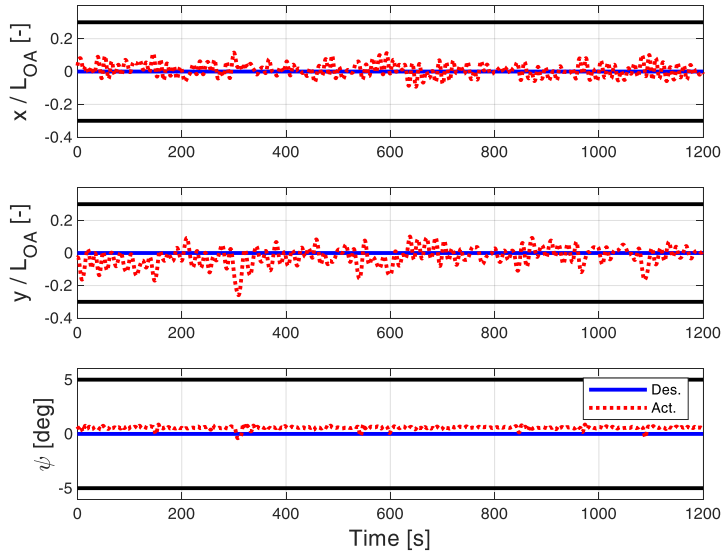

Figure 32. Dimensionless displacements – thrust optimised allocation.

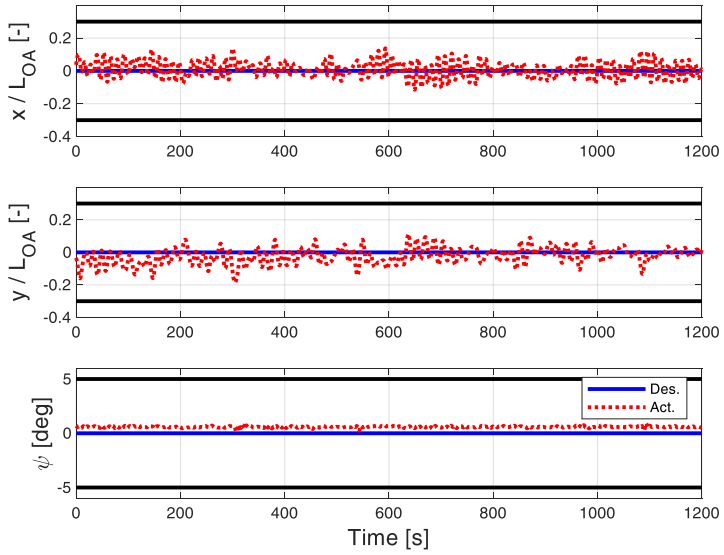

Figure 33. Dimensionless displacements – fixed angle allocation.

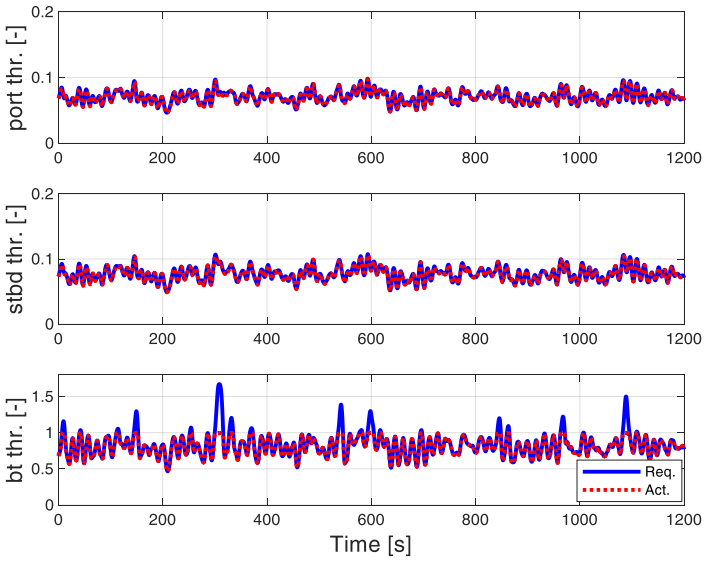

*Figure 34. **Dimensionless thrust** – thrust optimised allocation.*

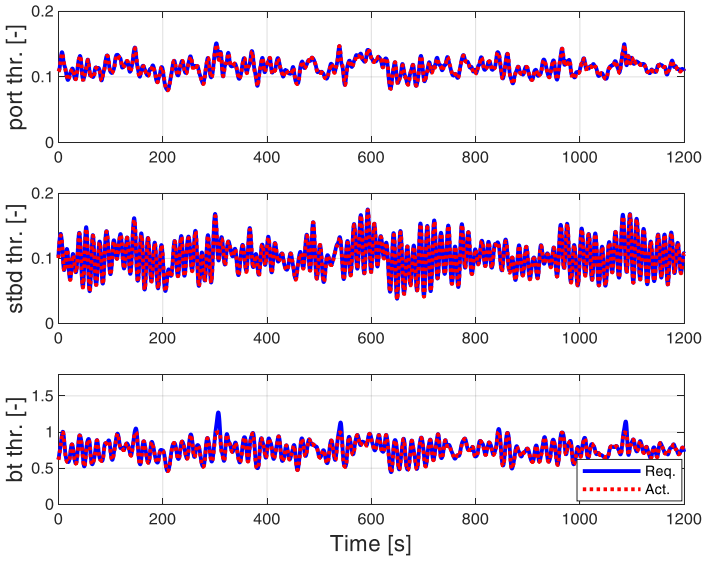

Figure 35. Dimensionless thrust – fixed angle allocation.

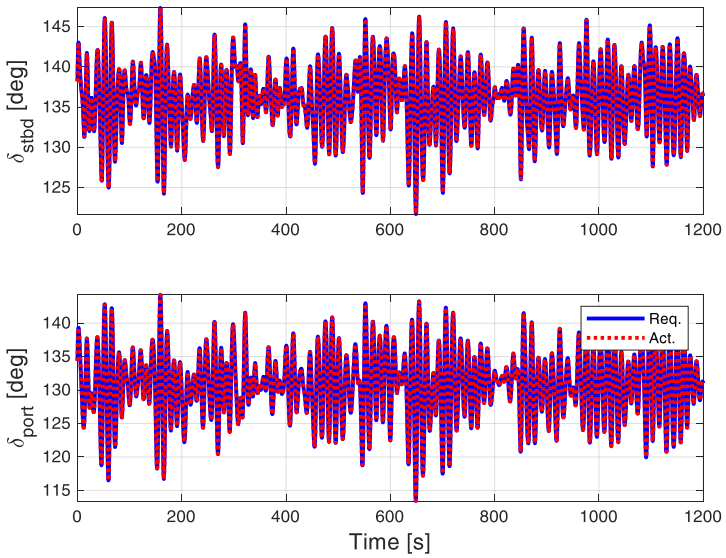

Figure 36. Requested & actuated az. angles – thrust optimised allocation.

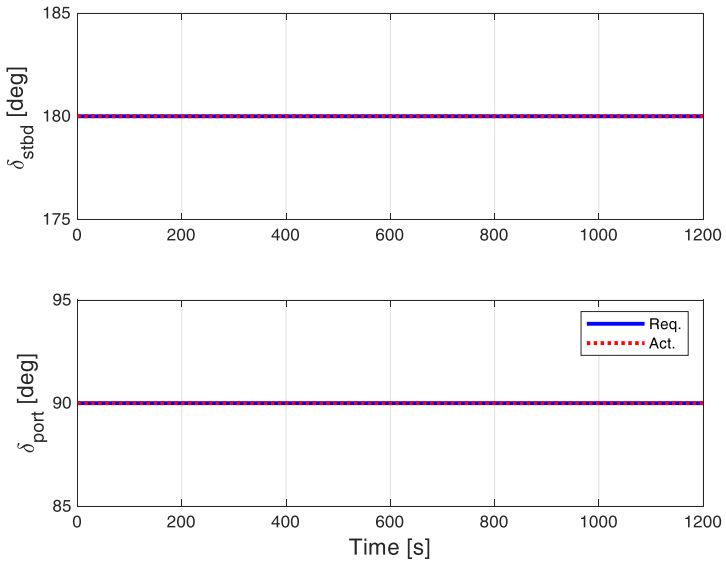

Figure 37. Requested & actuated az. angles – fixed angle allocation.

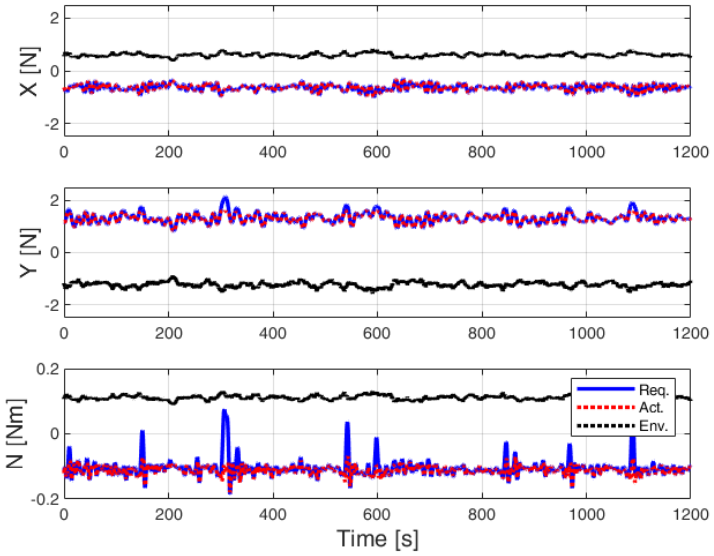

Figure 38. Requested, actuated & environmental forces and moment – thrust optimised allocation.

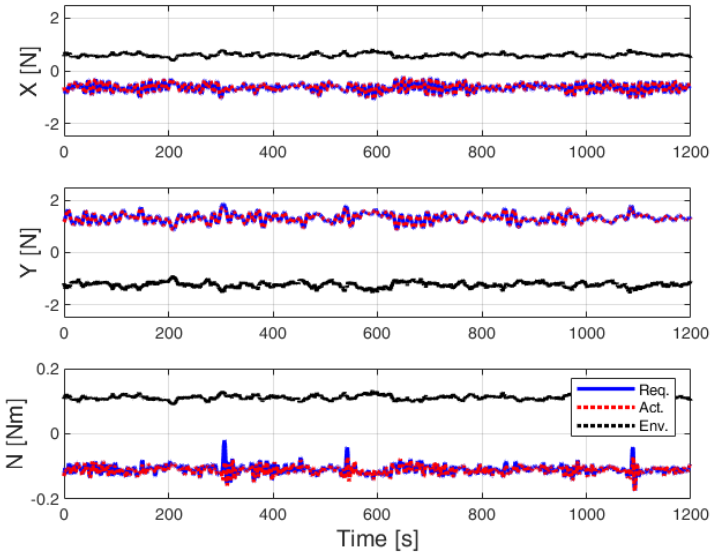

Figure 39. Requested, actuated & environmental forces, moment – fixed angle allocation.

4.3.4 Overall DPCPs Results Analysis

A comparison between the static and dynamic approach as well as for the two allocations designed is shown in Figure 40 to appreciate the variations in performances. The results shown are reported by employing a bar graph as a function of the main direction of the disturbance. In particular, the first bar (blue) represents the performance regarding the static, fixed angle position allocation, the second (red) shows the same allocation evaluated with the dynamic approach, the third (yellow) concerns the static thrust optimised allocation and finally, the fourth (purple) shows the same allocation evaluated with the dynamic approach. Moreover, they are reported in a dimensionless form by using the value relating to the static, fixed position allocation; for such a reason, the first bar will always be equal to 100%.

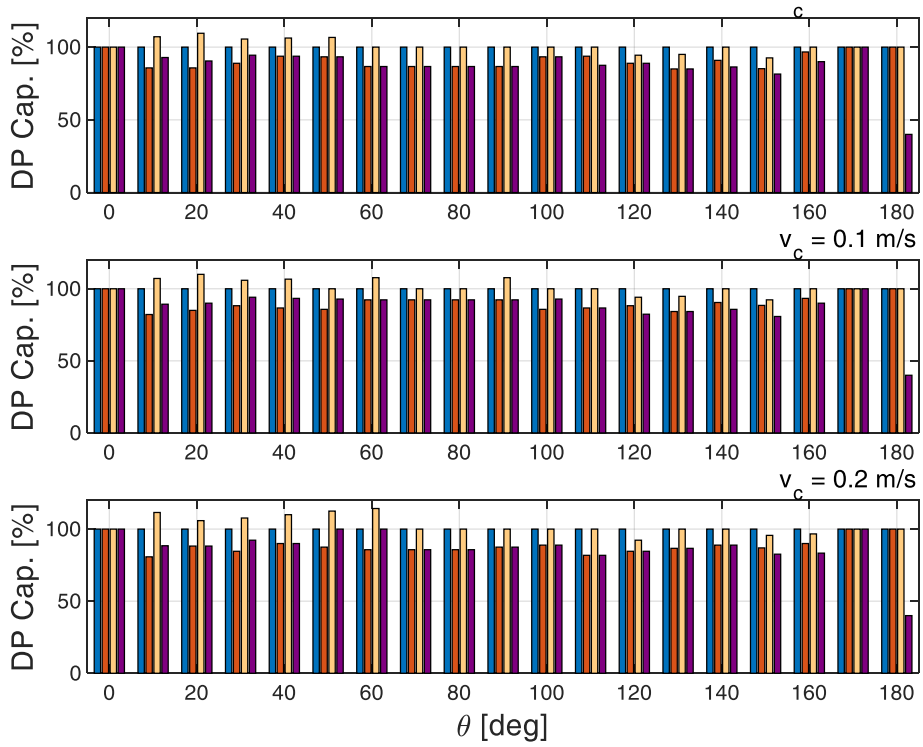

Figure 40 DPCP different approaches comparison

It can be observed that when the disturbances act in the bow quarter, the thruster optimisation allocation has a better performance behaviour of about 20%. On the other hand, the situation is the opposite in the aft quarter, and the margin is

less evident. In any case, as could be expected, the performances obtained through a dynamic approach are always lower than the corresponding statically assessed allocation. Furthermore, it is important to underline the difference in expected performance between the static and dynamic approaches. Indeed, the DP operators can overestimate the system capability with potential hazards for life, goods and system at sea.

Moreover, the importance to conduct a DP dynamic analysis is highlighted whenever the system performance in a realistic environment needs to be evaluated. The differences between static and dynamic approaches concern four main aspects: (i) environmental disturbance oscillations in both magnitude and directions; (ii) the influence of transients, in particular the controller behaviour, which is not considered in the assessment of the DP system capability, but affects performance during changes in environmental conditions during operations, (iii) the propulsion actuation delays, since, all the propulsion plant machinery have their response time; (iv) the limits and constraints of both machinery and DP system allowable errors.

Chapter 5

5.1 Sensor-based Collision Detection

As previously mentioned, the CA system is an essential element in developing a completely autonomous decision-making infrastructure and for achieving a decision support system. As shown in

Figure 1 and Figure 2, the CA system can be divided into three essential parts: obstacle detection, collision detection and re-planning route.

In a real scenario, the commonly used sensors involved in collision detection for long distances are RADAR and AIS, but as described in the Collision Detection and Avoidance paragraph, both represent limits of applicability. Therefore, the proposed research focused on developing an obstacle detection and subsequent obstacle tracking system workflow based on experimental data gathered by a LiDAR sensor. Indeed, the choice of this sensor was made with a double motivation.

Firstly, since the case study is a testing model of about 1m in length and the sensor's operating range is around 100 meters, the situational awareness domain around the boat is 50 ship lengths of radius, which is considered an acceptable distance to perform evasive manoeuvres.

The second reason is that the data processing process can also be used on real boats, of small dimensions, with the same purpose or be used by ships over 100 meters in length for port manoeuvres or to detect and trace the quay accurately in order to develop an autonomous mooring algorithm.

In general, the research work regarding this topic aims to develop a decision support system in the maritime sector and contribute to the unmanned surface vehicle research field to avoid and prevent collisions, mitigate economic effects for environmental safeguarding, and increase safety during the port navigation and the mooring operation. In order to meet situational awareness, it is necessary to have precise virtualization of the surrounding environment; the environment must be acquired by means of a sensors system that returns a virtualized model of the surrounding objects.

Obtaining a virtualized model of the environment means having the ability to recreate a real-time copy of the surrounding environment that can be analysed

through mathematical procedures. In recent times, LiDAR devices have been increasingly used to achieve this purpose; in such a case, the virtualized environment coincides with a sensor's point cloud.

Detecting an object within the point cloud means grouping the points that are part of it and separating them from the other points; this can be achieved in many ways by adopting different models and techniques. The choice of method will be further explained in the following sections.

Regardless of the selected method, this procedure can occur in two main scenarios, static and dynamic. In a static scenario, such as a boat about to moor surrounded by stationary objects, it is sufficient to take advantage of the virtualization of the environment to recognize the surrounding obstacles and develop a path that ensures the mission without collisions.

Instead, a dynamic scenario is more complicated; the same boat that is preparing to moor is now surrounded by moving objects. It will no longer be enough to recognize the obstacles. It will also be necessary to track them over time in order to update the path chosen in real-time, basing the activity on the position, direction and speed. If the scenario is dynamic, the use of a tracking strategy provides the ability to obtain a time history of the position occupied by the objects, updated in real-time, and to keep the memory of other variables of interest.

5.1.1 Proposed Obstacle Detection Workflow

Recently, research on collision avoidance detection in the maritime sector has begun to be investigated and studied in detail, mainly with deterministic geometric approaches. Contrarily, in the automotive field, the developments concerning detection are much broader and are widely based on machine learning [173]. Indeed, sizeable datasets to train the learning algorithms are available in open access; KITTI and ApolloScape are mainly used [174, 175]. These datasets contain the LiDAR point clouds, images, and positions data. These types of data are used in the deep learning approach [176, 177]. In particular, Convolutional Neural Networks (CNNs) are trained through the LiDAR point clouds to detect obstacles like pedestrians, cars, and trucks [178, 179]; clearly, this could not be used to recognise ships, buoys, yachts, and other floating objects.

The available marine dataset is not as widespread as the automotive ones; specifically, only one open-access dataset is available for the marine sector obtained by motorboats equipped with LiDAR, RADAR, infrared camera, and RGB camera sensors [180]. Moreover, no marine trained network is available for testing. Hence, nowadays, in the marine sector, the only way to use a machine learning approach based on a LiDAR point cloud neural network is to train a new one. The side effect is that training a neural network is a profoundly time-consuming activity, and a specific experimental campaign to collect data is needed. This critical aspect is widely felt; indeed, several studies regarding the maritime sector that show different approaches can be found [181, 182, 183]. For such reason, an alternative approach based on only LiDAR point clouds data has been developed. The proposed workflow is shown in Figure 41.

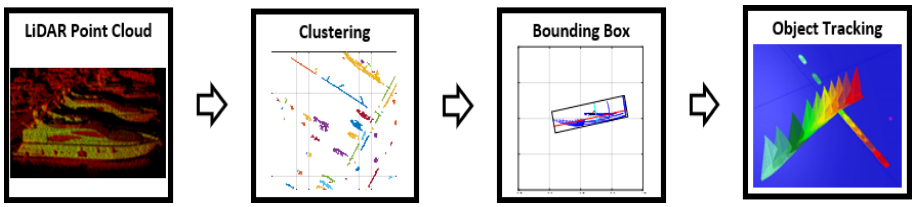

Figure 41. Unsupervised learning approach

5.2 LiDAR Sensor and Point Cloud

In general, the LiDAR sensor, previously described, lets to know the surrounding environment by means of infrared laser beams. In detail, the positions and shapes of surrounding objects are described by points located at the contact points between the laser beams and the environment surface. The data are contained in a point cloud structure in which spatial coordinates (x, y, z sensor reference) and intensity (as a function of colour, shape, and laser encounter angle) are available for each point acquired. Generally, the output includes both the position expressed in spherical and cartesian coordinates, where the origin represents the position occupied by the LiDAR and axis or angles are defined depending on the device.

The numerical array is produced for every scan. Each acquisition corresponds to a complete revolution of the rotor. As a result, the points of the same scan relative to different azimuth angles are not acquired simultaneously. In

particular, a quantifiable delay based on the frequency is present and assumes maximum values between the points acquired at azimuth angles equal to 359 ° and 0 °. Such an issue could imply evaluation errors in dynamic scenarios; fortunately, the relationship between the speeds involved and the acquisition frequency allows this phenomenon to be negligible in the marine field.

The LiDAR output can be typically organized in two distinct forms to assess obstacle detection tasks, organized or non-organized. A non-organized output is the raw standard LiDAR output. Each characteristic, e.g. x, y, z, distance and intensity, is collected in a column. Indeed, a complete scansion is represented as a 2D matrix *Aij* where each data of the *i-th* point is reported in the specific column j. The representation is the following in Figure 42.

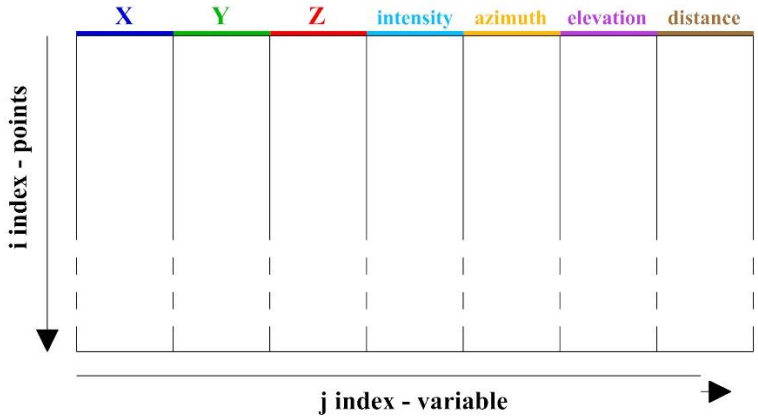

Figure 42. Raw LiDAR output

Instead, an organized LiDAR output associates a matrix to each characteristic, where values are rearranged by pitch and yaw angles using the spherical coordinate frame. As a result, a complete rotation output is represented by 3D tensor *Tijk*, Figure 43, where each layer k represents a characteristic and the matrix *ij*, is filled with the value of *k-th* characteristics as a function of i value of pitch and j value of yaw angles. The organization of the variables in matrixes and the output obtained is strictly related to the device's characteristics.

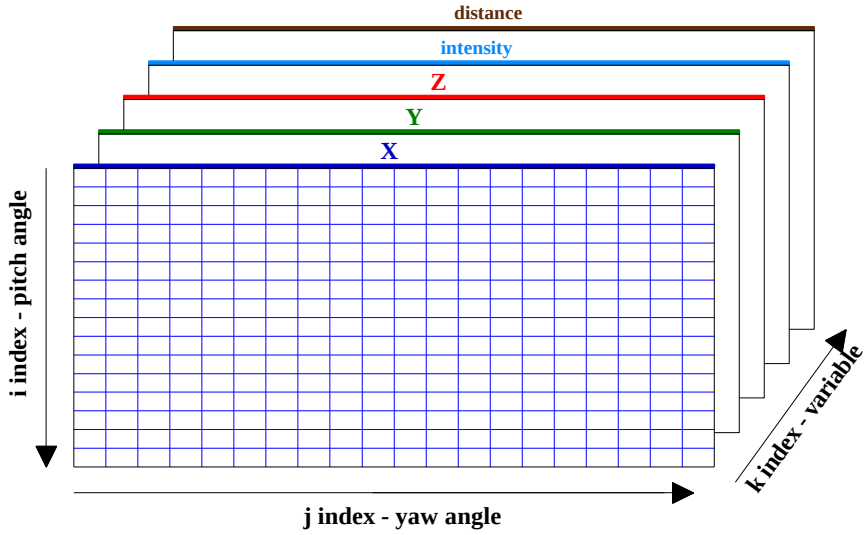

Figure 43. Spherical LiDAR output rearranged

To conclude the discussion, the same scenario, a harbour data collection, is reported by means of the two different approaches. In the first case, the unorganized point cloud is displayed using Cartesian coordinates by changing the colour of the points as the detected intensity varies.

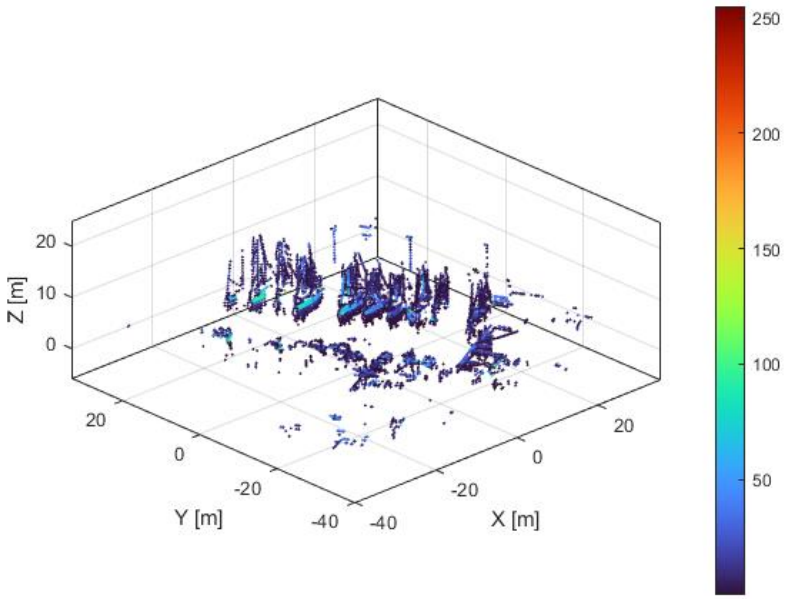

Figure 44. Unorganized LiDAR point cloud

In the visualization of the organized data, the single matrices are plotted as images, one for every characteristic. In fact, this method is used for fed CNNs since the point cloud rearranged in this way is a low-resolution image.

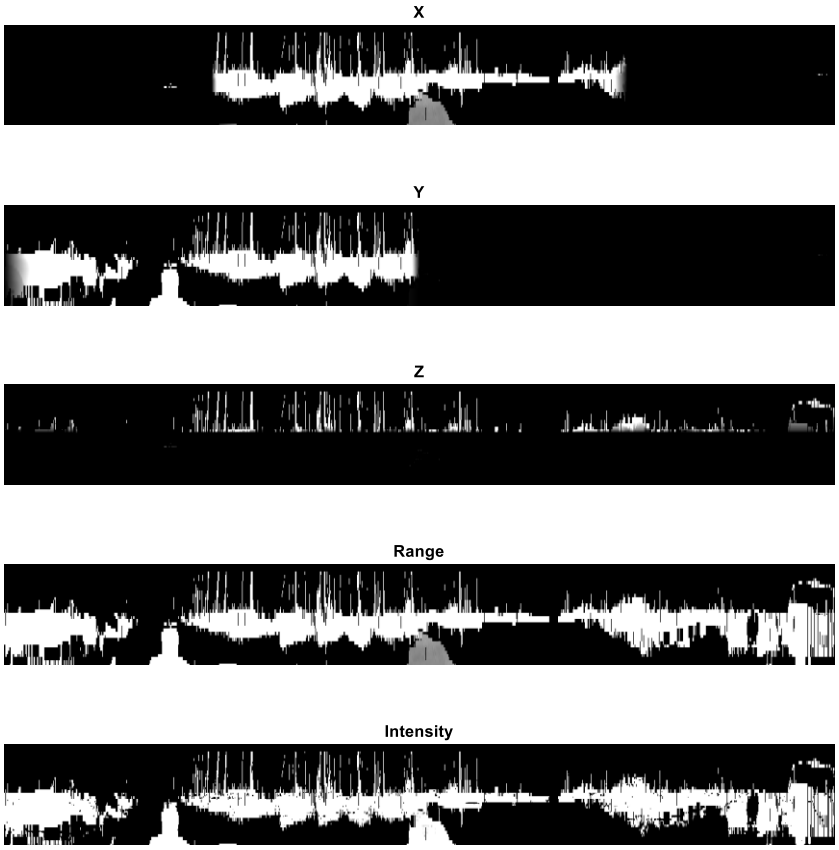

Figure 45. Organized LiDAR point cloud

5.2.1 Synthetic Scenario

The lack of a large available dataset in the marine environment forces the acquisition of multiple point clouds and relative images to develop and test the algorithms and tools necessary to carry out the activity. The possibility of having a tailored dataset of fast construction was one of the main objectives. In particular, this allows users to obtain a wide variety of datasets reducing the efforts significantly. Moreover, LiDAR data can be created indoors without

misspend, economic and time resources. In addition, LiDAR equipment is not necessary. For these reasons, a procedure designed to extract point clouds compatible with LiDAR technology from a virtual environment has been developed. The desired scenario has been built by means of three-dimensional modelling software. First, the LiDAR acquisition system is virtualized by drawing straight lines from the chosen observation point to mimic the laser beams. Eventually, the points are placed in the intersections between beams and objects.

The position of points is exported as a point cloud, and it represents a single LiDAR acquisition frame. In such a case, the point cloud is composed only of surrounding environment positions; the intensity is fixed to a constant value for all objects. This approach allows users to emulate several LiDARs and the different sensor settings, for instance, the rotor speed and the number of laser beams.

Moreover, this approach makes it possible to create a rendered image related to the acquired scenario. The desired materials and backgrounds are assigned, and the image is rendered. The possibility of customizing the product is wide. By acting on the parameters available in the rendering environments, it is possible to virtualize any image acquisition tool by imposing its technical specifications.

The extreme usefulness of this method lies in the possibility of total customization of the scenario; for example, it is possible to build a series of acquisitions in which one or more boats move by simulating path, manoeuvre or speed tailored to a specific required activity. Therefore, the proposed procedure results are an image-point cloud pair obtained relatively quickly.

Eventually, it is possible to reproduce any scenario acquired with any instrument for which the technical specifications are available. Despite countless advantages, the results produced by a virtual approach do not consider the information related to the real use of LiDAR in a hostile environment such as the marine one. Several expected results, such as water reflections and data loss, cannot be simulated sufficiently accurately due to the nature of these events.

Furthermore, it is not possible to directly impose the reflectivity of the laser beam inside the point cloud structure since the intensity is not a geometric parameter. However, it can be included in the point cloud structure with a post-processing activity. Nevertheless, it is challenging to accurately emulate the intensity acquired by a LiDAR in a real environment. Eventually, if the intensity must necessarily be used, the proposed approach presents some limits.

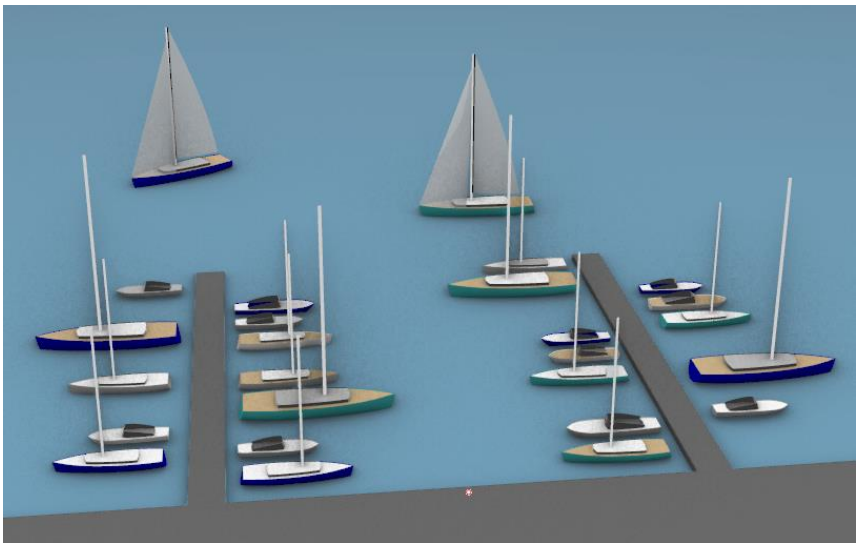

Figure 46. Synthetic scenario

5.2.2 Experimental Campaign

Several collections of LiDAR point clouds were carried out in the marine environment in order to obtain a real dataset, including real scenario noise. The main interest concerns obtaining a real dataset of lidar point clouds coupled with RGB images in order not to create an own dataset to be used in future developments to train a neural network fed with LiDAR data points and images, similar to the automotive sector.

An RGB camera (Nikon D7200) and LiDAR support has been created and printed by a 3D printer, Figure 51. In such a way, it is possible to know a priori the exact distance between the camera and the LiDAR. This information is crucial for the calibration procedure in data-fusion activity.

The data were acquired under different conditions within the Gulf of La Spezia. The main ones are:

1. static LiDAR position on the quay, acquiring static boats.
2. moving LiDAR position onboard of a motorboat, acquiring static boats.
3. static LiDAR position on the quay, acquiring fixed obstacles and navigating boats.

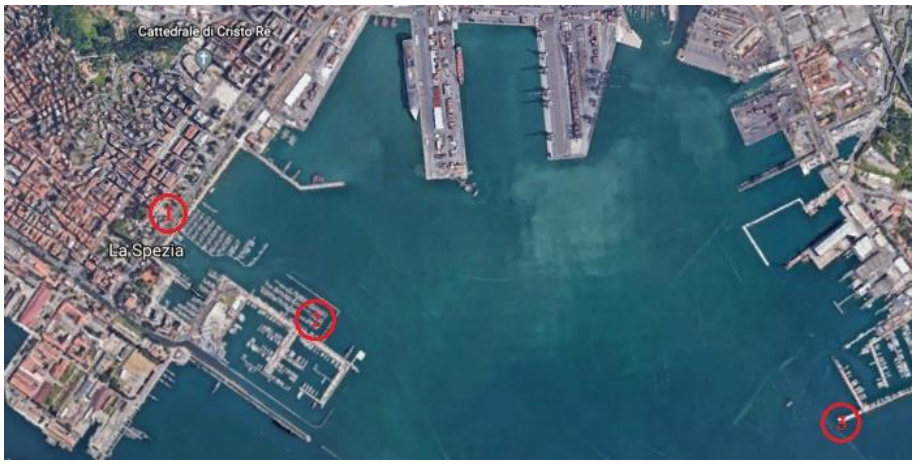

Figure 47. Data collection spots in the Gulf of La Spezia

In addition, a further experimental campaign was carried out during sea trials carried out on the Teseo I motor ship for research purposes at the Tringali shipyard near Augusta. The project involved remote control of the ship and tested an autonomous track-keeping system. The test was supervised in case of navigation system failure. A bridge operator aboard the motor ship could take control of engines and rudders.

During the aforementioned, the University of Genova recorded the surrounding environment described by a cloud of points and the GPS track with relative speed and ship rotation using a LiDAR device and inertial platform, respectively.

The LiDAR point cloud and the GPS track are reported in Figure 49 and Figure 50. In order to collect this data, mounting support containing both LiDAR and IMU was designed and printed using a 3D printer. This holder was carefully mounted on the ship that would allow for data recording, as shown in Figure 48

The undersigned wishes to thank SEASTEMA S.p.A (Fincantieri NexTech). for providing the possibility to participate in the sea trials. Furthermore, many thanks also to all Cantieri Tringali Srl staff for the help received during the sensor installation phase and for hospitality.

Figure 48. LiDAR and IMU mounting platform setup

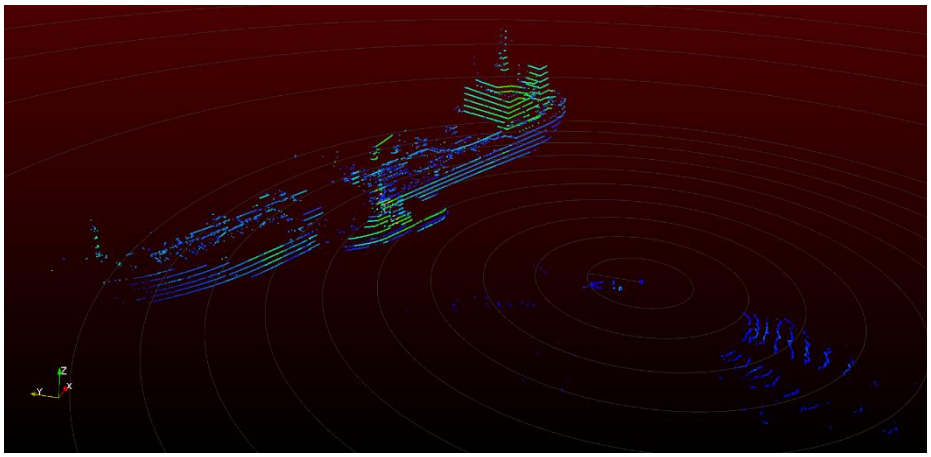

Figure 49. LiDAR point cloud - ship and tug

The LiDAR point cloud describes a 100-meter chemical tanker and a tugboat alongside its left side. At the bottom right, blue points representing the wake of Theseus I are present, the discussion on the noise acquired by the LiDAR has been carried out in the following paragraphs. The LiDAR was positioned in such a way that the Theseus I was not acquired

Figure 50. GPS track

Regarding the data collection campaign carried out in the Gulf of La Spezia, the first acquisition activity was the data collection of static objects with a static lidar spot in chronological order. As discussed in the following chapters, this has been useful to test and choose clustering algorithms. Subsequently, in order to investigate scan behaviour data gathering for a moving spot, the LiDAR was mounted on a small motorboat. The point clouds were acquired by sailing between boats quay moored. The acquisition of such a dataset will be helpful in future developments, including a possible Inertial Measurement Unit (IMU) to evaluate ship movements, as carried out during the Augusta sea trials, in order to adapt the acquired point cloud in a dynamic scenario. Eventually, a dataset of boats in motion acquired from a fixed location was carried out. The latter was the most relevant acquisition campaign because it allowed obtaining a dynamic dataset suitable to test the multi obstacle tracking algorithm on a real scenario with real environmental noise.

Figure 51. Camera and LiDAR experimental setup

The scanning frequency of the LiDAR was set to 5 Hz, guaranteeing a horizontal resolution of 0.09 °. The considered FOV is 360°. The camera was mounted to point in the -Y direction (for LiDAR axes).

Three coupled LiDAR-camera outputs are shown hereinafter; The RGB images are shown in Figure 52 (a), while the corresponding point clouds are shown in Figure 52 (b) by using cartesian representation, considering a 2D visualization, and coloured as a function of the intensity value. For the sake of clarity, the point clouds were reported in two dimensions, the XY plane, squeezing the z dimension. The experimental acquired scene was exploited to develop, test, and validate the tracking algorithm, as detailed in the following sections.

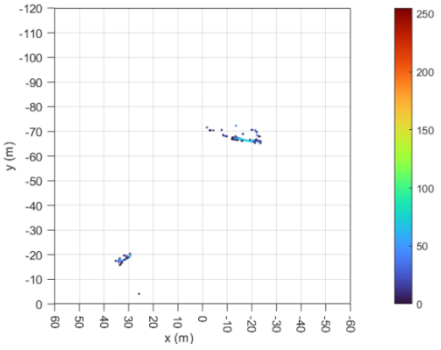

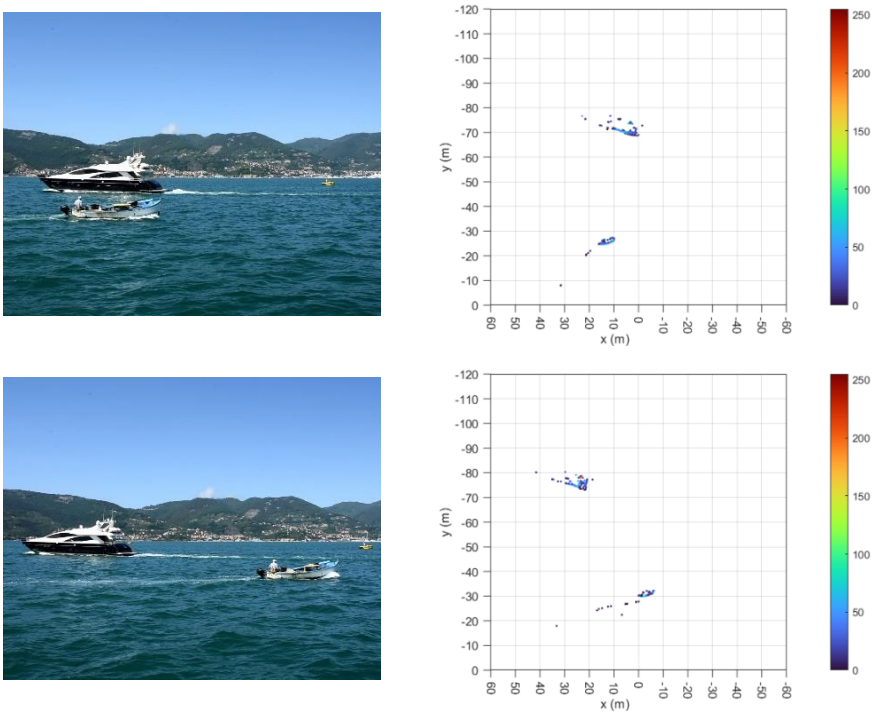

(a) RGB images *(b) 2D point-cloud*

Figure 52. RGB images and LiDAR point clouds coupled

A sudden change in shape can be noticed by analysing the point cloud describing the black motor-yacht due to the boat's position. In the first scan, mainly the left side is acquired, while the further the boat moves away, the fewer points acquired in the bow area, and the transom begins to be acquired.

During the on-field acquisition campaign, several phenomena were noticed. The first and probably the most relevant information found was the impossibility of acquiring seawater. This allows for a much cleaner scan than a similar one performed in an urban environment; in the marine scenario, the point clouds that describe the acquired objects are well-separated thanks to the empty spaces determined by the presence of the sea.

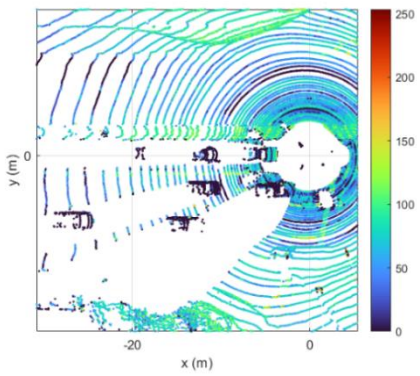

Figure 53. Urban environment

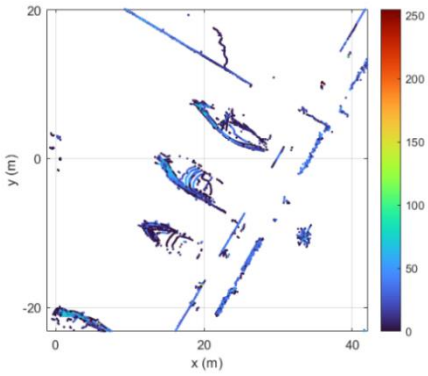

Figure 54. Marine environment

Figure 53 and Figure 54 show the LiDAR point cloud represented in 2D in an urban and marine environment. It is possible to notice how boats are well separated to respect cars and how the point cloud that describes the marine environment acquired is globally less populated. This characteristic means a lower computational effort due to the non-need for post-processing activities to eliminate the street plane, as happens for the ground in urban scans. Moreover, a marine scenario during navigation in open water has a lower number of points. Despite this great advantage, acquisition in the marine environment also presents drawbacks. While it is true that seawater is not acquired, this only occurs in calm sea conditions. The wake produced by boat motion and the breaking waves generates noisy points. The noisy points due to the wake that do not belong to the boat are acquired in the sea immediately abaft the vessel, distorting the point cloud that describes the object in both position and dimension. This issue is notable in the point cloud projected in 2D in Figure 56. For the sake of clarity, the relative image RGB has been shown; in Figure 55.

Figure 55. RGB wake boat

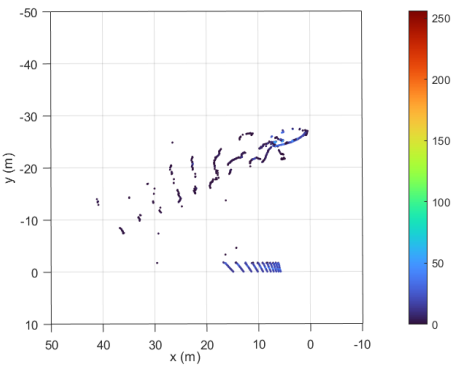

Figure 56. Noisy point due to boat wake

Another negative aspect linked to the marine environment is the reflection of points below the boats belonging to the sea. The characteristic of noisy points due to reflection is very low intensity. Moreover, several moored boats were acquired together with points mirrored below the sea surface. A schematic representation of the reflection phenomenon is shown in Figure 57, while an acquisition that presents this problem is shown in Figure 58.

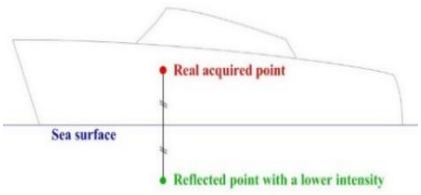

Figure 57. Representation of the reflection phenomenon

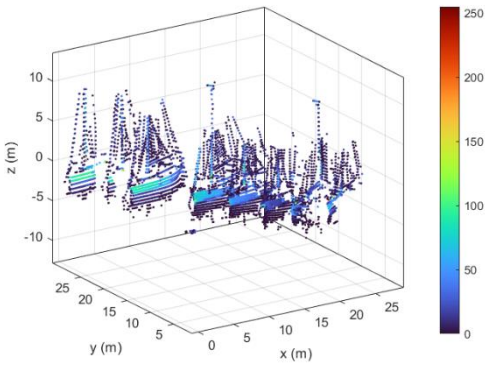

Figure 58. boats characterized by underwater reflection.

The last problem detected is not attributable to the presence of the sea but to the data acquisition method itself. Remembering that the intensity of the signal received by the instrument is linked to the object's reflectance, it is inevitable that objects of different colours are characterized by different intensity values

of the acquired points. This aspect is emphasized in the presence of black objects; in particular, a black object is characterized by a higher number of lost points and an intensity value on average much lower than objects of other colours.

Fig. 66 shows the reference RGB image and the point cloud that describes a white motor-yacht (top) and a black one (bottom). It can be noticed how the point cloud poorly describes the black motor-yacht; in particular, the lower black painted hull is completely not acquired. The only part quite well-acquired is the white superstructure. Moreover, even for the white yacht, the black glass components are not well acquired or are characterized by a lower intensity value.

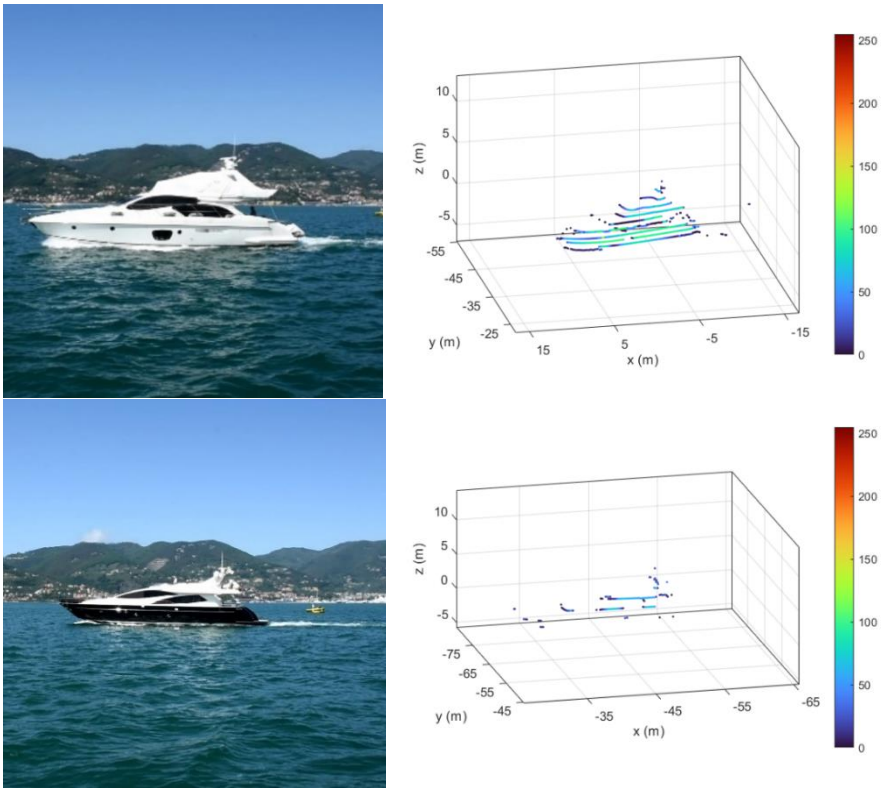

(a) RGB images *(b) Point cloud coloured by intensity*

Figure 59. LiDAR point cloud intensity comparison

This problem needs special attention. Each sensor has pros and drawbacks. Indeed, it is characterized by peculiarities that also determine its weak points.

A data-fusion activity with other sensors, for instance, RGB and IR cameras, would solve the deficiencies of a single sensor. The acquisition of such a large dataset in terms of point clouds and RGB images is a starting point for potential future activities to solve the lack of marine datasets.

5.3 LiDAR Point Cloud Data Processing

The LiDAR point cloud must be analysed to individuate objects and obstacles that populate the acquired environment. Object Detection is a common task discussed in Data Science (DS), specifically within Machine Learning (ML). There are two main approaches within the ML to achieve object detection: supervised learning and unsupervised learning. The supervised learning identifies an under-guidance ML method that uses a trained model able to recognise information patterns within a dataset. A priori knowledge has to be used as input; the model relies on a priori labelled training data from which the algorithm "learns" how to make accurate predictions. After the training period, the algorithm is ready to forecast on an unlabelled dataset. Supervision means that during the training of the model, the set of samples (or datasets) and the desired output signals are already known because they were previously labelled; in other words, a large dataset of input and output must be available a priori. Supervised learning methods are identified in Regression methods and Classification-Localization. In particular, Classification-Localization algorithms are used to locate and predict the label or the class of the desired target (or more than one) in a dataset; the most used algorithms, which are becoming increasingly popular in this period, are Artificial Neural Networks.

Unsupervised learning identifies techniques capable of observing the data structure and extrapolating meaningful information without requiring a training activity on known input-output pairs. The algorithms, therefore, find patterns in the dataset without requiring any guidance. The main techniques used are Clustering and Data Dimensionality Reduction. There is a considerable variety of Clustering algorithms oriented to different fields of analysis. Indeed, Clustering analysis allows the creation of groups of points based on their similarity, usually geometrical. Dimensionality Reduction is a learning technique used when the number of features (or dimensions) in a given dataset is too high. It reduces the number of data inputs to a manageable size preserving data integrity. Finding a new reference frame for a dataset with a lower number of features is a task achieved by a Dimensionality Reduction technique.

5.3.1 Clustering Activity

The clustering activity represents a task achieved by various algorithms that differ significantly in the manner of cluster construction. It is used for multiple purposes with various types of data. In the case study, the LiDAR point clouds as been used as input for several cluster methods. In particular, the point clouds have been analysed through different cluster patterns. The cluster activity consists of group points belonging to the same objects, separating them from other groups and the background. The points belonging to the same cluster share a similarity that could be geometrical or another aspect. In the proposed activity, the clustering algorithms are used to identify, among the detected points, those that belong to a single object and separate them from other points that define different objects.

The automotive sector's clustering methods based on LiDAR point clouds are widely documented. Contrarily, the clustering activity regarding the marine scenario is poorly studied. Moreover, the analysis of the acquisitions in the marine environment shows some differences concerning the urban scenario that must be carefully considered. For instance, the calm sea is not acquired by the LiDAR. This characteristic behaviour implies that no background activity has to be removed, as happens in the automotive sector. Avoiding the removal of background activity improves the computational time and accuracy in distinguishing floating objects.

On the other hand, several points that do not correspond to real objects are acquired; this happens in water reflections, breaking waves or waves generated usually from high speeds boats. Such an issue can be solved by using noise filters explicitly built for this purpose. Furthermore, in order to decrease the computational time of clustering activities, the point cloud is projected on the x-y plane. Such simplification has been done because it is reasonable, and no information is lost. Indeed, two different objects are very rarely one over the other during navigation. However, a deck landing or navigation under a bridge scenario could be studied by imposing a filter along z axes to consider a potential obstacle and perform the clustering activity in 2D or consider a 3D dataset as input clustering to obtain the point groups. Several clustering methods have been used to analyse the LiDAR point cloud dataset. In particular, DBSCAN [184], K-means [185], and Euclidean.

In detail, DBSCAN is a clustering algorithm based on the concept of density-reachability. It requires two input threshold values, a distance ε, representing the radius length and a minimum number of points belonging within the radius.

The algorithm presents a refined conception of noise and a very effective cluster definition. However, it has several disadvantages in the case study. Since the algorithm is based on observations density, it lacks when the density is not constant as the LiDAR point cloud. Indeed, the rotating multi-beam LiDAR has laser channels that diverge with the distance, so the point cloud has a variable density.

Moreover, when the density of data changes as a distance function, the density threshold imposed as an input parameter cannot be optimized for the whole distance range. In addition, the data are less dense in areas further away from the observation point because many laser channels have already encountered an object at shorter distances. In order to overcome a dataset with a variable density, the DBSCAN original version has been modified to take into account a density-variable dataset. Different solutions are present in the literature [186, 187].

Even if it were possible to overcome the issue of density variation, the main problem regarding the DBSCAN clustering remains the high computational time, making the algorithm unsuitable for real-time application. The computational time depends on the scene complexity. For instance, in a port scenario, where there is crowding of potentially dangerous objects, a rapid computational time is required to detect obstacles avoiding the collision. For such a reason, the DBSCAN clustering method currently is not suitable for applications that must run near real-time.

K-means is a partitional clustering algorithm that subdivides the data into k cluster groups. A centroid or midpoint identifies each cluster, adopting a minimizing within-cluster variances logic. The algorithm converges when the assignment no longer changes. The K-means algorithm is very discussed in the literature, and many variants exist. Unfortunately, the number of clusters k is an a priori imposition data, so a substantial limitation of the algorithm is present when the k-number is not available.

The case study is a LiDAR acquired port scenario, and the number of clusters is an unknown a priori data; indeed, it is a desirable result to obtain from the clustering analysis. Therefore, using an algorithm thus conceived does not represent a good choice for the required task.

Starting from the knowledge of the DBSCAN and K-means clustering pros and drawbacks, another approach is possible by combining them to overcome their drawbacks and perform the clustering activity. Indeed, LiDAR point clouds represent large datasets and clustering them by using the DBSCAN method implies a long computational time. On the other hand, K-means is not the

optimal choice when clusters, k-number, are not available a priori. Therefore, a technique much discussed in the literature is to perform a down-sampling operation on the dataset using the K-means algorithm and then analyse the output with the DBSCAN method.

The original point cloud is substituted by a new point cloud composed of k points. A group of points is substituted by its mean, which is considered the point that represents that cluster. DBSCAN analysis is performed on the representative point cloud instead of the original one. In this way, the number k of clusters to impose in the K-means algorithm is not the final number of the group but an intermediate step to decrease the number of observations to be analysed with DBSCAN.

DBSCAN benefits from down-sampling, decreasing the computational time, while the problem of knowing a priori the number of final clusters is no more present for the K-means method.

The clusters number k to impose is an arbitrary value and identifies the level of down-sampling, an approximation of the scenario. Unfortunately, if the number of groups imposed in the K-means method is high, the simplified dataset will be very similar to the original one comporting a computational cost negligible during the DBSCAN analysis.

To decrease the computational time, the number of k clusters imposed must be small, and also DBSCAN benefits by reducing the observations to analyse; but this implies a very rough description of the scenario, leading to significant information losses. On the other side, to preserve an adequate description of the data cloud, the reduction of the observations must be limited. The whole operation is a compromise between time reduction benefits and information losses.

Contextualizing this aspect in the LiDAR-detection task-oriented to the collision avoidance in the marine environment, a detailed description of the scenario is required. The admissible loss of information must necessarily be limited. Errors in estimating size and position or the loss of an entire object can have severe consequences.

Eventually, the need to limit the subsampling of the data means time benefits are practically negligible, making the analysis time-cost comparable to the time required by the only DBSCAN on the original point cloud.

The last method analysed is the Euclidean distance clustering. The Euclidean approach is a sort of simplification of DBSCAN. It is based on the simple

Euclidean distance for the definition of the groups, segmenting within the same group the points at a reciprocal distance less than or equal to the threshold distance imposed. However, such a simple algorithm gives less accurate results and does not have a specific noise cluster. Moreover, it is subject to group propagation phenomena through bridging objects. The term bridging object refers to a series of acquired points connecting two clusters and determining their union into a single cluster.

However, it is affected in a non-incisive way by the variation in the density of points if the threshold distance value is carefully chosen, or in any case, it is less affected by the problem than the DBSCAN. The significant advantage of the Euclidean method is that, thanks to its simplicity, it has extremely low computational time. Furthermore, the algorithm can easily implement a conception of noise by imposing a minimum and a maximum number of points for acceptable clusters.

Although it is not a definition as sophisticated as DBSCAN, it works accurately in the scenarios under consideration. Indeed, problems related to propagation phenomena due to bridging objects are surely present in the marine environment, but only in harbours, where boats are not moving and are connected by ropes and fenders. In such a scenario, it is acceptable to obtain sub-segmentations with clusters that include many boats moored and stationary since the interest is related to the obstacle entity as if it were an extension of the quay. Indeed, when a boat starts moving, it separates from the group, its distance increases, the sea that LiDAR does not acquire isolates the points of the moving object, and it is immediately recognized as a separate cluster.

For the sake of completeness, the clustering activities by means of the experimental and synthetic LiDAR datasets have been conducted. Although, for the sake of compactness, the real scenario affected by environmental noise results have been reported and discussed.

5.3.1.1 Clustering results

The results of the different clustering algorithm methods based on LiDAR point clouds relatively a real harbour scenario is reported hereinafter. Figure 60 shows the 3D scenario, while Figure 61 reports the same scenario in 2D projection.

It can be easily noticed that the density of the observations decreases with the distance. Moreover, the shadow cones of the objects hit by the LiDAR channel are notable. This aspect gets better in the 2D projection, Figure 61. Since the points over a certain distance do not represent objects precisely enough, the scenario is cut at a reasonable distance of 50 m before the clustering analysis. The original dataset size is composed of 120000 points, in particular, 40000 points for three coordinates each. The dimension reduction due to the 2D projection let to process 80000 points. Eventually, after the region of interest cuts, the total number of points is 30000.

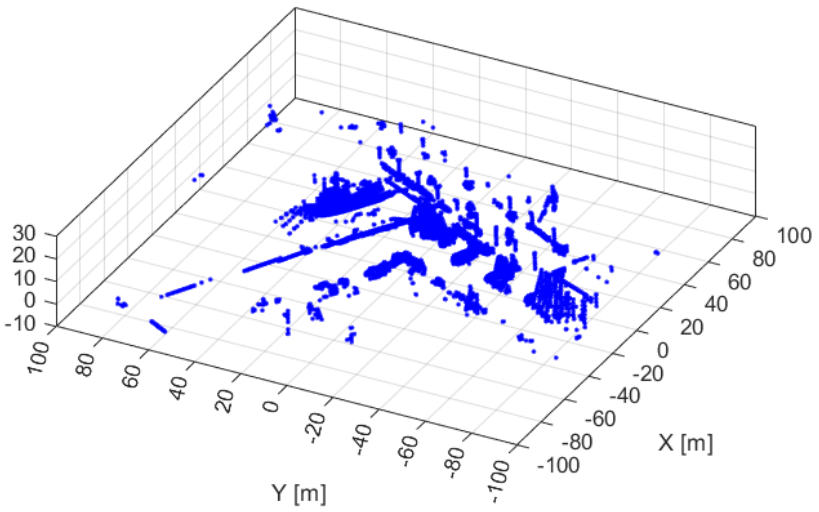

Figure 60. 3D representation of the real scenario.

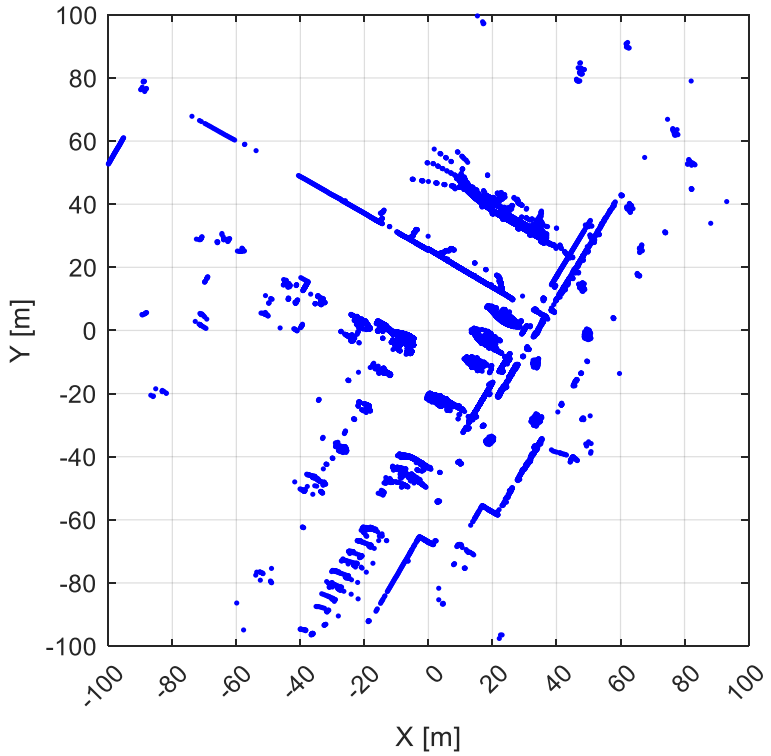

Figure 61. 2D projection of the real scenario.

Figure 62 reports the result of the DBSCAN analysis on the raw acquisition. Values used for the analysis are ten as the minimum point density and 1 m for the radius. The different clusters have been represented with different colours. Notably, the results are usable to perform the tracking activity. Using a standard office laptop, the computational time for such a scenario is about 15s.

Figure 63 shows the result of the DBSCAN analysis performed on the intermediate-step result of the K-means algorithm. The number of cluster k imposed in the down-sampling operation is 3000 in order to reduce the number of points by an order in magnitude. Input parameters for DBSCAN are the same as discussed before. However, the result is not as accurate as the one produced by DBSCAN or the Euclidean distance approach.

Figure 64 reports the result of the clustering analysis on the real acquisition of the algorithm based on Euclidean distance. The threshold distance value used is 1m and the minimum number of points to group them in a cluster is 20. Some boat moored is under-segmented due to the presence of bridging objects like

ropes and fenders and the nearness. The clustering results are comparable to the DBSCAN method, but in this case, the computational time is 1s.

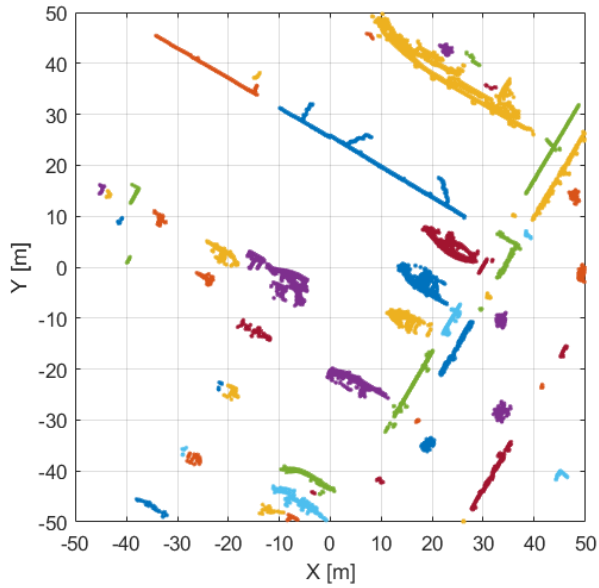

Figure 62. DBSCAN analysis on the real scenario.

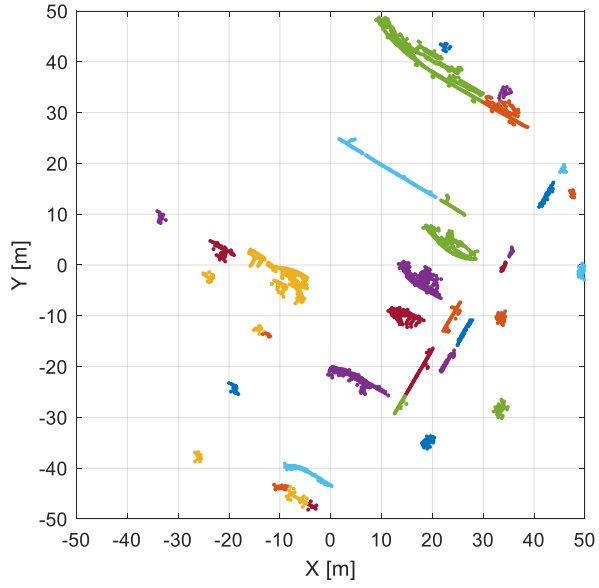

Figure 63. DBSCAN clustering analysis on real scenario down-sampled using K-means.

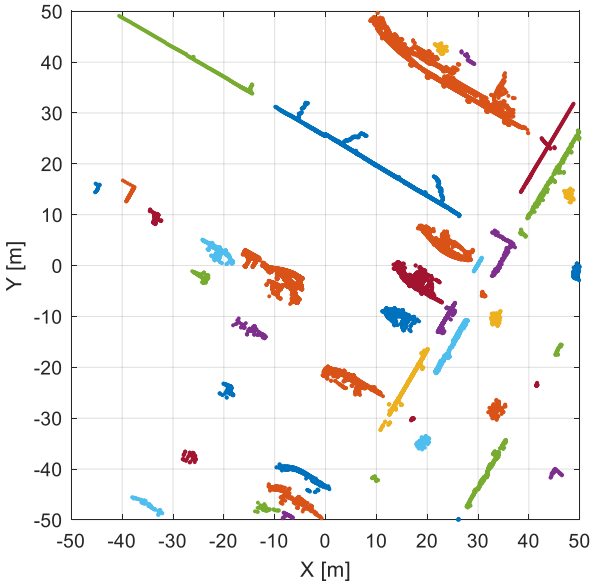

Figure 64. Euclidean distance clustering analysis on the real scenario.

Eventually, the presented results with different clustering methods are compared and discussed, focusing on accuracy and computational time. The clustering methods were conducted using a standard Laptop[1].

Figure 65 represents the time needed by the algorithms to perform the clustering analysis. The time is normalized on the computational cost of the Euclidean distance-based algorithm since it turns out to be the fastest in all conditions. It can be noticed that the time cost of the DBSCAN analysis performed on the down-sampled scenario is comparable to the one needed by the DBSCAN analysis directly on the original scenario. The results obtained show how the Euclidean distance-based algorithm guarantees a computational time lower more than an order of magnitude compared to the other; such runtime difference is mainly due to the simplicity of the algorithm, which adopts only one parameter (distance) contrary to the two parameters used by DBSCAN (radius and point density).

Furthermore, a higher computational cost of the synthetic scenario with respect to the real one can be noticed. Such a particular result is attributable to the presence of the quay, which is acquired through a high number of points; the

[1] CPU Intel Core i7-4510U 1.8 GHz, Graphics Nvidia GeForce GT 840M 4GB, 16GB RAM DDR3

greater number of points to be processed causes therefore an increase in the runtime despite the simpler scenario.

Figure 66 shows the number of clusters detected by the algorithms. The horizontal lines represent the likely number of groups that the algorithm should have produced. No distinct differences are present, even if it must be pointed out that the number of clusters is not itself a relevant parameter to identify the quality of the clustering activity since it strongly depends on the choice of input parameters of the chosen clustering method. It can be deducted that both algorithms show the same tendencies to over-segmentation in a marine scenario, such as those proposed. In particular, when the targets are at a great distance and are consequently poorly described, the algorithms are unable to form a single group, while for close targets connected by bridging objects, algorithms fail to perform the adequate separation.

In terms of accuracy, the DBSCAN and Euclidean methods produce comparable results, while the DBSCAN analysis based on the scenario down-sampled by the K-means method remains at an accuracy lower level. However, with the same accuracy, the choice of the chosen algorithm is Euclidean due to the lower computational cost.

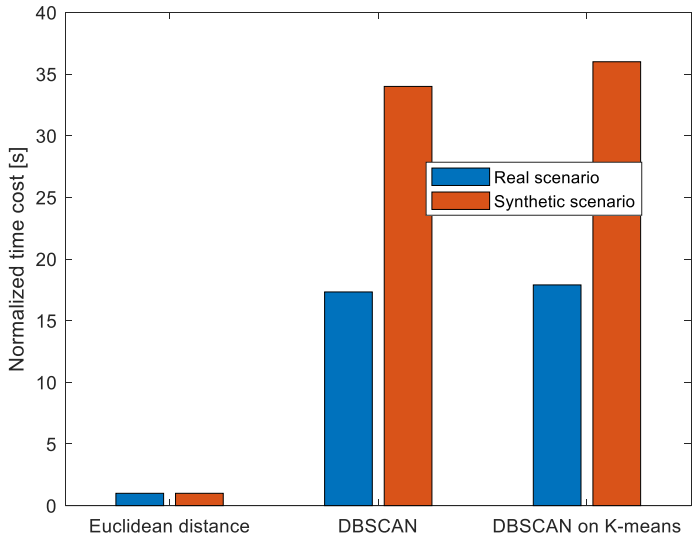

Figure 65. Normalized time-cost of clustering analysis for algorithms presented.

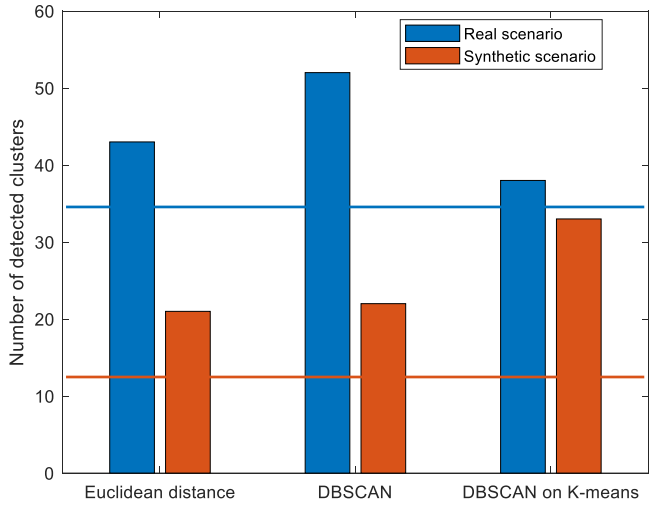

Figure 66. The number of clusters detected by algorithms.

5.3.1.2 Euclidean noise filter

In order to improve the Euclidean clustering accuracy performances, a filter concerning the marine scenario was added to the clustering method by pre-processing the dataset. Indeed, LiDAR acquisitions in the marine environment are characterized by anomalous reflection phenomena from the water. Indeed, despite the fact that the water is not acquired, the moored boats often present a noisy reflection that generates the acquisition of non-existent shadow points. Sometimes noisy points are located on the free surface of the sea, other times even under a sea surface. A similar phenomenon occurs during the acquisition of moving boat wakes or in the presence of breaking waves.

In a 2D projection, noisy points acquired due to reflection on water could increase the density of the moored boat points, which could be seen as an apparent positive contribution to the analysis. However, shadow points could also increase the dimension of the bridging object or create a false connection between objects, resulting in incorrect segmentation.

Points acquired in the presence of breaking waves or boat wakes always give a negative contribution to the analysis, leading to false boat dimensions and position.

For such reasons, a specific filter to solve these phenomena is needed.

Figure 67 shows a port acquisition where noisy reflection points are easily notable in dark blue. Indeed, the colours used in the image are proportional to the intensity of the reflected channel. So, a dark blue point means a low reflection intensity value. It can be noticed that almost all the noisy reflected points share the same colour, so the same intensity. This intensity hierarchy is true also for breaking waves, or boat wake acquired points.

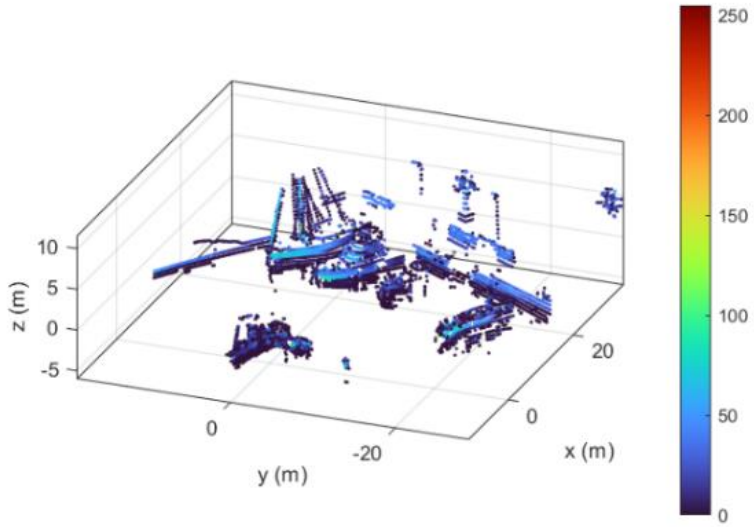

Figure 67. Detail of the noisy points acquired below the boat.

Although the point cloud is projected in 2D, the information on the vertical direction is still available. A filter that excludes points with a vertical position lower than a specific threshold value that identifies the sea level and, simultaneously, a value of intensity lower than the value that identifies noisy phenomena has been implemented. In this way, the detected sea points are deleted while preserving the points belonging to the hull that would be eliminated with a single filter on the vertical positioning.

The value of intensity that identifies noisy phenomena must be evaluated for each specific LiDAR device. The LiDAR used during the data collection campaign produces an intensity output value between 0 and 256. After an extended analysis of the acquisition dataset, it can be stated with sufficient precision that, in the case study, noisy points due to water acquisition share an intensity value of 90% below the value of 15. Increasing the lower intensity threshold value ensures eliminating all the water points, but this could also

affect low-intensity hull points near the sea surface, decreasing the total accuracy of the scenario. For such a reason, a value of intensity that identifies only water points is preferable. Indeed, the value proposed, equal to 15, means to accept losing about 10% of water points not to be erased. The water points that remain in the scenario, particularly those that are isolated from the others, are deleted by the post-processing noise algorithm that sets a minimum number of points to create a cluster.

A secondary, but not negligible, effect of eliminating noisy points is the decrease in the number of points processed by the clustering algorithm and, consequently, the computational cost.

Figure 68 and Figure 69it show the filter action on a moving boat characterized by a highly noisy phenomenon of waves and wake acquisition.

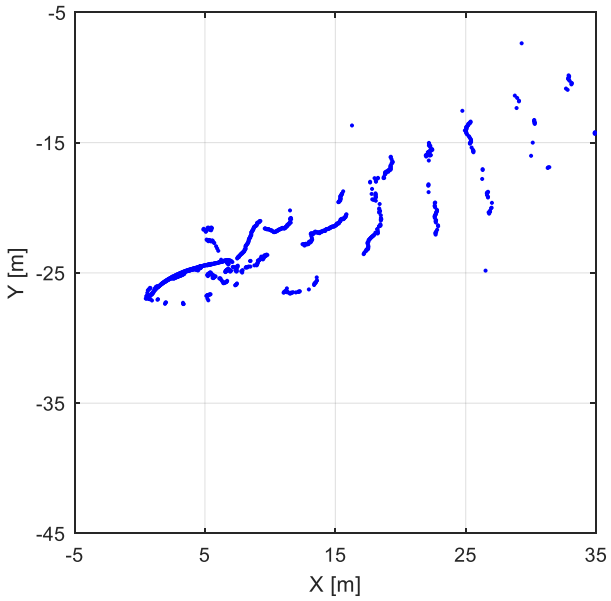

Figure 68. Boat acquisition with wake and waves noise production.

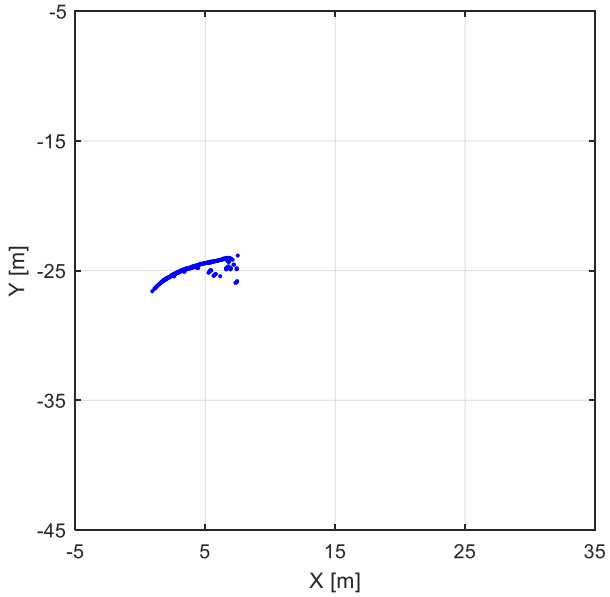

Figure 69. Filtered acquisition

5.3.2 Bounding Box Evaluation

The clustering algorithm labels every point that composes the LiDAR point cloud based on the geometrical aspect. Indeed, assuming that the LiDAR point cloud data is represented by an *m by n* matrix where *m* is the information from 0° to 359° for all laser channels and *n* is the information types (usually equal to 5, e.g., x, y, and z position, distance, and intensity), the clustering output is represented by column array (*m by 1*).

The task of the bounding box approach is to find a representative point for each identified clustered group in order to simplify the tracking procedure. Indeed, to track an object will be enough following its representative point. Therefore, the clustering output must be processed to obtain a single representative point for each detected group to achieve a tracking algorithm and assign a dimension and orientation to each group.

This procedure has been done via the bounding box (BB) approach to find its centroid.

The clustering procedure has been carried out in the x-y plane (2D dimension) for such a reason the BB procedure has been carried out in 2D to reduce the computational effort and facilitate the implementation of the process in a possible real-time system.

Many methods and procedures to obtain a BB starting from a point group are present in the literature. Some bounding box methods are discussed hereinafter to find a suitable approach for the case study application.

An effortless and fast way to enclose a group of points within a BB is based on the limit values of the cluster. In particular, the bounding box is built through 4 specific points. The box vertices are calculated as follows:

V_1: [x_{min}; y_{min}], V_2: [x_{min}; y_{max}], V_3: [x_{max}; y_{max}], V_4: [x_{max}; y_{min}]

where:
$xmin = \min(\boldsymbol{X})\,;\ \ xmax = \max(\boldsymbol{X})\,;\ ymin = \min(\boldsymbol{Y})\,;\ \ ymax = \ max(\boldsymbol{Y})$.

Furthermore, **X** and **Y** are the vectors of the x and y coordinates of the group, respectively. This method is straightforward and fast but leads to several critical disadvantages. First of all, the bounding box area is overestimated. Moreover, the bounding box is alienated from the global frame cartesian axis even if the object has the main dimension not aligned with them. Such aspects become more relevant when dealing with a vessel with a dimension much bigger than the other one, particularly when the main vessel dimension is acquired with a relative position, with respect to LiDAR, with an angle ± 45°. Therefore, a BB obtained in such a way could lead to a misrepresentation of the object geometry. The box centroid C (x_c; y_c) can be defined as the geometrical centre coordinates of the BB.

Figure 70 shows the bounding box obtained with the discussed method and its centroids. The BB does not accurately represent the clustered point group, and its centroid does not approximate enough the position of the real centroid of the object.

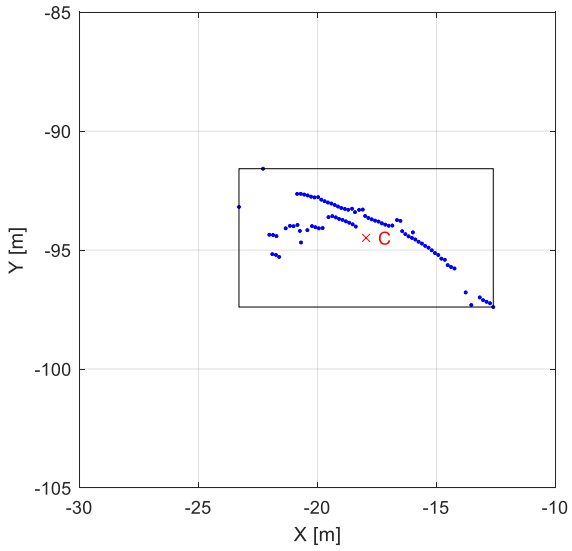

Figure 70. Max and min BB method

Another approach is represented by cuboid fitting [188]. Several methods discussed in the literature to obtain a bounding box are based on a geometric fitting of a figure on the points cluster. Procedures to fit a figure on a point cloud are available in many programming languages. In particular, the chosen method obtains a cuboid solid that better approximates a 3D point cloud based on an L-shape finding logic, and it also works in a 2D simplification. Since a fitting technique requires some iterations, it is not as fast as the min-max limits method.

The accuracy justifies the higher computational time in approximating the main dimension of the object with the cuboid. However, the L-shape fitting has been built specifically for the automotive environment. For such a reason, the L-shape cuboid fitting is not always easily detectable in the marine environment and could lead to some problems in the orientation of the cuboid when dealing with boats.

This method represents a good starting point for a first-hypothesis orientation of the bounding box. The geometric centre of the cuboid is considered the cluster centroid.

Figure 71 shows the result obtained with the discussed procedure. The bounding box is much more realistic than the one produced by the min-max limit methods, but it can be noticed that the box's orientation is not as accurate as expected.

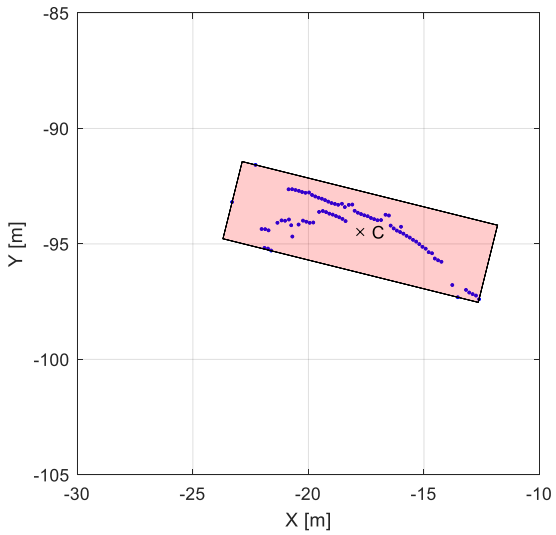

Figure 71. L-shape BB method

The last method is to build a BB based on the principal component analysis (PCA) [189, 190, 191]. In particular, the PCA is a dimensionality reduction method used to decrease the dimensionality of large datasets, preserving as much information as possible. The aim is to obtain a projection of variables in a new frame for whose directions the variance of the data is maximized. Principal components are computed under the uncorrelation condition, e.g. directions in which data are projected must be perpendicular. This identifies a cartesian system of the group in which the projected points can be used to compute the limits of the cluster extension in the new frame.

The main idea regarding the construction of the bounding box is to obtain the cartesian frame for which the variance of data is maximized. Projected data on the new frame is used to obtain the limits values for the directions under analysis (2 in the case study). Then, the bounding box's vertices are evaluated as a vector sum by using the limit points described in the new reference frame as boundaries. Also, in this case, the centroid is the geometric centre of the bounding box, as seen before.

Figure 72 shows the BB obtained starting from the PCA method. The geometric centre definition is much more realistic than the previously shown methods.

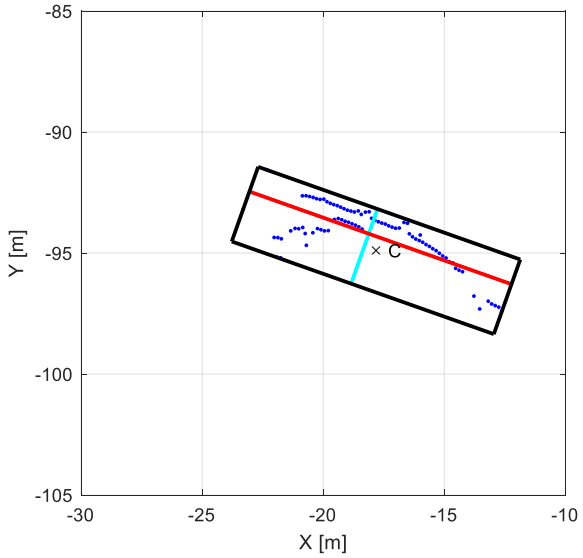

Figure 72. BB PCA method.

5.3.2.1 BB result comparison

In order to carry out a comparison concerning the discussed BB construction methods, a virtual LiDAR dataset has been prepared, as shown in Figure 73. Two different types of surface vehicles are modelled and located at different positions with respect to the LiDAR device. On the top, it is located the surface vehicle number 1 (12 m), in yellow, while at the bottom, in cyan, is located the surface vehicle number 2 (8 m). The vessel positions have been chosen to verify simultaneously two-point groups composed of points arranged very differently regarding the LiDAR device.

Indeed, the advantage of using a virtual scenario to identify a LiDAR point cloud is to construct the precise geometrical BB through the 3D software. Moreover, such aspect permits knowing the vessel BB, its centroid, and its orientation a priori, as shown in Figure 74 and Figure 75, in order to compare them with the results obtained by the previously discussed methodologies.

In Figure 76 and Figure 77 are reported the results obtained using the min-max limits method.

In Figure 78 and Figure 79 are reported results obtained adopting the geometric fitting on the point cloud, while in Figure 80 and Figure 81 are reported bounding boxes obtained by using the method based on the principal component analysis (PCA).

Figure 82 reports the error regarding the centroid estimation obtained as the distance between the calculated centroid with respect to the original one. The definition of the centroid as the geometric centre of the bounding box has been adopted to compare results.

Figure 83 shows the errors of the area obtained as the difference between the 3D modelling BB area and the BB area of the discussed methods.

The error regarding the heading angle is evaluated as the difference between the orientation of the reference BB main dimension and the orientation of BB obtained with the different construction methodologies. The analysis is shown in Figure 84. The definition of the heading angle as the bow angle taken from the north direction and increasing clockwise has been adopted.

Figure 85 reports the time cost spent by the presented methods to compute the bounding box. The results have been normalized on the min-max limits method computational time. It must be considered that the order of magnitude of the time cost for the min-max methodology is around 10^{-3} s. For such a reason, both methodologies have a negligible computation time compared to clustering methods.

Analysing the reported and discussed results, it can be stated that the method based on PCA meets the case study requirements. In particular, the PCA method ensures a low computational time while preserving a precise BB orientation and the estimation of its centroid.

On the other hand, the geometric fitting needs a computational time equal to the PCA method, while the results are not as accurate.

Results obtained with the Min-Max limits method are not as accurate as required, but on the other hand, it needs an extremely low computational time. This characteristic makes the Min-Max method suitable for applications where lowering the time is the most important aspect, while a higher level of approximation can be accepted.

BB construction based on the Principal Component Analysis has been selected for the case study.

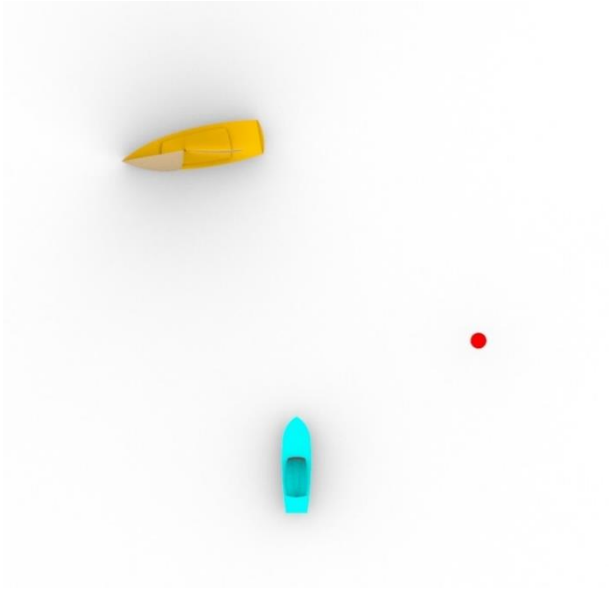

Figure 73. Representation of the virtual scenario built to compare bounding box methods. In red is reported the LiDAR location. In yellow surface vehicle number 1, in cyan surface vehicle number 2.

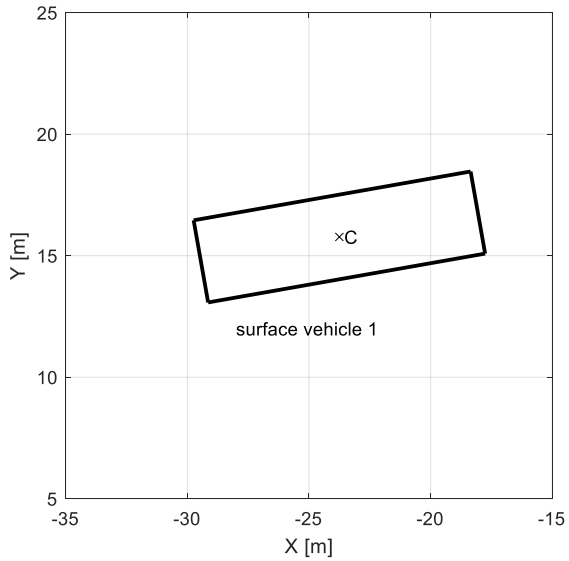

Figure 74. BB dimension and actual centroid position for surface vehicle number 1.

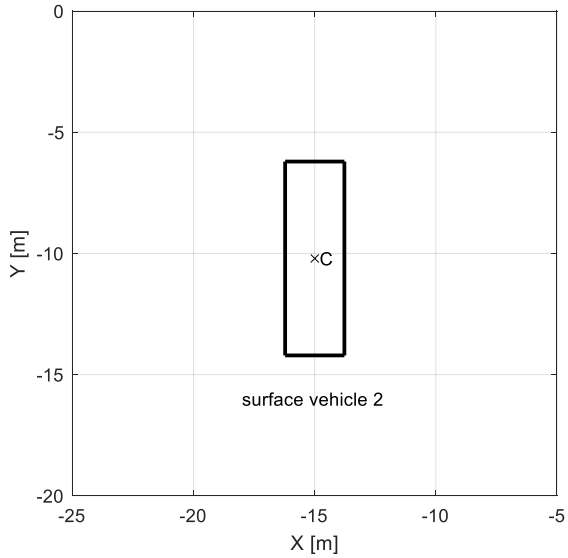

Figure 75. BB dimension and actual centroid position for surface vehicle number 2.

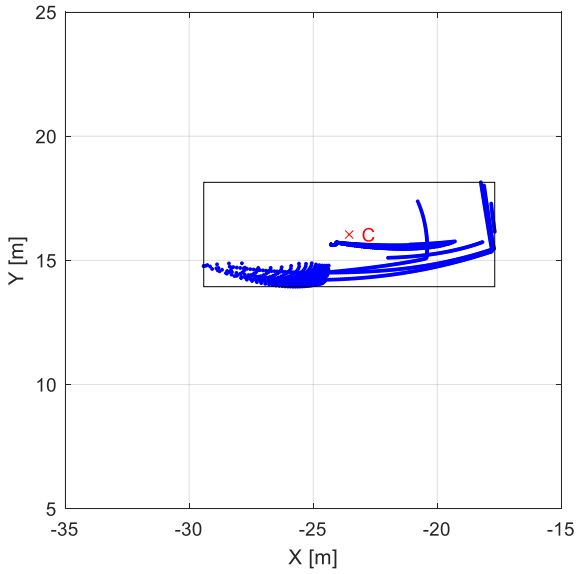

Figure 76. BB computed with the min. and max. limits method. Surface vehicle number 1.

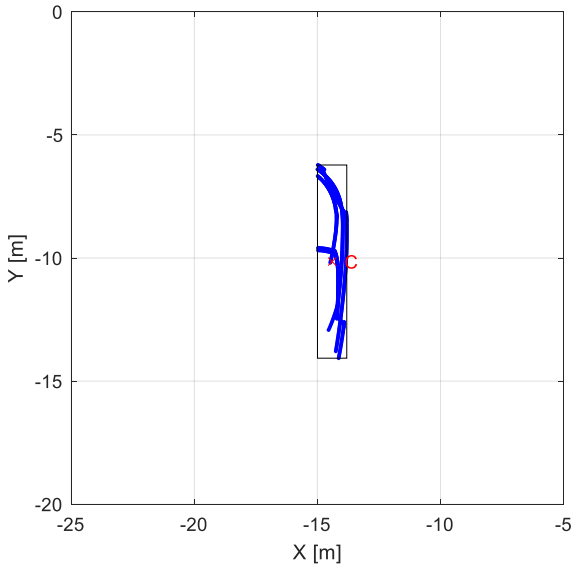

Figure 77. BB computed with the min. and max. limits method. Surface vehicle number 2.

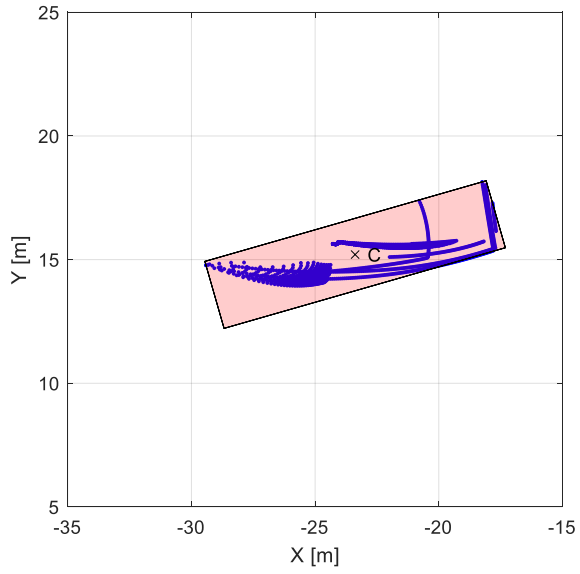

Figure 78. BB computed with the geometric fitting method. Surface vehicle number 1.

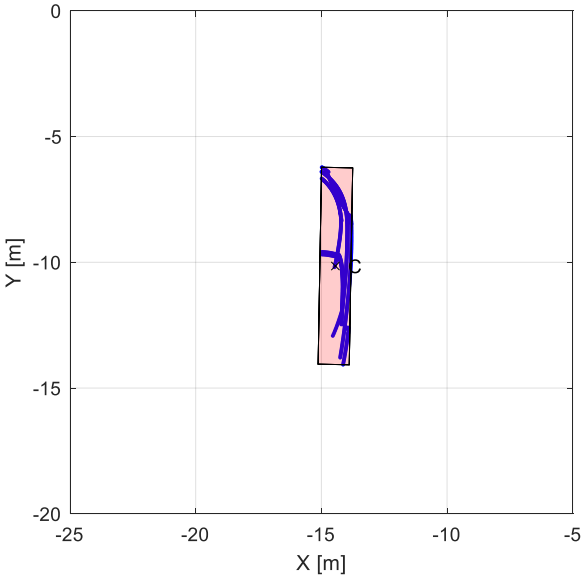

Figure 79. BB computed with the geometric fitting method. Surface vehicle number 2.

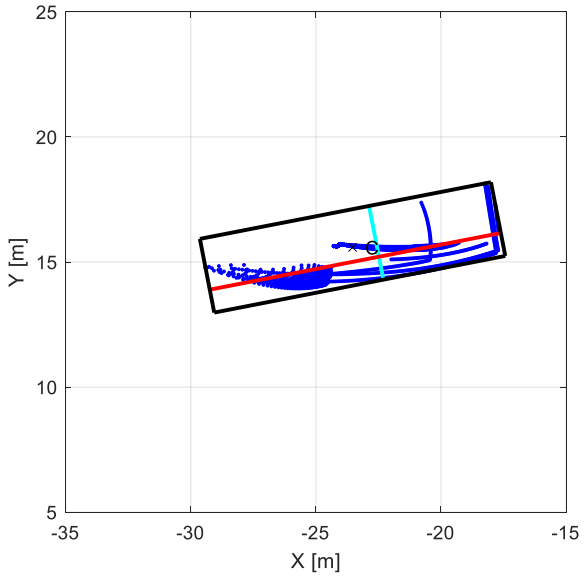

Figure 80. BB computed with PCA method. Surface vehicle number 1.

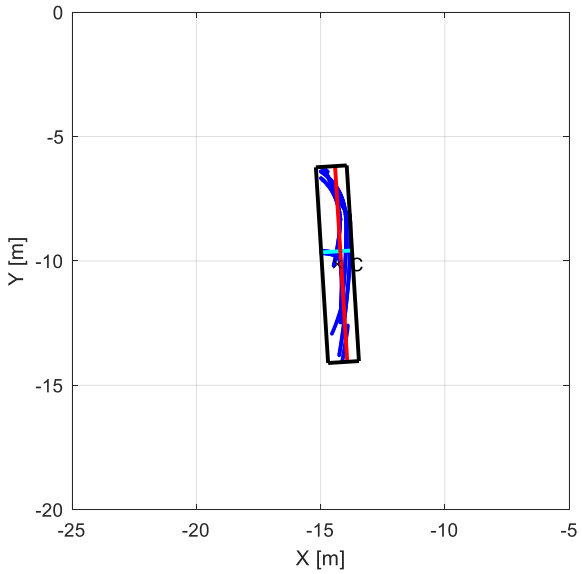

Figure 81. BB computed with PCA method. Surface vehicle number 2.

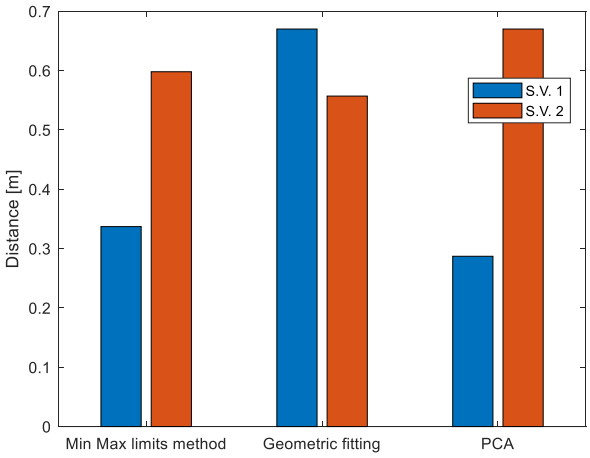

Figure 82. Error on the position of the BB centroid.

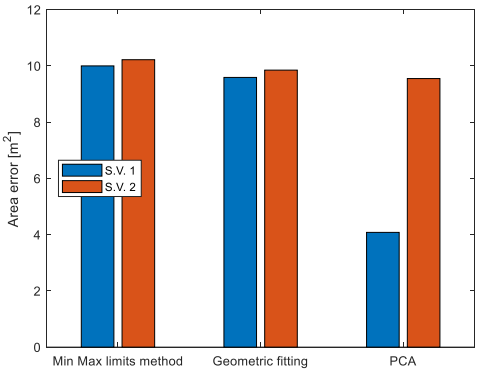

Figure 83. Error on the BB area obtained to the respect of the real one.

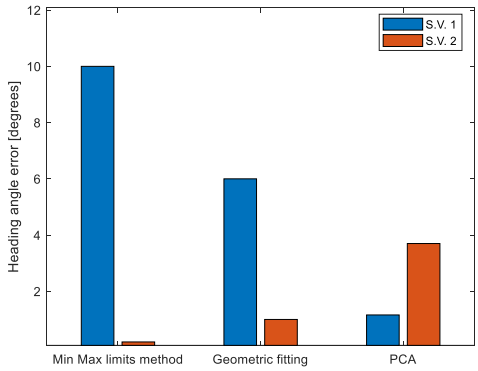

Figure 84. Error on the heading angle of the main dimension of the BB to respect the real heading angle of the vessel.

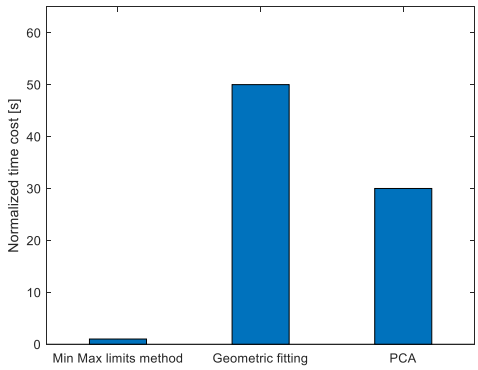

Figure 85. Normalized time to compute the BB of methods presented.

5.3.3 Tailored Multi-Obstacle Tracking

Tracking activity is crucial for the Guidance, Navigation, and Control of autonomous systems or decision support systems in order to support the helmsman during navigation. Indeed, knowing characteristics like position, speed, and orientation as a function of time is essential for making effective operative decisions autonomously or as feedback support to increase vessel safety.

Tracking term means a task that aims to achieve situational awareness by knowing the state, as the kinematic parameters and attributes that characterize one or more objects (targets) over the time domain and possibly predict their future values.

The aim is to obtain a fast method tailored for the marine environment that allows for tracking near to real-time LiDAR data collection. Procedures already discussed are exploited to associate each object - vessel or obstacle - with a representative point that is used as a target for the tracking activity. In particular, the clustering procedure is able to label the point cloud into groups that correspond to the real objects. BB is built to associate a representative point and a set of geometric information as dimension and orientation for every cluster group. Indeed, clustering and BB building procedures are necessary conditions for tracking activity.

The aim is to obtain a LiDAR sensor-based multi obstacle tracking. The working principles algorithm is reported in Figure 86. Although tracking algorithms are also discussed for a group of points in the literature, for the case study, the tracking activity is performed on BB centroids, considering centroids as representative points of the entire objects.

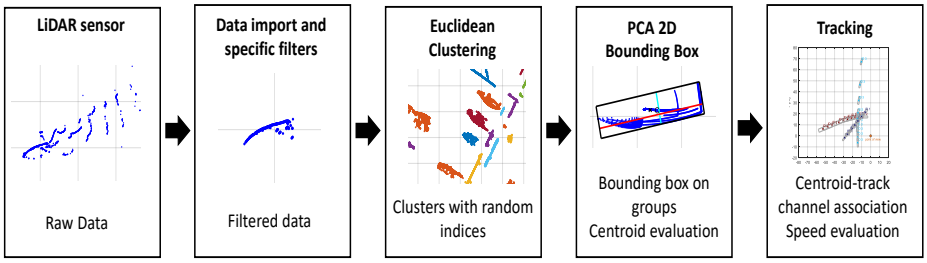

Figure 86. Complete tracking algorithm workflow.

Tracking a single object in the area of interest allows adopting the simplest tracking algorithms known as single-target tracking (STT). Tracking a standalone target does not require a data association process because the detection can be directly used to evaluate the state of the object.

Dealing with multiple targets requires the association of the target to a track channel. By knowing the present and past variables' values is possible to evaluate the state of the target. This system is used in a modern tracking system that usually involves a Multiple Target Tracking (MTT) model. MTT association problem is a challenging aspect and is the method adopted that generally distinguishes the different tracking algorithms present in the literature.

In modern MTT systems, the assignment is achieved by means of a prediction and a gating activity. The prediction is generally delegated to the MTT internal filter (such as a Kalman filter) and is used to carry out the gating activity; a validation gate is built around the predicted track based on the predicted state and associate covariance to individuate the candidates' track for the assignment. The gating activity's purpose is to decrease the computational effort of the detection-track association algorithm feeding it only with validated candidates.

Joint Probabilistic Data Association (JPDA) algorithm [192, 193, 194] and Global Nearest Neighbour (GNN) algorithm [195] are well-known tracking algorithms, often proposed in the literature to track LiDAR and RADAR data. They are generally adopted when it is necessary to associate multiple object measurements with multiple sensors in a cluttered environment in order to achieve target tracking, even if JPDA usually performs better in a high clutter environment than GNN.

GNN algorithm employs a rigid detection assignment to a track; in particular, the global nearest observations within candidates validated from the gating activity are assigned to the selected existing tracks. A new track is initialized when an observation is not associated with any existing track.

On the other hand, the JPDA algorithm performs a soft assignment; all detections that fall in a track's validation gate can contribute to the track by means of weight based on their probability of association. If the probability of assignment of detection is lower than an imposed threshold, the algorithm initializes a new track.

The description of the literature tracking systems is not meant to be a detailed explanation of the tracking algorithms but a brief introduction necessary to better understand the existing problems.

JPDA and GNN approaches are pretty sophisticated and require filters to make predictions, increasing the computational cost. On the other hand, LiDAR point cloud detections in the marine environment do not involve high clutter phenomena as applications in which JPDA and GNN are generally adopted. Therefore, the advantages of using these algorithms are limited, while containing the computational cost is essential for the case study. A simplified model capable of achieving a good level of accuracy in the tracking activity was developed.

5.3.3.1 Object ID association issue – proposed tracking method

The premises for the development of this model are not to use a predictive tool and to contain the computational effort. Therefore, the development was oriented on the use of elementary operations considering the peculiarities of the marine environment. Moreover, the tracking system must be structured in such a way as to take into account the outputs received from the clustering and BB construction modules already discussed in the previous chapters.

Assume having two acquisitions at consequent times t and $t+1$ and that the clustering and BB building activities are already performed. Cluster labels and the associated BB and its centroids are information available. The clustering algorithm starts to analyse datasets in a random seed point. For such a reason, it must be considered that the same label p will probably identify a different object at time t and at time $t+1$. In other words, the object acquired at time $t+1$ could be identified with a cluster label different to the label assigned to the same object at time t. Moreover, it is not ensured that the number of clusters at time t will be the same at the time $t+1$. The continuous change in the cluster label of an object is typically overcome using tracking channels or a track-list.

The tracking activity problem is how to manage the assignment of an object to a track channel over time. The aim is to evaluate a method based on the data at disposal that allows assigning, with reasonable accuracy, centroids evaluated at a different time instant to the same track channel in order to represent the same object.

The proposed method to achieve the tracking task is based on a closeness logic. Indeed, an object at time $t+1$ is assigned to the track channel that identifies the closest object at time t.

For each time step, the algorithm calculates the distance between the clusters at the time t and at the time $t+1$. A matrix D_{ij} is built where the location ij

represents the distance of the object *j* at the time *t+1* from the object *i* at the time *t*. Then, a generic object *j* is assigned to the track that minimizes the distance. If at time *t+1* there are more tracks than at the time *t*, the unassigned object produces a new track. If at time *t+1* the number of tracks is less than at the time *t*, the track - or the tracks - that remain without new objects are cancelled.

This algorithm could seem to be an excessively simplified methodology but contextualized on the case study it guarantees several advantages. First, its simplicity allows assigning a vessel to a track without performing any time-consuming prediction concerning the path, making it a high-speed method.

The ambiguity tracking represents the main problem due to closely spaced targets. Indeed, geometric positions of different targets at time *t+1* and at time *t* could be disposed to lead to a wrong switch of the assigned track channels. Such an issue is an existing problem, shown in Figure 87. Tracked points are the centroids of the BB built on the clusters detected in LiDAR acquisition. It means that a minimum distance between centroids is always maintained due to the physical geometry of surface vehicles.

LiDAR used in the case study can perform five scans per second (5 *Hz*). Assuming the worst case of a 6 m long boat that is sailing at 20 knots in harbour water, in one second, the centroid is shifted by about 10 m. If the LiDAR acquires a new scan every 0.2 s, it means that the centroid shift between two consequent scans is of the order of 2 m. In other words, the centroids representing the boat at time t and at time t+1 are enclosed in the boat's shape at time t+1, making it impossible to switch on the track assignment with another vessel due to the closeness Figure 88. Moreover, it must be considered that such a high speed is not typical – and not even permitted – in a port scenario where boats sail slowly.

The only case in which the closeness criterion could fail, depending on the speed, is when two small boats stand side by side for a boarding operation. Nevertheless, in this specific case, a failure of the clustering algorithm is detected before the tracking operation. Indeed, the two very close boats will be clustered as a unique object belonging to the same cluster, and a single centroid will represent them. Then, when the boats start to drift away, and the clustering algorithms recognize them as separate objects, what has been said previously is valid, and the problem does not arise. This behaviour could probably lead to a switch of the track channel but does not depend on the tracking assignment criterion. The same thing happens in an impact event. Such a limit is not suitable for the following track or following the leader logic where it requests

to follow a specific target. Indeed, the track can be lost in such a case during a particular manoeuvre. Therefore, except for particular scenarios, it can be stated that the proposed track assignment criterion produces accurate results for most cases.

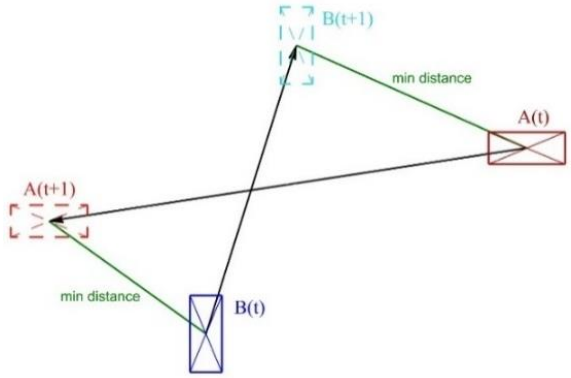

Figure 87. Failure scenario for the closeness criterion.

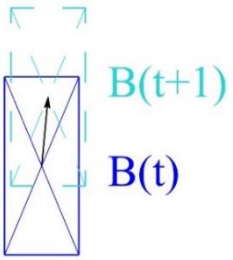

Figure 88. The behaviour of the centroid shift between two consequent LiDAR acquisitions.

The pseudocode, representing the assignment of the centroids to the track-list, is shown below:

READ centroids (previous scan) from the track-list
READ centroids (current scan)
FOR i = 1 to number of previous centroids
    Compute the distance of i^{th} previous centroid from each current centroid
    Find the index k of the current centroid with a minimum distance
    Add the k^{th} current centroid to the i^{th} track channel
END
IF number of current centroids > number of previous centroids
    Assign current centroids not already assigned to new track channels
IF the number of current centroids < number of previous centroids
    Remove the no update track channels
ELSE
  Update all track channels
END

After carrying out the centroid-track association, the speeds are assessed. The object's speeds are concerning to the LiDAR reference frame, Vx and Vy [Figure 89]. The centroid's speed V is evaluated as follows:

$$Vx = \frac{X(t) - X(t-1)}{\Delta t}$$
$$Vy = \frac{Y(t) - Y(t-1)}{\Delta t} \quad (30)$$
$$V = \sqrt{Vx^2 + Vy^2}$$

Where X and Y are the coordinates of the centroid associated with the ID (or track channel) for which the speed is evaluated; *t* and *t-1* indicate the frame for which the speeds are evaluated, while Δt is the time interval between the two scans.

V_x and V_y are the speed components projected on the LiDAR's reference frame. The angle that the centroid's speed (V) forms with the X-axis can then be calculated as follows:

$$\chi = arctan\frac{Vy}{Vx} \quad (31)$$

From a hydrodynamic point of view, the χ angle includes both the route angle ψ and the drift angle δ, as shown in Figure 90.

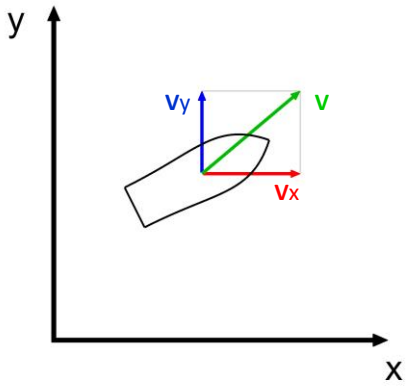

Figure 89. Speeds on LiDAR reference frame.

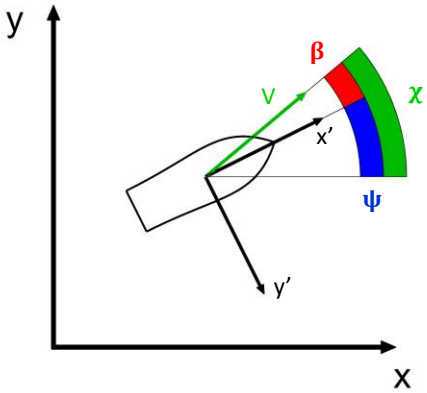

Figure 90. Speed angle on LiDAR reference frame.

As has been shown in the previous section, the centroid calculation is strongly influenced by LiDAR data collection accuracy; therefore, the χ angle obtained is a purely indicative estimate. Moreover, the drift angle β cannot be evaluated with the available data, and so the route angle ψ of the target remains an unknown variable.

The proposed tracking method has been tested and validated by means of the synthetic and experimental data collected scenario.

5.3.3.2 Real scenario – proposed tracking method

The proposed tracking algorithm has been tested in a real marine scenario where two boats navigate in opposite directions and maintain an average safety distance. The considered frames for the analysis are 38, assuming to evaluate the tracking algorithm every second.

Therefore, the analysed scenario has a temporal duration of 38 s. The scenario has been collected by using an acquiring speed equal to 5 Hz. For such a reason, every frame is acquired every 0.2 s. Choosing one second as the time step allows the algorithm to consider an under-sampling case and puts the analysis in favour of safety. However, the algorithm is able to process a scan every 0.2 s under certain conditions, i.e., in the open sea. In this case, the analysis started has a frame step equal to 5 frames.

In Figure 91 are reported the point clouds regarding the two vessels for each numbered frame.

In Figure 92 are reported the bounding boxes and the track number identifier (ID).

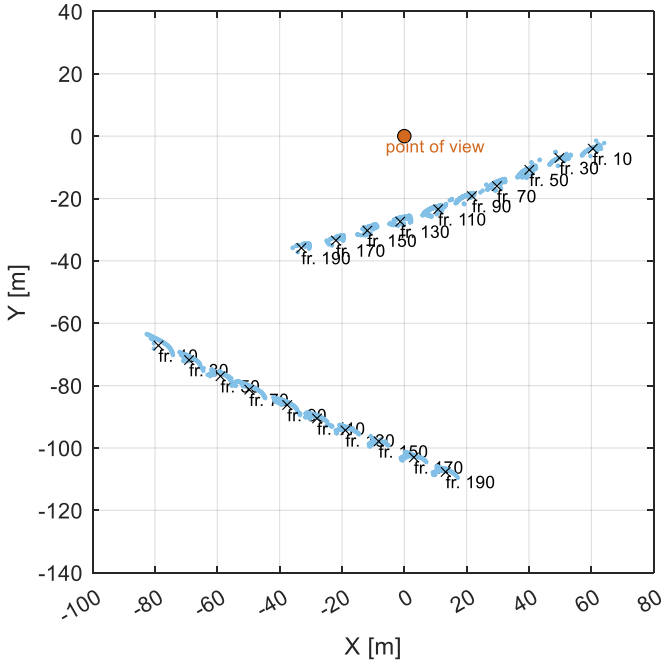

Figure 91. Real scenario tracking – point clouds and centroids.

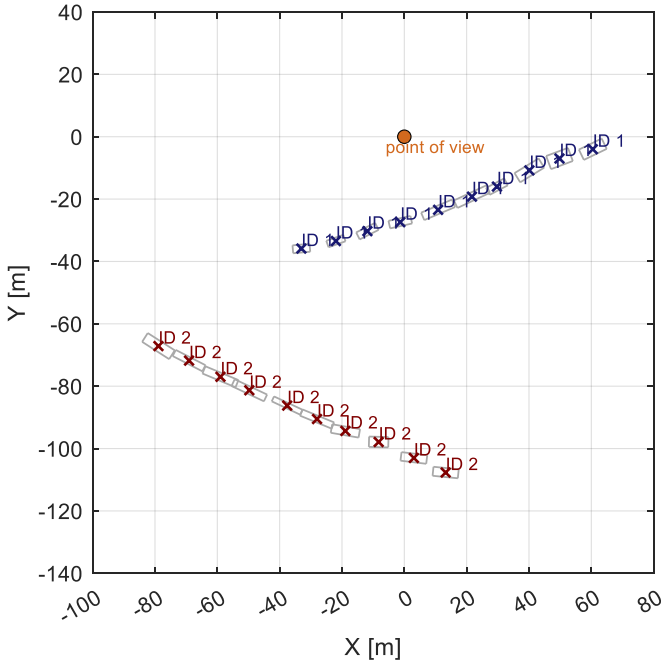

Figure 92. Real scenario tracking – bounding boxes and vehicle ID.

Figure 93 shows the speed, in knots, of vessels for x and y directions and the speed module. ID 1 is reported in a blue line with circle markers, while ID 2 with a red line with cross markers. A fluctuation of the velocity value is observable. The centroid movement is not entirely attributable to the only vessel motion but also to the differences in its description caused by LiDAR acquisition peculiarity. Depending on the time step adopted, a very high sampling frequency produces a more significant oscillation in the instantaneous speed. Indeed, the instantaneous speed does not provide a reliable value but can be used to estimate the mean speed through time history.

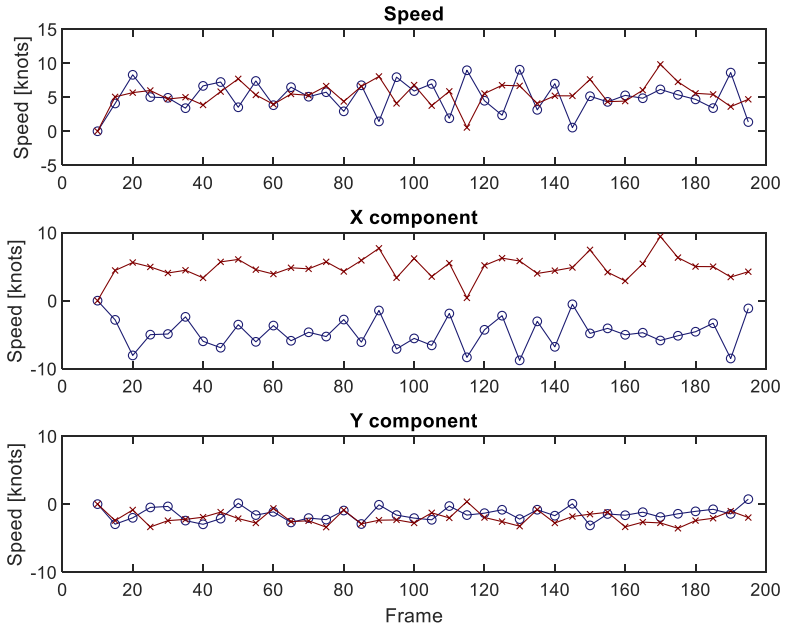

Figure 93. Speed comparison for both vessels. The ID track number identifies objects.

5.3.3.3 Virtual scenario – proposed tracking method

In order to test the tracking algorithm on a more challenging scenario, a synthetic scenario has been created to stress the multi-object tracking algorithm testing an improbable navigation scenario where no safety distance has been respected. The virtual scenario has been developed in order to obtain a trajectory intersection among a motorboat (8 m), a sailboat (12 m), and a *gozzo* (6 m). The motorboat has south to north route direction. The sailboat navigates with an east to west route direction. The *gozzo* has a southwest to northeast

route direction. The motions of the boats within the scenario are the following: the motorboat slows down, then passes aft of the sailboat and accelerates straight ahead. The sailboat maintains a quasi-constant speed while the *gozzo* crosses the two trajectories passing very close to the motorboat. The minimum distance is less than 4 meters. The boat movements vary from less than one meter up to several meters for each step, depending on the speed of the ships. The time step adopted for the analysis is one second. The model built to test the tracking procedure is reported in Figure 94. For the sake of clarity, the colours identify the same instant frames for the different ships, in particular, starting from red to green.

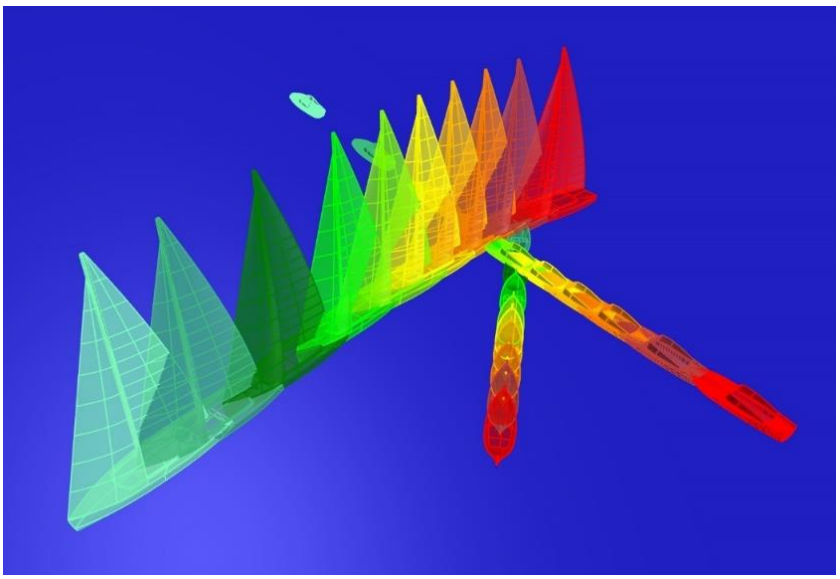

Figure 94. Virtual scenario tracking – 3D shape.

Figure 95 and Figure 96 show the track history on the 2D plane, showing different information, the point cloud and centroid, and the BBs and the ID, respectively, for each frame. For the sake of clarity, the data has been reported as skipping one frame avoiding plotting every frame. Otherwise, the plots would have been useless for understanding purposes. It is essential to underline that the point cloud that describes the gozzo is poorly acquired in the sixth frame due to the motorboat shadow cone. This aspect implies a wrong evaluation of bounding box orientation, area sizing, and centroid position.

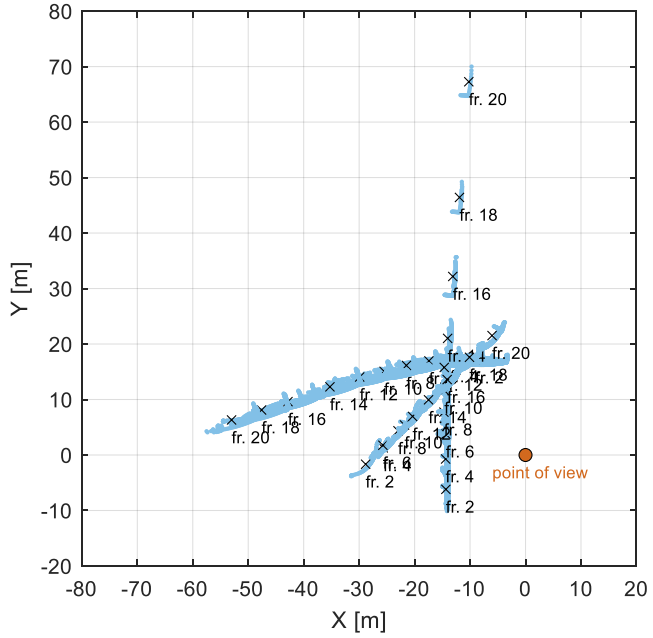

Figure 95. Virtual scenario tracking – point clouds and centroids.

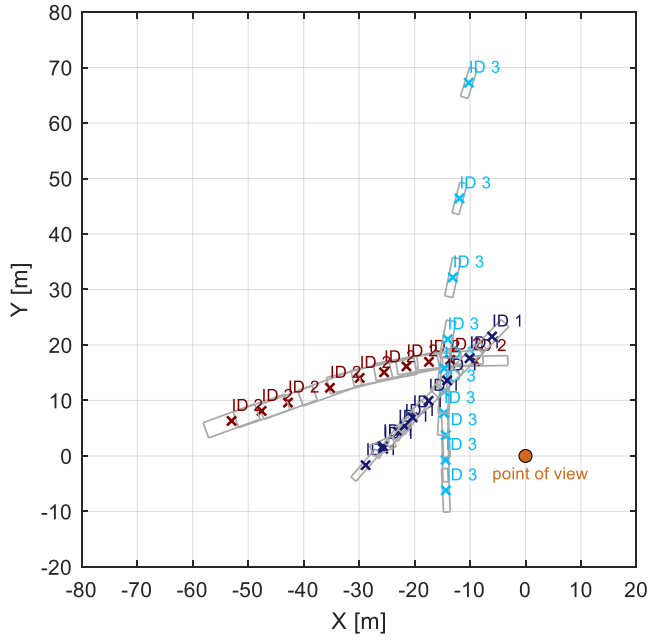

Figure 96. Virtual scenario tracking – bounding boxes and vehicle ID.

Figure 97 reports the speeds for the track channels. The blue line with the circle markers identifies ID1 (*gozzo*), the red line with the cross markers identifies ID2 (sailboat), and the cyan line with diamond markers identifies ID3 (motorboat).

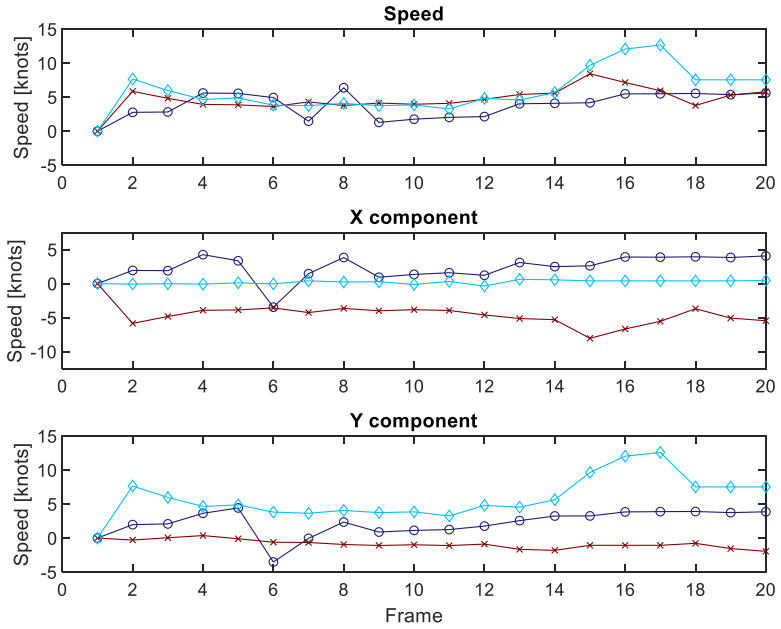

Figure 97. Speed of vessels.

A tailored scenario allows comparing the speeds calculated by means of the tracking activity respect with to speeds assessed by the 3D virtual scenario. The comparison between the tracking calculated speeds and that set in the model (Figure 98, Figure 99, Figure 100) are reported hereinafter.

The calculated speed is shown with a blue line and circular markers, while the model set speed is shown with an orange line and x markers. The high difference concerning the speed for the ID 3 in the last frames is attributable to the motorboat's position and the distance between the boat and the sensor. Frames 6, 7, and 8 are characterized by an incorrect evaluation of the speeds of ID1. Such a result is a superimposition consequence of ID3 and ID1 that implies a worse acquisition of ID1, which is partially positioned inside the shadow cone caused by the presence of ID3.

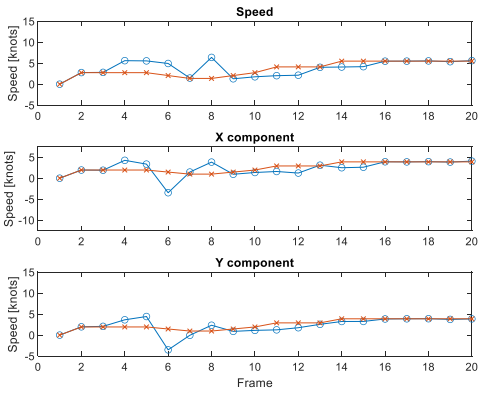

Figure 98. Calculated speed compared to the actual one for track ID number 1.

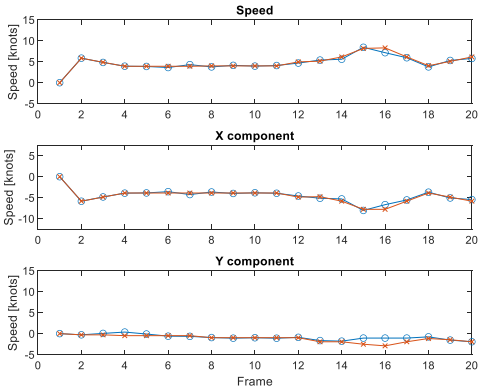

Figure 99. Calculated speed compared to the actual one for track ID number 2.

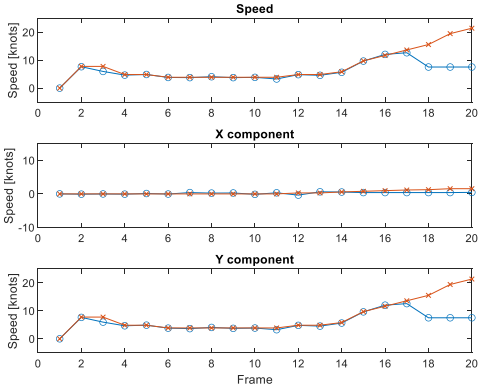

Figure 100. Calculated speed compared to the actual one for track ID number 3.

5.3.3.4 Computational time comparison – proposed tracking method

The tracking results are entirely overlapping regarding the real environment and the virtual one, considering the other tracking system (JPDA & GNN).

Figure 101 reports the comparison of the average time needed by each algorithm to analyse a single scan of the real scenario already discussed. Again, time results are normalized on the time cost of the proposed tracking procedure. Even if the proposed procedure does not ensure any prediction, contrary to what the standard tracking algorithms do, for the case study, it produces sufficiently accurate results and, on the other hand, guarantees a computational time of the order of 10^{-3} s. Such a low computational cost allows for completing the entire procedure, starting from clustering to obstacle-tracking, almost in real-time. Moreover, the computational time is comparable with LiDAR acquisition time intervals. Predicting the trajectory is generally linked to the risk of having no observation for a consistent time due to data loss. Nevertheless, since the algorithm could work processing more than one scan for a second, some scans' lack of an object does not produce particular issues.

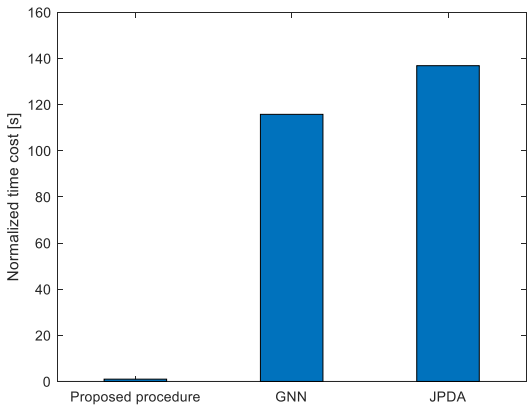

Figure 101. The normalized time cost of the tracking algorithm for one single LiDAR scan.

The results suggest that using more complete algorithms such as JPDA and GNN for the environment under analysis does not lead to appreciable benefits, instead increasing the computational time. However, using GNN and JPDA can be helpful in very complex scenarios where the tracked object is likely to be hidden and lost for short periods, and path prediction is essential to avoid the potential collision.

Chapter 6

6.1 Conclusion

The proposed research project aims to develop enabling technologies to achieve autonomous navigation or a decision support system. In particular, two main topics have been treated, the dynamic positioning system and the collision avoidance system, highlighted the experimental obstacle detection. Moreover, has been presented the experimental facility and devices, thanks to the research project, have been carried out.

Regarding the dynamic positioning system, the importance of using a dynamic approach to dimension and more accurately knowing the behaviour of a system was shown. Hence, significant differences concerning the static-approach results have been demonstrated. Furthermore, using a dynamic approach allows evaluating the transients and analysing how the DP control logic responds to the different disturbance magnitude and oscillations; this information will not be available with other design methods.

Indeed, the static approach is valid for designing the propulsion system's main characteristics and stationary performance during a design concept phase. On the other hand, it is impossible to understand, from the static results, if the marine vehicle will overcome the transient safely or if the vehicle can withstand, even small, oscillations around the equilibrium reached configuration.

Moreover, the presented DP system was developed with two force allocation logics (FALs), one optimised thrust allocation and one with a fixed propeller position that can be used in both open-loop and closed-loop for the station-keeping purpose. The results showed that each allocation has some benefits and drawbacks, and it is possible to think about switching between them in the function of external disturbances direction.

The collision avoidance system was presented in its first level, e.g., managing the first part of the system. The obstacle detection was tailored for the marine environment. In particular, a sensor-based multi-tracking obstacle was developed that detects and tracks wandering obstacles in the marine field using the latest generation sensors and integrates effective data management and analysis. The proposed approach contributes to the steps necessary for the

construction of a decision support system and the autonomous navigation research field.

The use of LiDAR sensors guarantees effective virtualization of the surrounding environment by means of a point cloud structure. The LiDAR point cloud was analysed by exploiting the proposed machine learning approach based on unsupervised learning techniques, particularly Clustering and Principal Component Analysis steps.

This approach ensures obtaining a high level and fast object detection, avoiding the onerous training activity required by a supervised learning approach. Furthermore, the peculiarities of LiDAR scanning in the marine field allow the construction of a simplified tracking system, which results in a much lower computational load than more complete methods, guaranteeing an equally precise result.

A method for obtaining a virtual scenario suitable for testing and developing algorithms was also shown. This approach allows the researchers to test their algorithms on synthetic point clouds obtained without real devices. This approach is recommended in the early stage of the project when the devices are unavailable or to optimize the resources to avoid experimental data collection campaigns.

6.2 Future Research

Future development will concern the dynamic positioning system's experimental tests on the model-scale tugboat and compare the observed manoeuvring behaviour with the presented numerical results.

The different force allocations developed will be implemented on the test model in order to obtain a comparison between simulated and experimental data. Furthermore, the video tracking system shown with a single camera can be improved by providing for the use of multiple cameras simultaneously in order to enlarge the available field of view. In this way, the developed allocations can be used not only in order to perform dynamic positioning manoeuvres but also to change positioning.

Concerning the obstacle detection topic, despite the experimental and virtual validation of the multi-tracking obstacle, several issues were detected, such as

the LiDAR acquisition of black objects due to optical phenomena and propagation of the groups identified by the Clustering algorithm in the presence of bridging objects.

A future development already under analysis is the data-fusion activity to overcome the inevitable and peculiar shortcomings of the single sensors. Enlarging the number of information collected and data sources allows for overcoming the specific lacks of each sensor. Moreover, the Inertial Measurement Unit (IMU) used to evaluate ship movement and position will be essential to process the acquired LiDAR point cloud to use the application in real-time in a dynamic scenario.

Figure 102 shows a proposal for a data-fusion activity coupling an RGB camera and a LiDAR sensor. In particular, the point cloud is processed through the unsupervised proposed method, while a supervised approach employing Convolutional Neural Networks (CNN) is adopted for RGB image processing, particularly YOLOv4.

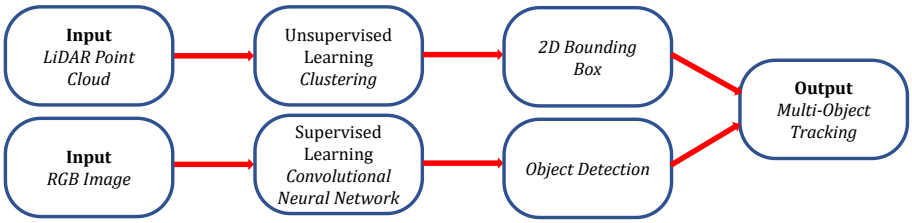

Figure 102. LiDAR-camera data-fusion workflow.

In particular, thanks to the CNN know-how of SEASTEMA (Fincantieri NexTech) Company, this research topic has been carried out, and the object detection via RGB image has been concluded, as shown in Figure 103.

The topic under development is to the information hierarchy level in order to decide the priority of data (data-fusion activity). More pieces of information are available in [196].

Indeed, the natural continuation of the proposed project has to include the integration of different sensors and the time synchronization of the acquired data to improve the system's accuracy and flexibility.

Figure 103. Object detection via YOLOv4

In particular, the aspects concerning the development of situational awareness must be deepened and analysed in the immediate future. They will acquire ever greater importance for remotely guided or autonomous ships.

For example, this aspect is evidenced by an important project, called "Ocean Infinity" that has the purpose of designing and constructing a new series of six multi-purpose offshore vessels, all of which will be operated from shore. Indeed, in this project, the development of a situational awareness system through the integration of a multitude of sensors of different nature e.g., RGB images, RADAR, SONAR and LiDAR data, will be essential to the success of the project. The project data fusion hierarchy is still under discussion and study.

Acknowledgements

I apologize to my foreign readers but I promise that this part is not at all a technical one, this wants to be just an acknowledgement for every person that I met during my academic path. For such a reason I'm going to use my mother tongue to capture the shades of words.

Come ogni cosa nella vita tutto ha un inizio ed una fine, e questa tesi può essere considerata come il mio personale canto del cigno. A differenza di molti che conoscono la propria strada con fermezza e decisione, conoscendo la propria meta sin dal principio, io posso affermare che ho sempre vissuto cercando di compiere la scelta che ritenevo giusta senza perseguire una precisa destinazione.

Sinceramente, ho sempre pensato che più importante della meta sia il viaggio, ed in questo viaggio, iniziato ben prima del dottorato, posso affermare di aver incontrato persone decisamente degne di essere conosciute che, fortunatamente, ora posso chiamare amici.

Non farò nomi e cognomi, parafrasando persone più importanti di me, per non dimenticare qualcuno e non allungare questo sproloquio di sentimentalismi, ma, a tutti loro va la mia riconoscenza e gratitudine.

Gli innumerevoli consigli, i più o meno aspri confronti e gli incoraggiamenti ricevuti, mi hanno reso sicuramente una persona migliore, sotto molti punti di vista, rispetto allo studente che ero diversi anni fa.

Riprendendo la già citatata figura di Ulisse, sicuramente io non sarò un navigatore altrettanto eccellente ma, come lui, ho navigato per mari, talvolta burrascosi e ricchi di insidie, ed infine, a differenza sua, ho portato la nave in porto attraccando alla mia Itaca.

References

1. Chaal M, Valdez Banda OA, Glomsrud J, Basnet S, Hirdaris S, Kujala P.A framework to model the STPA hierarchical control structure of an autonomous ship. Saf Sci 2020.
2. World Maritime News Staff. Maersk CEO: unmanned Containerships Not in My Lifetime 2018. https://www.offshore-energy.biz/maersk-ceo-unmanned-containerships-not-in-my-lifetime/(accessed May 27, 2020).
3. Tesla, N. (1898). Method of and Apparatus for Controlling Mechanism of Moving Vessels. Pat, (613), 809.
4. Shenoi, R. A., Bowker, J. A., Dzielendziak, A. S., Lidtke, A. K., Zhu, G., Cheng, F., ... & Westgarth, R. (2015). Global marine technology trends 2030.
5. EMSA – Preliminary Annual Overview of Marine Casualties and Incidents 2014-2020 (2021, April).
6. United States Coast Guard – 2020 Recreational Boatin Statistics (2021, June).
7. Allianz Global Corporate and Specialty. Safety and Shipping Review 2021. (2021).
8. Banda, O. A. V., & Kannos, S. (2017). Hazard analysis process for autonomous vessels. In Technical Report.
9. Banda, O. A. V., Kannos, S., Goerlandt, F., van Gelder, P. H., Bergström, M., & Kujala, P. (2019). A systemic hazard analysis and management process for the concept design phase of an autonomous vessel. Reliability Engineering & System Safety, 191, 106584.
10. Wróbel, K., Gil, M., & Chae, C. J. (2021). On the influence of human factors on safety of remotely-controlled merchant vessels. Applied Sciences, 11(3), 1145.
11. Burmeister, H. C., Bruhn, W. C., Rødseth, Ø. J., & Porathe, T. (2014). Can unmanned ships improve navigational safety?. In Proceedings of the Transport Research Arena, TRA 2014, 14-17 April 2014, Paris,.
12. Zhang, M., Montewka, J., Manderbacka, T., Kujala, P., & Hirdaris, S. (2021). A big data analytics method for the evaluation of ship-ship collision risk reflecting hydrometeorological conditions. Reliability Engineering & System Safety, 213, 107674.
13. Gou, X., & Lam, J. S. L. (2019). Risk analysis of marine cargoes and major port disruptions. Maritime Economics & Logistics, 21(4), 497-523.
14. Felski, A., & Zwolak, K. (2020). The ocean-going autonomous ship—Challenges and threats. Journal of Marine Science and Engineering, 8(1), 41.
15. Perera, L. P. (2020). Deep learning toward autonomous ship navigation and possible COLREGs failures. Journal of Offshore Mechanics and Arctic Engineering, 142(3).
16. de Vos, J., Hekkenberg, R. G., & Banda, O. A. V. (2021). The impact of autonomous ships on safety at sea–a statistical analysis. Reliability Engineering & System Safety, 210, 107558.
17. Haider, J., Ou, Z., & Pettit, S. (2019). Predicting corporate failure for listed shipping companies. *Maritime Economics & Logistics*, *21*(3), 415-438.
18. Etges, A. P. B. D. S., Souza, J. S. D., & Kliemann, F. J. (2017). Risk management for companies focused on innovation processes. *Production*, *27*.
19. Bhalodi, A. (2019). Digitalisation in Maritime Industry.
20. Kretschmann, L., Burmeister, H. C., & Jahn, C. (2017). Analysing the economic benefit of unmanned autonomous ships: An exploratory cost-comparison between an

autonomous and a conventional bulk carrier. Research in transportation business & management, 25, 76-86.
21. Akbar, A., Aasen, A. K., Msakni, M. K., Fagerholt, K., Lindstad, E., & Meisel, F. (2021). An economic analysis of introducing autonomous ships in a short-sea liner shipping network. International Transactions in Operational Research, 28(4), 1740-1764.
22. Msakni, M. K., Akbar, A., Aasen, A. K., Fagerholt, K., Meisel, F., & Lindstad, E. (2020). Can autonomous ships help short-sea shipping become more cost-efficient?. In Operations Research Proceedings 2019 (pp. 389-395). Springer, Cham.
23. DNV GL. Remote-controlled and autonomous ships. Position Paper DNV GL Høvik, Norway, 2018.
24. Ziajka-Poznańska, E., & Montewka, J. (2021). Costs and Benefits of Autonomous Shipping—A Literature Review. Applied Sciences, 11(10), 4553.
25. BIS Research (2018). Global Autonomous Ship and Ocean Surface Robot Market: Focus on Mode of Operation, Subsystem, End User, and Application – Analysis and Forecast, 2018-2028 – BIS Research Report, 2018. https://bisresearch.com/industry-report/global-autonomous-ship-ocean-surface-robot-market.html
26. Liu, Z., Zhang, Y., Yu, X., & Yuan, C. (2016). Unmanned surface vehicles: An overview of developments and challenges. *Annual Reviews in Control*, *41*, 71-93.
27. Schiaretti, M., Chen, L., & Negenborn, R. R. (2017, October). Survey on autonomous surface vessels: Part II-categorization of 60 prototypes and future applications. In *International Conference on Computational Logistics* (pp. 234-252). Springer, Cham.
28. Gu, Y., Goez, J. C., Guajardo, M., & Wallace, S. W. (2021). Autonomous vessels: state of the art and potential opportunities in logistics. *International Transactions in Operational Research, 28(4)*, 1706-1739.
29. Curcio, J., Leonard, J., & Patrikalakis, A. (2005, September). SCOUT-a low cost autonomous surface platform for research in cooperative autonomy. In Proceedings of OCEANS 2005 MTS/IEEE (pp. 725-729). IEEE.
30. Bremer, R. H., Cleophas, P. L., Fitski, H. J., & Keus, D. (2007). Unmanned surface and underwater vehicles. TNO DEFENCE SECURITY AND SAFETY THE HAGUE (NETHERLANDS).
31. Motwani, A. (2012). A survey of uninhabited surface vehicles. Marine and Industrial Dynamic Analysis, School of Marine Science and Engineering, Plymouth University, Tech. Rep.
32. Roberts, G. N., & Sutton, R. (Eds.). (2006). Advances in unmanned marine vehicles (Vol. 69). Iet.
33. Vaneck, T. W., Rodriguez-Ortiz, C. D., Schmidt, M. C., & Manley, J. E. (1996). Automated bathymetry using an autonomous surface craft. NAVIGATION, Journal of the Institute of Navigation, 43(4), 407-418.
34. Delft University of Technology, Dynamic Positioning for Tito Neri Tug Boats. https://www.studeersnel.nl/nl/document/technische-universiteit-delft/mechatronics-in-mt/overige/dp-guide-2017-0228-reader/924363/view?has_flashcards=false (2017)
35. Haseltalab, A., Garofano, V., Afzal, M. R., Faggioni, N., Li, S., Liu, J., ... & Negenborn, R. R. (2020). The collaborative autonomous shipping experiment (case): motivations, theory, infrastructure, and experimental challenges. In International ship control systems symposium (iSCSS 2020). IMaReST.
36. Manley, J. E. (1997, October). Development of the autonomous surface craft" aces". In Oceans' 97. MTS/IEEE Conference Proceedings (Vol. 2, pp. 827-832). IEEE.

37. Goudey, C. A., Consi, T., Manley, J., & Graham, M. (1998). A robotic boat for autonomous fish tracking. Marine Technology Society. Marine Technology Society Journal, 32(1), 47.
38. Majohr, J., & Buch, T. (2006). Modelling, simulation and control of an autonomous surface marine vehicle for surveying applications Measuring Dolphin MESSIN. IEE Control Engineering Series, 69, 329.
39. Manley, J. E., Marsh, A., Cornforth, W., & Wiseman, C. (2000, September). Evolution of the autonomous surface craft AutoCat. In OCEANS 2000 MTS/IEEE Conference and Exhibition. Conference Proceedings (Cat. No. 00CH37158) (Vol. 1, pp. 403-408). IEEE.
40. Bertram, V. (2008). Unmanned surface vehicles-a survey. Skibsteknisk Selskab, Copenhagen, Denmark, 1, 1-14.
41. Roberts, G. N., & Sutton, R. (Eds.). (2006). Advances in unmanned marine vehicles (Vol. 69). Iet.
42. Yakimenko, O. A., & Kragelund, S. P. (2011). Real-time optimal guidance and obstacle avoidance for umvs. Autonomous underwater vehicles, 67-98.
43. Breivik, M., Hovstein, V. E., & Fossen, T. I. (2008). Straight-line target tracking for unmanned surface vehicles.
44. Caccia, M., Bono, R., Bruzzone, G., Spirandelli, E., Veruggio, G., Stortini, A. M., & Capodaglio, G. (2005). Sampling sea surfaces with SESAMO: an autonomous craft for the study of sea-air interactions. IEEE robotics & automation magazine, 12(3), 95-105.
45. Alves, J., Oliveira, P., Oliveira, R., Pascoal, A., Rufino, M., Sebastiao, L., & Silvestre, C. (2006, June). Vehicle and mission control of the DELFIM autonomous surface craft. In 2006 14th mediterranean conference on control and automation (pp. 1-6). IEEE.
46. Gomes, P., Silvestre, C., Pascoal, A., & Cunha, R. (2006). A path-following controller for the DELFIMx autonomous surface craft. Proceedings of the 7th IFAC MCMC, Lisbon, Portugal.
47. Idland, T. K. (2015). Marine cybernetics vessel cs saucer:-design, construction and control (Master's thesis, NTNU).
48. Yang, W. R., Chen, C. Y., Hsu, C. M., Tseng, C. J., & Yang, W. C. (2011). Multifunctional inshore survey platform with unmanned surface vehicles. International Journal of Automation and Smart Technology, 1(2), 19-25.
49. Mahacek, P. (2005). Dynamic analysis of a SWATH vessel. MBARI Internship Report, 1-13
50. Higinbotham, J. R., Hitchener, P. G., & Moisan, J. R. (2006, September). Development of a new long duration solar powered autonomous surface vehicle. In OCEANS 2006 (pp. 1-6). IEEE.
51. Ebken, J., Bruch, M., & Lum, J. (2005, May). Applying unmanned ground vehicle technologies to unmanned surface vehicles. In Unmanned Ground Vehicle Technology VII (Vol. 5804, pp. 585-596). International Society for Optics and Photonics.
52. Larson, J., Bruch, M., & Ebken, J. (2006, May). Autonomous navigation and obstacle avoidance for unmanned surface vehicles. In Unmanned systems technology VIII (Vol. 6230, p. 623007). International Society for Optics and Photonics.
53. Sauze, C., & Neal, M. (2006). An autonomous sailing robot for ocean observation.
54. Bingham, B., Kraus, N., Howe, B., Freitag, L., Ball, K., Koski, P., & Gallimore, E. (2012). Passive and active acoustics using an autonomous wave glider. Journal of field robotics, 29(6), 911-923.
55. Desa, E., Maurya, P. K., Pereira, A., Pascoal, A. M., Prabhudesai, R. G., Mascarenhas, A., ... & Afzulpurkar, S. (2007). A small autonomous surface vehicle for ocean color remote sensing. IEEE Journal of Oceanic Engineering, 32(2), 353-364.

56. Martins, A., Ferreira, H., Almeida, C., Silva, H., Almeida, J. M., & Silva, E. (2007). Roaz and roaz ii autonomous surface vehicle design and implementation. In International Lifesaving Congress 2007.
57. Ferreira, H., Martins, R., Marques, E., Pinto, J., Martins, A., Almeida, J., ... & Silva, E. P. (2007, June). Swordfish: an autonomous surface vehicle for network centric operations. In Oceans 2007-Europe (pp. 1-6). IEEE.
58. Li, Z., & Bachmayer, R. (2013, September). The development of a robust Autonomous Surface Craft for deployment in harsh ocean environment. In 2013 OCEANS-San Diego (pp. 1-7). IEEE.
59. Holler, J., Striz, A., Bretney, K., Kavett, K., & Bingham, B. (2007). Design, construction, and field testing of an autonomous surface craft for engineering and science education. In OCEANS 2007 (pp. 1-6). IEEE.
60. Cruz, N., Matos, A., Cunha, S., & da Silva, S. O. (2007). Zarco-an autonomous craft for underwater surveys. 7th Geomatic Week.
61. Yan, R. J., Pang, S., Sun, H. B., & Pang, Y. J. (2010). Development and missions of unmanned surface vehicle. Journal of Marine Science and Application, 9(4), 451-457.
62. Breivik, M. (2010). Topics in guided motion control of marine vehicles.
63. Bibuli, M., Caccia, M., Lapierre, L., & Bruzzone, G. (2012). Guidance of unmanned surface vehicles: Experiments in vehicle following. IEEE Robotics & Automation Magazine, 19(3), 92-102.
64. Giger, L., Wismer, S., Boehl, S., Büsser, G. A., Erckens, H., Weber, J., ... & Siegwart, R. (2009). Design and construction of the autonomous sailing vessel avalon. In Proceedings of The World Robotic Sailing Championship and International Robotic Sailing Conference. Eidgenössische Technische Hochschule Zürich.
65. Bibuli, M., Bruzzone, G., Caccia, M., Ippoliti, G., Longhi, S., Orlando, G., & Pelusi, G. M. (2012). Discrete-time sliding mode control for guidance of an unmanned surface vehicle. IFAC Proceedings Volumes, 45(27), 441-446.
66. Zizzari, A. A., Indiveri, G., Bibuli, M., Bruzzone, G., & Caccia, M. (2009). Path following guidance control with bounded control effort: Application to the charlie unmanned surface vehicle. IFAC Proceedings Volumes, 42(18), 109-114.
67. Beck, E., Kirkwood, W., Caress, D., Berk, T., Mahacek, P., Brashem, K., ... & Wheat, G. (2009). SeaWASP: A small waterplane area twin hull autonomous platform for shallow water mapping. Marine Technology Society Journal, 43(1), 6-12.
68. Sliwka, J., Reilhac, P. H., Leloup, R., Crepier, P., Malet, H. D., Sittaramane, P., ... & Jaulin, L. (2009, July). Autonomous robotic boat of ensieta. In 2nd International Robotic Sailing Conference, Matosinhos, Portugal (Vol. 35).
69. Miller, P., Beal, B., Capron, C., Gawboy, R., Mallory, P., Ness, C., ... & Spears, H. (2010). Increasing performance and added capabilities of usna sail-powered autonomous surface vessels (asv). NAVAL ACADEMY ANNAPOLIS MD DEPT OF NAVAL ARCHITECTURE OCEAN AND MARINE ENGINEERING.
70. Zyvex Marine and Zyvex Technologies. Piranha USV. Available: http://www.zyvexmarine.com/piranha/
71. Ghani, M. H., Hole, L. R., Fer, I., Kourafalou, V. H., Wienders, N., Kang, H., ... & Peddie, D. (2014). The SailBuoy remotely-controlled unmanned vessel: Measurements of near surface temperature, salinity and oxygen concentration in the Northern Gulf of Mexico. Methods in Oceanography, 10, 104-121.
72. Hitz, G., Pomerleau, F., Garneau, M. E., Pradalier, C., Posch, T., Pernthaler, J., & Siegwart, R. Y. (2012). Autonomous inland water monitoring: Design and application of a surface vessel. IEEE Robotics & Automation Magazine, 19(1), 62-72.

73. Singh, Y., Sharma, S., Sutton, R., Hatton, D., & Khan, A. (2018). A constrained A* approach towards optimal path planning for an unmanned surface vehicle in a maritime environment containing dynamic obstacles and ocean currents. Ocean Engineering, 169, 187-201.
74. Singh, Y., Sharma, S., Sutton, R., Hatton, D., & Khan, A. (2018). A constrained A* approach towards optimal path planning for an unmanned surface vehicle in a maritime environment containing dynamic obstacles and ocean currents. Ocean Engineering, 169, 187-201.
75. Wirtensohn, S., Reuter, J., Blaich, M., Schuster, M., & Hamburger, O. (2013, August). Modelling and identification of a twin hull-based autonomous surface craft. In 2013 18th International Conference on Methods & Models in Automation & Robotics (MMAR) (pp. 121-126). IEEE.
76. Perera, L. P., Moreira, L., Santos, F. P., Ferrari, V., Sutulo, S., & Soares, C. G. (2012). A navigation and control platform for real-time manoeuvring of autonomous ship models. IFAC Proceedings Volumes, 45(27), 465-470.ù
77. Pandey, J., & Hasegawa, K. (2015, October). Study on manoeuverability and control of an autonomous Wave Adaptive Modular Vessel (WAM-V) for ocean observation. In 2015 International Association of Institutes of Navigation World Congress (IAIN) (pp. 1-7). IEEE.
78. Von Ellenrieder, K., & Wampler, J. (2016). Unmanned surface vessel (USV) systems for bridge inspection.
79. Stelzer, R., & Jafarmadar, K. (2012, November). The robotic sailing boat asv roboat as a maritime research platform. In Proceedings of 22nd international HISWA symposium.
80. Le Bars, F., & Jaulin, L. (2013). An experimental validation of a robust controller with the VAIMOS autonomous sailboat. In Robotic Sailing 2012 (pp. 73-84). Springer, Berlin, Heidelberg.
81. Wang, J., Gu, W., & Zhu, J. (2009, January). Design of an autonomous surface vehicle used for marine environment monitoring. In 2009 International Conference on Advanced Computer Control (pp. 405-409). IEEE.
82. Gray, A., Shahrestani, N., Frank, D., & Schwartz, E. (2013). Propagator 2013: Uf autonomous surface vehicle. AUVSI Foundation's 6th Annual RoboBoat Competition, Virginia Beach, VA.
83. Frank, D., Gray, A., & Schwartz, E. (2014, November). Propagator 2: A planing autonomous surface vehicle with azimuth rimdriven thrusters. In Proceedings of the 14th Annual Early Career Technical Conference (pp. 1-6).
84. Fumagalli, E., Bibuli, M., Caccia, M., Zereik, E., Del Bianco, F., Gasperini, L., ... & Bruzzone, G. (2014). Combined acoustic and video characterisation of coastal environment by means of unmanned surface vehicles. IFAC Proceedings Volumes, 47(3), 4240-4245.
85. Oh, H. N. H., Tsourdos, A., & Savvaris, A. (2014). Development of collision avoidance algorithms for the c-enduro usv. IFAC Proceedings Volumes, 47(3), 12174-12181.
86. Iovino, S., Savvaris, A., & Tsourdos, A. (2018). Experimental testing of a path manager for unmanned surface vehicles in survey missions. IFAC-PapersOnLine, 51(29), 226-231.
87. Codiga, D. L. (2015). A marine autonomous surface craft for long-duration, spatially explicit, multidisciplinary water column sampling in coastal and estuarine systems. Journal of Atmospheric and Oceanic Technology, 32(3), 627-641.

88. Valada, A., Velagapudi, P., Kannan, B., Tomaszewski, C., Kantor, G., & Scerri, P. (2014). Development of a low cost multi-robot autonomous marine surface platform. In field and service robotics (pp. 643-658). Springer, Berlin, Heidelberg.
89. Cabrera-Gámez, J., de Miguel, A. R., Domínguez-Brito, A. C., Hernández-Sosa, J. D., Isern-González, J., & Fernández-Perdomo, E. (2014). An embedded low-power control system for autonomous sailboats. In Robotic Sailing 2013 (pp. 67-79). Springer, Cham.
90. Domínguez-Brito, A. C., Valle-Fernández, B., Cabrera-Gámez, J., Ramos-de-Miguel, A., & García, J. C. (2015, August). A-TIRMA G2: an oceanic autonomous sailboat. In World Robotic Sailing championship and International Robotic Sailing Conference (pp. 3-13). Springer, Cham.
91. Liu, C., Zheng, H., Negenborn, R. R., Chu, X., & Wang, L. (2015, September). Trajectory tracking control for underactuated surface vessels based on nonlinear Model Predictive Control. In International Conference on Computational Logistics (pp. 166-180). Springer, Cham.
92. Plumet, F., Petres, C., Romero-Ramirez, M. A., Gas, B., & Ieng, S. H. (2014). Toward an autonomous sailing boat. IEEE Journal of Oceanic Engineering, 40(2), 397-407.
93. Nakatani, T., Hyakudome, T., Sawa, T., Nakano, Y., Watanabe, Y., Fukuda, T., ... & Yoshida, H. (2015, October). Development of an autonomous surface vehicle for monitoring underwater vehicles. In OCEANS 2015-MTS/IEEE Washington (pp. 1-5). IEEE.
94. Delft University of Technology, All algorithms on deck! Working on robotic ships. DELTA 49(6), https://tudelftroboticsinstitute.nl/news/all-algorithms-deck-working-robotic-ships (2016).
95. Conte, G., Scaradozzi, D., Mannocchi, D., Raspa, P., & Panebianco, L. (2016, June). Development and testing of low-cost ASV. In The 26th International Ocean and Polar Engineering Conference. OnePetro.
96. Prempraneerach, P., Janthong, M., Klanthip, T., Boonyarak, S., Choosui, C., Phothongkum, K., ... & Kulvanit, P. (2015, November). Autonomous way-point tracking navigation of surveying surface vessel with real-time positioning system. In 2015 International Computer Science and Engineering Conference (ICSEC) (pp. 1-6). IEEE.
97. Santos, D., Silva Junior, A. G., Negreiros, A., Vilas Boas, J., Alvarez, J., Araujo, A., ... & Gonçalves, L. M. (2016). Design and implementation of a control system for a sailboat robot. Robotics, 5(1), 5.
98. Negenborn R.R., Autonomous Vessel Family of the Waterborne Transport Technology Lab at Delft University of Technology. http://www.mtt.tudelft.nl/, Delft University of Technology, The Netherlands (2017)
99. Demetriou, G. A., Hadjipieri, A., Panayidou, I. E., Papasavva, A., & Ioannou, S. (2016, April). ERON: A PID controlled autonomous surface vessel. In 2016 18th Mediterranean Electrotechnical Conference (MELECON) (pp. 1-5). IEEE.
100. Li, Y., Wang, L., Liao, Y., Jiang, Q., & Pan, K. (2018). Heading MFA control for unmanned surface vehicle with angular velocity guidance. Applied Ocean Research, 80, 57-65.
101. Azevedo, D., Beltram, S., DelVecchio, G., & Hopner, B. (2016). MARV: Marine Autonomous Research Vessel.
102. Peng, Z., Wang, D., Wang, W., & Liu, L. (2016). Neural adaptive steering of an unmanned surface vehicle with measurement noises. Neurocomputing, 186, 228-234
103. Klinger, W. B., Bertaska, I. R., von Ellenrieder, K. D., & Dhanak, M. R. (2016). Control of an unmanned surface vehicle with uncertain displacement and drag. IEEE Journal of Oceanic Engineering, 42(2), 458-476.

104. Sarda, E. I., Qu, H., Bertaska, I. R., & von Ellenrieder, K. D. (2016). Station-keeping control of an unmanned surface vehicle exposed to current and wind disturbances. Ocean Engineering, 127, 305-324.
105. AMS Institute: Roboat (2016), http://www.ams-institute.org/roboat/
106. Fernandes, P. C., Marques, M. M., & Lobo, V. (2016, September). Barlavento-considerations about the design of an autonomous sailboat. In World Robotic Sailing championship and International Robotic Sailing Conference (pp. 19-30). Springer, Cham.
107. Heins, P. H., Jones, B. L., & Taunton, D. J. (2017). Design and validation of an unmanned surface vehicle simulation model. Applied Mathematical Modelling, 48, 749-774.
108. Makhsoos, A., Mousazadeh, H., Mohtasebi, S. S., Abdollahzadeh, M., Jafarbiglu, H., Omrani, E., ... & Kiapey, A. (2018). Design, simulation and experimental evaluation of energy system for an unmanned surface vehicle. Energy, 148, 362-372.
109. Odetti, A., Bruzzone, G., Altosole, M., Viviani, M., & Caccia, M. (2020). SWAMP, an Autonomous Surface Vehicle expressly designed for extremely shallow waters. Ocean Engineering, 216, 108205.
110. Villa, J., Aaltonen, J., & Koskinen, K. T. (2020). Path-following with lidar-based obstacle avoidance of an unmanned surface vehicle in harbor conditions. IEEE/ASME Transactions on Mechatronics, 25(4), 1812-1820.
111. Gonzalez, A., Sanchez, P., Collado, I., Mendivil, R., Martinez, S., Gil, M., ... & Garrido, L. RoboBoat 2020: VantTec Technical Design Report VTec S-III.
112. Chang, H. C., Hsu, Y. L., Hung, S. S., Ou, G. R., Wu, J. R., & Hsu, C. (2021). Autonomous Water Quality Monitoring and Water Surface Cleaning for Unmanned Surface Vehicle. Sensors, 21(4), 1102.
113. Rødseth, Ø. J., & Burmeister, H. C. (2012). Developments toward the unmanned ship. In Proceedings of International Symposium Information on Ships–ISIS (Vol. 201, pp. 30-31).
114. Rolls-Royce (2016) Remote and autonomous ships. The next steps. https ://www.rolls -royce .com/~/media /Files /R/Rolls -Royce/docum ents/custo mers/marin e/ship-intel /aawa-white paper -210616.pdf. Accessed 20 Nov 2018
115. Rolls-Royce (2018) Rolls-Royce and Finferries sign cooperation agreements to optimise ship safety and efficiency. https://www.rolls-royce.com/media/press-releases/2018/17-05-2018-rr-and-finferries-sign-cooperation-agreement-to-optimise-ship-safety-andefficiency.aspx.
116. Rolls-Royce (2018) Rolls-Royce and Finferries demonstrate the world's first Fully Autonomous Ferry. https://www.rolls-royce.com/media/press-releases/2018/03-12-2018-rr-and-finferries-demonstrate-worlds-first-fully-autonomous-ferry.aspx.
117. Bolbot, V., Theotokatos, G., Andreas Wennersberg, L., Faivre, J., Vassalos, D., Boulougouris, E., ... & Van Coillie, A. (2021). A novel risk assessment process: Application to an autonomous inland waterways ship. Proceedings of the Institution of Mechanical Engineers, Part O: Journal of Risk and Reliability, 1748006X211051829.
118. Kongsberg Maritime (2017) Autonomous ship project, key facts about YARA Birkeland. https://www.kongsberg.com/maritime/support/themes/autonomous-ship-project-key-facts-about-yarabirkeland/?OpenDocument=
119. Alfheim, H. L., Muggerud, K., Breivik, M., Brekke, E. F., Eide, E., & Engelhardtsen, Ø. (2018). Development of a dynamic positioning system for the revolt model ship. IFAC-PapersOnLine, 51(29), 116-121.
120. European Space Agency. (2019). Trondheimsfjorden Test Area. Available at: https://navisp.esa.int/project/details/59/show

121. Maritime Autonomy Research Site (MARS). Available at: https://smartshipscoalition.org/maritime-autonomy-research-site-mars/
122. OCEANα. 2019. The world's largest, Asia's first unmanned marine test site officially opened. Available at: https://www.oceanalpha.com/news_list/the-worlds-largest-asias-first-unmanned-marine-test-site-officially-opened/
123. The Nippon Foundation MEGURI. Available at: https://www.nippon-foundation.or.jp/en/news/articles/2022/20220118-66716.html
124. INAS. Members of INAS. Available at: http://autonomous-ship.org/members.html
125. Vagale, A., Oucheikh, R., Bye, R. T., Osen, O. L., & Fossen, T. I. (2021). Path planning and collision avoidance for autonomous surface vehicles I: a review. Journal of Marine Science and Technology, 1-15.
126. T. B. Sheridan and W. L. Verplank, Human and Computer control of Undersea Teleoperators, Massachusetts: MIT, 1978.
127. Denmark et al., IMO MARITIME SAFETY COMMITTEE, 98th session, Agenda item 20. Maritime Autonomous Surface Ships, Proposal for a regulatory scoping exercise. Submitted by Denmark, Estonia, Finland, Japan, the Netherlands, Norway, the Republic of Korea, the United Kingdom and the United States. 27th February 2017. IMO Document MSC 98/20/2.
128. Rødseth, O.J., Nordahl, H. , 2017. Norwegian Forum for Autonomous Ships. Definitions for Autonomous Merchant Ships. Available at: https://nfas.autonomous-ship.org/wp-content/uploads/2020/09/autonom-defs.pdf
129. Lloyd´s Register, 2017. Design Code for Unmanned Marine Systems. Available at: https://www.lr.org/en/unmanned-code/
130. Bureau Veritas, 2019. Guidelines for Autonomous Shipping. Available at: https://erules.veristar.com/dy/data/bv/pdf/641-NI_2019-10.pdf
131. DNV GL, 2018. Autonomous and remotely operated ships. Available at: https://rules.dnv.com/docs/pdf/DNV/cg/2018-09/dnvgl-cg-0264.pdf
132. Bratić, K., Pavić, I., Vukša, S., & Stazić, L. (2019). A review of autonomous and remotely controlled ships in maritime sector. Transactions on Maritime Science, 8(02), 253-265.
133. Huang, Y., Chen, L., Chen, P., Negenborn, R. R., & Van Gelder, P. H. A. J. M. (2020). Ship collision avoidance methods: State-of-the-art. Safety science, 121, 451-473.
134. Wang, L., Wu, Q., Liu, J., Li, S., & Negenborn, R. R. (2019). State-of-the-art research on motion control of maritime autonomous surface ships. Journal of Marine Science and Engineering, 7(12), 438.
135. Kumar, S. (2020). Dynamic Positioning for Engineers. CRC Press.
136. Balchen, J. G., Jenssen, N. A., & Sælid, S. (1976, September). Dynamic positioning using Kalman filtering and optimal control theory. In IFAC/IFIP Symposium on automation in offshore oil field operation (Vol. 183, p. 186).
137. Specht, C., Dabrowski, P. S., Pawelski, J., Specht, M., & Szot, T. (2019). Comparative analysis of positioning accuracy of GNSS receivers of Samsung Galaxy smartphones in marine dynamic measurements. Advances in Space Research, 63(9), 3018-3028.
138. Burmeister, H. C., Bruhn, W. C., Rødseth, Ø. J., & Porathe, T. (2014). Can unmanned ships improve navigational safety?. In Proceedings of the Transport Research Arena, TRA 2014, 14-17 April 2014, Paris.
139. Hassani, V., Sørensen, A. J., & Pascoal, A. M. (2012). Evaluation of three dynamic ship positioning controllers: from calm to extreme conditions. IFAC Proceedings Volumes, 45(5), 158-163.

140. Hassani, V., Sørensen, A. J., & Pascoal, A. M. (2013, June). A novel methodology for robust dynamic positioning of marine vessels: Theory and experiments. In 2013 American Control Conference (pp. 560-565).
141. Donnarumma, S., Figari, M., Martelli, M., Vignolo, S., & Viviani, M. (2017). Design and validation of dynamic positioning for marine systems: A case study. IEEE Journal of Oceanic Engineering, 43(3), 677-688.
142. Donnarumma, S., Martelli, M., & Vignolo, S. (2015). Numerical models for ship dynamic positioning. In 6th International Conference on Computational Methods in Marine Engineering, MARINE (pp. 15-17).
143. Sørensen, A. J., Sagatun, S. I., & Fossen, T. I. (1996). Design of a dynamic positioning system using model-based control. Control Engineering Practice, 4(3), 359-368.
144. Loueipour, M. (2019). Design of Dynamic Positioning Control System for an ROV with Unknown Dynamics Using Modified Time Delay Estimation. International Journal of Maritime Technology, 11, 53-59.
145. Hosseinnajad, A., & Loueipour, M. (2020). Dynamic Positioning System Design for A Marine Vessel with Unknown Dynamics Subject to External Disturbances Including Wave Effect. China Ocean Engineering, 34(5), 651-663.
146. Ahani, A., & Ketabdari, M. J. (2019). Alternative approach for dynamic-positioning thrust allocation using linear pseudo-inverse model. Applied Ocean Research, 90, 101854.
147. Værnø, S. A., Skjetne, R., Kjerstad, Ø. K., & Calabrò, V. (2019). Comparison of control design models and observers for dynamic positioning of surface vessels. Control Engineering Practice, 85, 235-245.
148. Tam, C., Bucknall, R., & Greig, A. (2009). Review of collision avoidance and path planning methods for ships in close range encounters. The Journal of Navigation, 62(3), 455-476.
149. Ito M, Zhnng F, Yoshida N. 1999 Aug. Collision avoidance control of ship with genetic algorithm. Proceedings of the 1999 IEEE International Conference on Control Applications (Cat. No.99CH36328); Kohala Coast (HI). Vol. 2. p. 1791–1796.
150. Alvarez A, Caiti A, Onken R. 2004. Evolutionary path planning for autonomous underwater vehicles in a variable ocean. IEEE J Ocean Eng. 29:418–429. doi: 10.1109/JOE.2004.827837
151. Smierzchalski R, Michalewicz Z. 2000. Modeling of ship trajectory in collision situations by an evolutionary algorithm. IEEE Trans Evol Comput. 4(3):227–241. doi: 10.1109/4235.873234
152. Fang, M.C.; Tsai, K.Y.; Fang, C.C. A Simplified Simulation Model of Ship Navigation for Safety and Collision Avoidance in Heavy Traffic Areas. J. Navig. 2018, 71, 837–860.
153. Shimoda S, Kuroda Y, Iagnemma K. 2005. Potential field navigation of high speed unmanned ground vehicles on uneven terrain. Proceedings – IEEE International Conference on Robotics and Automation; Barcelona, Spain. Vol. 2005. p. 2828–2833.
154. Barraquand J, Langlois B, Latombe JC. 1992. Numerical potential field techniques for robot path planning. IEEE Trans Syst Man Cybernet. 22(2):224–241. doi: 10.1109/21.148426
155. Hwang Y, Ahuja N. 1992. A potential field approach to path planning. IEEE Trans Robot Autom. 8(1):23–32. doi: 10.1109/70.127236
156. Karaman S, Frazzoli E. 2011b. Sampling-based algorithms for optimal motion planning. Int J Robot Res. 30(7):846–894. doi: 10.1177/0278364911406761
157. Zaccone, R., & Martelli, M. (2020). A collision avoidance algorithm for ship guidance applications. Journal of Marine Engineering & Technology, 19(sup1), 62-75.

158. L. Perera, J. Carvalho and C. Guedes Soares, Intelligent guidance in collision avoidance of maritime transportation, pp. 9-17, 11 2012.
159. R. Zaccone, M. Martelli and M. Figari, "A COLREG-Compliant Ship Collision Avoidance Algorithm," 2019 18th European Control Conference (ECC), 2019, pp. 2530-2535, doi: 10.23919/ECC.2019.8796207.
160. Shokri-Manninen, F., Vain, J., & Waldén, M. (2020, September). Formal Verification of COLREG-Based Navigation of Maritime Autonomous Systems. In International Conference on Software Engineering and Formal Methods (pp. 41-59). Springer, Cham.
161. Chiang, H. T. L., & Tapia, L. (2018). COLREG-RRT: an RRT-based COLREGS-compliant motion planner for surface vehicle navigation. IEEE Robotics and Automation Letters, 3(3), 2024-2031.
162. COLREGs: Convention on the International Regulations for Preventing Collisions at Sea, 1972.
163. Sørensen, A.J., (2011). A survey of dynamic positioning control systems. In Annual Reviews in Control, 35(1), 123-136, https://doi.org/10.1016/j.arcontrol.2011.03.008.
164. Halvorsen, H. S., Øveraas, H., Landstad, O., Smines, V., Fossen, T. I., & Johansen, T. A. (2020). Wave motion compensation in dynamic positioning of small autonomous vessels. Journal of Marine Science and Technology, 1-20.
165. Smogeli, Ø., Trong, N. D., Børhaug, B., Pivano, L., & AS, M. C. (2013, October). The next level dp capability analysis. In Proceedings of the Dynamic Positioning Conference, Marine Technology Society.
166. Egeland, O., & Gravdahl, J. T. (2002). Modeling and simulation for automatic control (Vol. 76). Trondheim, Norway: Marine Cybernetics.
167. Martelli, M., Faggioni, N., & Berselli, G. (2019). Fuel saving in a marine propulsion plant by using a continuously variable transmission. Proceedings of the Institution of Mechanical Engineers, Part M: Journal of Engineering for the Maritime Environment, 233(4), 1007-1021.
168. Kuiper, G. (1992). The Wageningen propeller series (No. BOOK). Marin.
169. Oltmann, P. & Sharma, S.D. (1984). Simulation of Combined Engine and Rudder Maneuvers using an improved Model of Hull-Propeller-rudder Interactions, Proc. 15thONR, pp.83-108.
170. Davenport, A. G. (1961). The spectrum of horizontal gustiness near the ground in high winds. Quarterly Journal of the Royal Meteorological Society, 87(372), 194-211.
171. Alessandri, A., Donnarumma, S., Martelli, M., & Vignolo, S. (2019). Motion control for autonomous navigation in blue and narrow waters using switched controllers. Journal of Marine Science and Engineering, 7(6), 196.
172. Alessandri, A., Donnarumma, S., Luria, G., Martelli, M., Vignolo, S., Chiti, R., & Sebastiani, L. (2014). Dynamic positioning system of a vessel with conventional propulsion configuration: Modeling and simulation. In Proc. Martech 2nd Int. Conf. Maritime Technol. Eng. (pp. 725-733), Lisbon, Portugal.
173. Li, Y., Ma, L., Zhong, Z., Liu, F., Chapman, M. A., Cao, D., & Li, J. (2020). Deep learning for LiDAR point clouds in autonomous driving: a review. IEEE Transactions on Neural Networks and Learning Systems.
174. Geiger, A., Lenz, P., Stiller, C., & Urtasun, R. (2013). Vision meets robotics: The kitti dataset. The International Journal of Robotics Research, 32(11), 1231-1237.
175. Huang, X., Wang, P., Cheng, X., Zhou, D., Geng, Q., & Yang, R. (2019). The apolloscape open dataset for autonomous driving and its application. IEEE transactions on pattern analysis and machine intelligence, 42(10), 2702-2719.

176. Gao, H., Cheng, B., Wang, J., Li, K., Zhao, J., & Li, D. (2018). Object classification using CNN-based fusion of vision and LIDAR in autonomous vehicle environment. IEEE Transactions on Industrial Informatics, 14(9), 4224-4231.
177. Wu, B., Wan, A., Yue, X., & Keutzer, K. (2018, May). Squeezeseg: Convolutional neural nets with recurrent crf for real-time road-object segmentation from 3d lidar point cloud. In 2018 IEEE International Conference on Robotics and Automation (ICRA) (pp. 1887-1893). IEEE.
178. Wu, B., Zhou, X., Zhao, S., Yue, X., & Keutzer, K. (2019, May). Squeezesegv2: Improved model structure and unsupervised domain adaptation for road-object segmentation from a lidar point cloud. In 2019 International Conference on Robotics and Automation (ICRA) (pp. 4376-4382). IEEE.
179. Xu, C., Wu, B., Wang, Z., Zhan, W., Vajda, P., Keutzer, K., & Tomizuka, M. (2020, August). Squeezesegv3: Spatially-adaptive convolution for efficient point-cloud segmentation. In European Conference on Computer Vision (pp. 1-19). Springer, Cham.
180. Autonomous Underwater Vehicles Laboratory (AUV Lab). (2017). MIT Sea Grant Marine Perception Dataset. Available at https://seagrant.mit.edu/auvlab-datasets-marine-perception-1/
181. Villa, J., Aaltonen, J., & Koskinen, K. T. (2020). Path-following with lidar-based obstacle avoidance of an unmanned surface vehicle in harbor conditions. IEEE/ASME Transactions on Mechatronics, 25(4), 1812-1820.
182. Sorial, M., Mouawad, I., Simetti, E., Odone, F., & Casalino, G. (2019, October). Towards a real time obstacle detection system for unmanned surface vehicles. In OCEANS 2019 MTS/IEEE SEATTLE (pp. 1-8). IEEE.
183. Muhovič, J., Bovcon, B., Kristan, M., & Perš, J. (2019). Obstacle tracking for unmanned surface vessels using 3-d point cloud. IEEE Journal of Oceanic Engineering, 45(3), 786-798.
184. M. Ester, H. P. Kriegel, J. Sander and X. Xu, "A density-based algorithm for discovering clusters in large spatial databases with noise," kdd, vol. 96, no. 34, pp. 226-231, 1996.
185. X. a. W. D. a. W. X. Hu, "Varying density spatial clustering based on a hierarchical tree," in International Workshop on Machine Learning and Data Mining in Pattern Recognition, 2007.
186. Y. a. T. Zhu, K. M. a. Carman and M. J, "Density-ratio based clustering for discovering clusters with varying densities," Pattern Recognition, vol. 60, pp. 983--997, 2016.
187. X. a. W. D. a. W. X. Hu, "Varying density spatial clustering based on a hierarchical tree," in International Workshop on Machine Learning and Data Mining in Pattern Recognition, 2007.
188. X. Zhang, C. D. Wenda Xu and J. M. Dolan, "Efficient L-Shape Fitting for Vehicle Detection Using Laser Scanners," IEEE Intelligent Vehicles Symposium, 2018.
189. G. A. F. Seber, "Multivariate Observations," Wiley, 1984.
190. J. E. A. Jackson, in User's Guide to Principal Components, Wiley, 1988.
191. I. T. Jolliffe, in Principal Component Analysis. 2nd ed., Springer, 2002.
192. Y. Bar-Shalom, F. Daum and J. Huang, "The probabilistic data association filter," IEEE Control Systems Magazine, vol. 6, no. 29, pp. 82-100, 2009.
193. T. Fortmann, Y. Bar-Shalom and M. Scheffe, "Sonar Tracking of Multiple Targets Using Joint Probabilistic Data Association.," IEEE Journal of Ocean Engineering., vol. 8, no. 3, pp. 173-184, 1983.

194. D. Musicki and R. Evans., “Joint Integrated Probabilistic Data Association: JIPDA.,” IEEE transactions on Aerospace and Electronic Systems, vol. 40, no. 3, pp. 1093-1099, 2004.
195. S. Blackman and R. Popoli, Design and Analysis of Modern Tracking Systems., Boston: Artech House Radar Library, 1999.
196. Faggioni, N., Leonardi, N., Ponzini, F., Sebastiani, L., & Martelli, M. (2022). Obstacle detection in Real and Synthetic Harbour Scenarios. International Conference on Modelling and Simulation for Autonomous Systems. MESAS 2021. Lecture Notes in Computer Science(13207), 26-38. Springer.